Bulk and Microfluidic-Assisted Preparation of Bioreducible Polyplexes for Gene Therapy

Filipe Diogo Sousa Coelho
Mestrado em Química
Departamento de Química e Bioquímica
2017

Orientador
Prof. Doutor Eduardo Jorge Figueira Marques,
Departamento de Química e Bioquímica,
Faculdade de Ciências da Universidade do Porto

Coorientador
Doutor Bruno Fernando Brás da Silva,
Department of Life Sciences,
INL – International Iberian Nanotechnology Laboratory

Todas as correções determinadas pelo júri, e só essas, foram efetuadas.

O Presidente do Júri,

Porto, _____/_____/_____

Acknowledgments

To my supervisor, Prof. Eduardo Marques for providing me this great professional opportunity, that otherwise I would not possibly get. Also, I would like to thank for all the support given throughout the entire project and especially for the intellectual development.

To my co-supervisor, Bruno Silva, for accepting me with such kindness, also for the patience and effort. Thank you for all the support.

To Isabel Oliveira for being my helping hand every time I was in need, and for being so professional and fun.

To Sara Abalde-Cela for being such an inspiring person, and considerate positive-minded friend, that was always there when I needed. Thank you!

To Sandra, Silvina, Ana Rita, João, Alexandre, Bárbara, Ricardo and the rest of the microfluidics group at INL and the physical chemistry research group at FCUP for the friendship and companionship.

To Juliana Sousa for all the fun training rides, coffee breaks and encouraging words.

To my parents for the life lessons, for pushing me forward and always keeping me down to earth. Most importantly, for the financial support you provided.

To my dear grandparents for all the concern and support.

To my sister for always being there for me no matter what.

To Diogo for being my right hand in life. Thank you for the encouragement, warm words, and positivity you always have.

To Nádia and Teresa, for being my duo gals. Thank you for always making sure I remembered all the deadlines. Thank you for being so accepting of me. You are true friends.

To all my friends, thank you for the company.

Resumo

A terapia génica pode ser definida como a introdução de material genético numa célula para a complementação ou silenciamento de genes defeituosos, podendo ser aplicada no tratamento de doenças, tais como cancro, imunodeficiências, distrofia muscular e fibrose cística. Os vetores não virais baseados em polímeros catiónicos – poliplexos - apresentam-se como uma das mais promissoras tecnologias para este fim, devido à reduzida imunogenicidade e elevada flexibilidade de funcionalização.

Este trabalho teve como objetivo genérico a produção e caracterização de poliplexos (complexos de ácidos nucleicos com policatiões) com capacidade de degradação em contacto com o ambiente oxido-redutor do citosol celular – poliplexos biorredutíveis. Como objetivos mais específicos, pretendeu-se estabelecer uma melhor compreensão sobre o efeito do processo de mistura sobre a estrutura dos poliplexos, por recurso à técnica de microfluídica, a qual permite um melhor controlo sob o processo de mistura dos diferentes componentes.

No decorrer do projeto, o sistema DNA plasmídico/poli-L-lisina (PLL) foi produzido e caracterizado em solução e em ambiente microfluídico, servindo como sistema de referência, enquanto que o sistema DNA plasmídico/poli-L-lisina biorredutível (bPLL) foi produzido e caracterizado em solução.

Estes sistemas de poliplexos foram preparados em meio aquoso, numa vasta gama de razão de carga polímero:DNA (+/-). A estabilidade destes complexos foi estudada em tampão fisiológico e em tampão a diferente força iónica. Todos os complexos preparados foram estruturalmente caracterizados por determinação de tamanho e potencial zeta. Os dois sistemas, pDNA/PLL e pDNA/bPLL, demonstraram possuir características idênticas em meio aquoso, mas estabilidades em tampão bastante distintas entre si, diferenciando-se de forma significativa na presença de elevada força iónica.

Este trabalho visa assim contribuir para uma melhor compreensão sobre a influência do processo de mistura sobre a estrutura final do poliplexo, assim como para um melhor conhecimento sobre o efeito que a propriedade de biorredutibilidade tem nas propriedades físico-químicas dos complexos policatião/DNA.

Abstract

Gene therapy may be defined as the introduction of genetic material into a cell for the complementation or silencing of defective genes and may be applied in the treatment of diseases such as cancer, immunodeficiencies, cystic fibrosis and muscular distrophy. Non-viral vectors based on cationic polymers - polyplexes - are one of the most promising technologies for this purpose due to the low immunogenicity and high flexibility of functionalization.

In this work, our general goal was the preparation an and characterization of bioreducible polyplexes that degrade in contact with the redox environment of the cellular cytosol. As more specific objectives, we intended to establish a better understanding of the effect of the mixing process on the structure of the polyplexes, thus using the microfluidic technique which allows better control over the mixing process of the different components.

During the project, the plasmid DNA/poly-L-lysine (PLL) system was produced and characterized in bulk and microfluidic environment, serving as a reference system, whereas the plasmid DNA/bioreducible poly-L-lysine (bPLL) system was produced and characterized in bulk.

These polyplex systems were prepared in water over a wide range of polymer:DNA (+/-) charge ratios. The stability of these complexes was studied in physiological buffer, and also in buffer with different ionic strengths. All complexes prepared were structurally characterized by their size and zeta potential. The two systems, pDNA/PLL and pDNA/bPLL, have shown similar characteristics in water, but rather different stabilities in buffer, varying significantly in the presence of high ionic strength.

This work is a contribution to a better understanding of the influence of the mixing process on the final structure of the polyplex, providing information about the effect that the bioreducibility property has on the physicochemical properties of the complex.

Keywords

Polyplexes, bioreducible, polylysine, colloids, gene delivery, dynamic light scattering, electrophoretic mobility, size, zeta potential, microfluidics, laminar flow, ionic strength, polydispersity.

Content

List of Figures

List of Tables

List of symbols and abbreviations

A	Channel cross-section area
BM	Bulk mixing
bp	Base pair
bPLL	Bioreducible poly-L-lysine
CR	Charge ratio
ctDNA	Calf thymus DNA
DEAE	Diethylaminoethyl cellulose
D	Diffusion coefficient
$\mathbf{D_h}$	Hydraulic parameter
$\mathbf{d_H}$	Hydrodynamic diameter
DLS	Dynamic Light Scattering
EM	Electrophoretic mobility
GSH	Glutathione
GSSG	Glutathione disulfide
h	Channel height
$\boldsymbol{\kappa^{-1}}$	Debye length
$\boldsymbol{k_B}$	Boltzmann constant
MF	Microfluidics
MW	Molecular weight
PAAs	Polyamidoamines
pDNA	Plasmid DNA
PDI	Polydispersity index
PDMS	Polydimethylsiloxane

PEI	Polyethylemine
PLL	Poly-L-lysine
$\mathbf{P_{wet}}$	Wet parameter of the channel
$\boldsymbol{q}$	Wave vector
Q	Flow rate
$\mathbf{Q_R}$	Ratio of flow rates
$\mathbf{Q_T}$	Total flow rate
Re	Reynold's number
v	Average velocity of the flow
T	Absolute temperature
$\boldsymbol{w}$	Width of the channel
$\boldsymbol{\Gamma}$	Decay constant
$\boldsymbol{\zeta}$	Zeta potential
$\boldsymbol{\theta}$	Scattering angle
$\boldsymbol{\lambda}$	Wavelength
$\boldsymbol{\mu}$	Fluid viscosity
$\boldsymbol{\mu_2}$	Electrophoretic mobility
$\boldsymbol{\rho}$	Fluid density
$\boldsymbol{\tau}$	Delay time

1. Introduction

Since the understanding of the role of nucleic acids in encoding and translating genetic information into biological function[1-2], the increasing biochemical and biophysical knowledge gained also opened new opportunities for therapeutic interventions at the molecular level. Variations at the nucleic acid codification may directly cause illnesses or be associated with disease development. Therefore, the introduction of artificial therapeutic nucleic acids into the cell matrix should be able to lessen the severity and even cure diseases. This strategy clearly has other potential applications, including in cardiovascular[3-4], inflammatory[5] and infectious diseases[6-9], cancer[10] as well as organ transplant[11]. The delivery of the various therapeutic nucleic acids to their required cellular site of action has appeared as a major problem that delayed medical progress. Complexation of nucleic acid with polymeric carriers into polyplex nanoparticles is one possible approach to facilitate the delivery and hence overcome some of the problems.

1.1 Gene therapy

Research efforts have been focused on designing effective carrier vectors that compact and protect nucleic acids for gene therapy, since free oligonucleotides and DNA are rapidly degraded by serum nucleases in the blood if injected intravenously[12]. Initial research concentrated on using viral carriers to transport the genetic material into the cell. Viruses have been optimized by nature for nucleic acid transfer into host cells and represent the most efficient delivery vehicles. Despite their high transfer efficiency[13], viral carriers present substantial limitations, such as immunogenicity, limited cargo capacity, restricted cell tropism, or sophisticated analytics and production[14].

Non-viral vector systems, including cationic lipids[15-17], polymers[18-19], dendrimers[20], and peptides[21], all offer potential routes for DNA complexation for systemic delivery. However, unlike viral analogues that have evolved significantly to overcome cellular barriers and immune defense mechanisms, non-viral gene carriers consistently exhibit low transfection efficiency as they are blocked by many intra- and extracellular barriers. However, these systems are very attractive to this type of therapy, due to their capacity to self-assembly and high level functionalization[22]. Therefore, this type of carrier needs to present properties such as: stability in the extracellular environment, interaction with

target cell surface and cell uptake, release from endosomal vesicles and finally DNA unpacking[23-25] (figure 1).

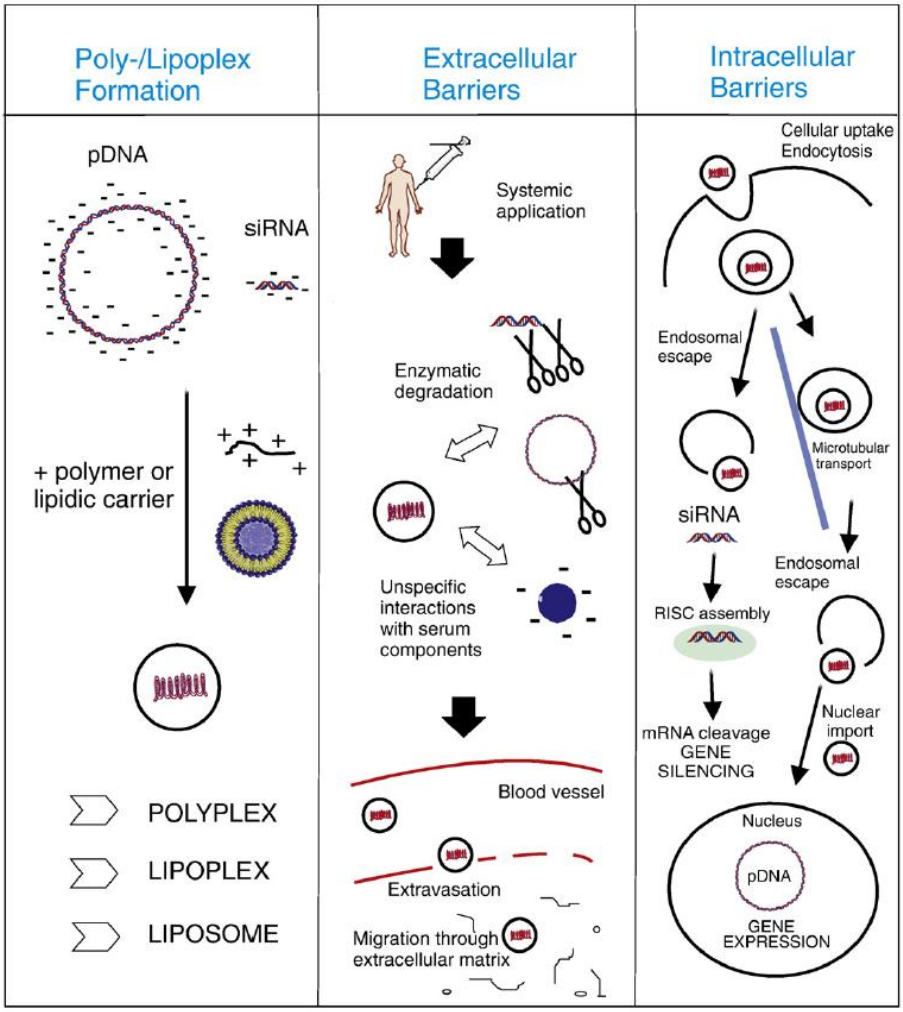

*F*ig. 1 – Schematics of the polyplex/lipoplex formation and latent cellular barriers. Adapted from[26].

1.1.1 DNA Complexation

Cellular uptake of free DNA via plasma membrane permeation is hindered by the size and negative charge of the DNA. While several studies have shown that free DNA can be introduced into cells through electroporation, gene gun, or direct injection into target tissue, the clinical relevance of these methods is limited[25]. Systemic circulation of free DNA is hampered by nuclease degradation.

At the cell level, mandatory compaction of the genome is obtained by complexation with agents such as multivalent ions, cationic surfactants, cationic polymers, or small polycationic proteins combined with monovalent and divalent ions into large

nucleoprotein complexes[27]. It has been reported that only 50% of all the negative charge of DNA is neutralized by polycation proteins, such as histones, while the other 50% is neutralized by positive ions[28]. It is also important to note that the transition from elongated coil to a condensed state only occurs when 89-90% of the negative charges are neutralized by positive counterions[29]. The understanding of the genome compaction lead to the first studies of DNA complexation using polycationic agents in the 1970s. These agents range from multivalent ions, cationic surfactants and cationic polymers[30-33].

The properties of the media where the complexation between the polymer and DNA occurs play an important role in the final structure of the formed particle (polyplex). The interactions between the two cosolutes are essentially electrostatic. Each charged molecule has a diffuse electrical double layer with some strongly bond counterions; upon release of these counterions due to complexation, there is a strong gain of entropy.

Some strategies can be used to alter complex formation and stability, including (i) addition of monovalent salt, and (ii) pH changes. Regarding effect (i), the addition of small electrolytes can aid the self-assembly of polyplexes by shielding the intramolecular charge repulsions, thus increasing the flexibility of the polymers and their ability to self-assemble[34]. On the other hand, high salt concentrations can lead to strong electrostatic screening between polyplexes leading to swelling and subsequent aggregation of swollen complexes. Also, the presence of high salt concentration before complexation decreases the entropic gain due to counterion release, thus decreasing the nucleation rate. Regarding effect (ii), polymers can be classified as either weak or strong whether they undergo partial or full ionization at physiological pH. For example PEI – polyethylenimine – is a weak polyelectrolyte with a pKa ≈ 7 [35], while PLL – poly-L-lysine – is a strong polyelectrolyte due to NH_2 groups with a pKa ≈ 10 [36]. As a result, and contrary to strong polyelectrolytes, the charge density of weak polyions will strongly depend on the pH found in different tissues and organelles. The variation within the pH range can lead to significant changes in polyelectrolyte binding and stability depending on the loss or gain of valency, i.e. charges per molecule[37].

1.1.2 Extra and Intracellular Delivery

The polycation should be able to confer protection to nucleic acids, and be strong enough to remain complexed in the presence of physiological competitors, such as serum proteins. An aspect that is common to almost every study is that polyplexes with a charge ratio (positive charge/negative charge) less or equal to 1 exhibit a poor gene transfer, while higher charge ratios yield high efficiency[21, 38]. Consequently, efficient polyplexes are formed when the number of positive charges overcomes the number of negative charges, and the physicochemical properties may be controlled by this charge ratio.

The polyplex size is a very important parameter for systemic administration, with a great impact in biodistribution and pharmacokinetics[25]. Nanoparticles with a hydrodynamic diameter below 6 nm are rapidly removed by the kidneys. On the other hand, particles sized up to 400 nm may facilitate accumulation on highly vascularized tumors[39-41]. Thus, the success of gene delivery is dependent of both size and surface charge, since these properties influence the circulation time, cellular binding and uptake, and intracellular trafficking of polyplexes[42].

The importance of polyplex stability in blood and other fluids is also a critical issue to regard. This stability is threatened by electrolytes, proteins, or cellular surfaces which may cause complex distabilization[43]. Some complications could arise from this, such as loss of delivery efficacy, binding of positively charged polyplexes with serum complement protein, activation of the innate immune system[44] or self-aggregation into larger microstructures[45]. A possible counteracting measure is to introduce elements within the polymer backbone to shield it against undesired interactions with the bioenvironment; however, cell binding and uptake may be affected.

The first barrier to the entrance of the polyplex in the cell is the cell membrane. The entry across the cell membrane does not occur passively, and so this presents the first challenge relating to intracellular delivery. Unless there is any chemical messenger on the surface of the polyplex, the binding typically occurs by particle/membrane electrostatic interaction[46]. The direct transfer to cytosol by protein channels and carriers only works for small molecules. It is also possible for some enveloped viruses[47], which bind and fuse their membrane with the target cell membrane releasing directly their payload. Nonenveloped viruses and polypeptides use an alternative two-step entry mechanism: first, engulfment into intracellular vesicles; second, escape from the vesicles to the cytosol. Other non-lipid particles are also subject to this same process, although the endosomal escape is quite inefficient. Many endocytosis processes exist[48].

Transcytosis, trafficking into Golgi organelles and endoplasmic reticulum, or maturation into lysosomes that enzymatically degrade their content, are some of the fates referred previously. Clearly, the latter fate is to be avoided for prolific delivery of nucleic acids.

The next stage of the polyplex life cycle is the cytoplasm diffusion and vector dissociation, which also represents a problem. Several strategies have been studied to facilitate the disassembly of polyplexes by taking advantage of the different conditions experimented during the cellular trafficking, such as different pH and redox potential gradient. Bioreducible polymers containing disulfide bonds are extracellularly stable providing stability to the complex, while the reducing environment of the intracellular medium leads to polymer breakdown and acid nucleic release[49]. Studies involving bioreducible polymers show an increase in gene transfection when compared to nonreducible ones[50-51]. Gene-encoding plasmid DNAs have their destination in the nucleus, whereas mRNA or siRNA targets are in the cytosol, where migration is size-dependent[52-53]. For efficient delivery, the DNA must be transported along microtubes toward the nuclear envelope to be imported into nucleus by active mechanisms or alternative pathways, and be retained there in active form. Improved delivery into the nucleus by active transport domains, in particular small peptides, has been reported in many studies[54-55].

1.2 Polymer-based Carriers

Polymers are natural candidates for the transport of therapeutic nucleic acid, because they contain the necessary features to fulfill the extracellular and intracellular requirements. They can bind, condense, protect and release nucleic acids. In addition, they can bind to cell surfaces, trigger intracellular uptake, and mediate endosomal membrane destabilization required for cytosolic release. They cannot comply these actions in the desired time sequence required. Thus, within the bioenvironment, they are subjected to many secondary interactions that hinder activity and increase cytotoxicity[25, 56-57].

The first batch of polymers ever studied, with application in gene delivery, were biomolecules already known, such as DEAE-dextran, traced back to 1965[58-59], or peptides such as polylysine and polyornithine. In a study made in 1975 by Farber, spermine , polyornithine, DEAE-dextran, polylysine and polyarginine, represented in figure 2, were evaluated for the transfection of exogenous mammalian DNA, proving that polyornithine had the best performance[60]. Early spectroscopic and electron microscopy studies provided a window into the mechanism of complexation of polymer/DNA. It was shown that polycations bind and condense nucleic acids into organized and regular nanostructures like rods and toroids[30, 33, 61-63].

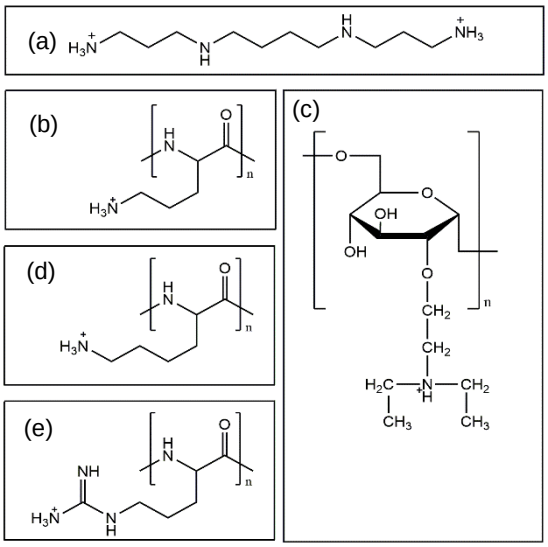

Fig. 2 - Structure of polymers used in the 1975 study of transfection efficiency of polyplexes. (a) Spermine; (b) polyornithine; (c) DEAE-dextran; (d) polylysine; (e) polyarginine.

The development of ever more efficient polyplexes went alongside the understanding of the mechanism of transfection. As mentioned before, polyplexes are engulfed within the cell membrane, penetrating the cell through vesicle formation, namely endosomes, by a variety of pathways[64]. Once in endocytic vesicles, the trapped non-viral vectors suffer a pH drop from natural to around 6. In this stage, called early endosome stage, two pathways are available: in the first path, the endosome content is externalized and, in the second and more frequent path, the vesicles turn into late endosomes, becoming more acidic. The last step involves the fusion of late endosomes with lysosomes with a further pH reduction to pH 4.5, through the action of degrative enzymes. Therefore, if

nucleic acids are trapped in these vesicles until this stage, their degradation will occur and the process of gene delivery fails.

It was discovered that by coupling the polyplexes with an antimalarial agent, chloroquine, the transfection would greatly increase. This strategy was first reported in 1983 by Luthman and Magnusson[65]. The effect of chloroquine[66-68] is largely based on the natural acidification process that occurs in endosomes due to ATPase. This enzyme actively transports protons to reach the desired pH. ATPase generates a proton gradient with a pH ~ 6 in early endosomes and down to 4.5 to late endosomes and lysosomes[69-70]. The unprotonated form of this drug can diffuse across lipid membranes into the cell and in the acidic environment of endosomes and lysosomes, it becomes protonated and thus entrapped. With the continued activity of ATPase, the drug further accumulates in the vesicles, triggering an inflow of chloride counterions, via specific carriers, and water. This results in increased osmotic pressure and swelling, leading to membrane destabilization and rupture, releasing the vectors to the cytoplasm. The scheme of this mechanism is shown in figure 3. A way to improve the transfection and eliminate possible side effects from chloroquine and analogues, would be to incorporate this proton-sponge feature into the polymer[71].

Polyamides are the first group of polymers that may be used when looking for proton-sponge features. They are only partly protonated at neutral extracellular pH and would still condense the DNA by electrostatic interactions, but they would increase their protonation and charge density within the acidic vesicle. This process should destabilize the polyplex-containing endosomal vesicle. The criteria would not be fulfilled by the already mentioned polylysine, polyarginine, or polyornithine, due to their full cationic state at physiological pH. This approach led to the discovery and use of polyethylemine (PEI) and polyamidoamines (PAAs) as very efficient carriers[71].

Recent strategies used to enhance the escape of nucleic acids from endosome are based on the design of new vectors regarding their buffering capacity. A widely used buffering moiety is the imidazole ring of histidine that is a weak base with a pKa ≈ 6, conferring the ability to acquire capture proton when the pH of the environment drops below 6. The attachment of these amino acids moieties to polymers, lipids or peptides has shown to enhance their transfection efficiency and often reduce their cytotoxicity[72-73].

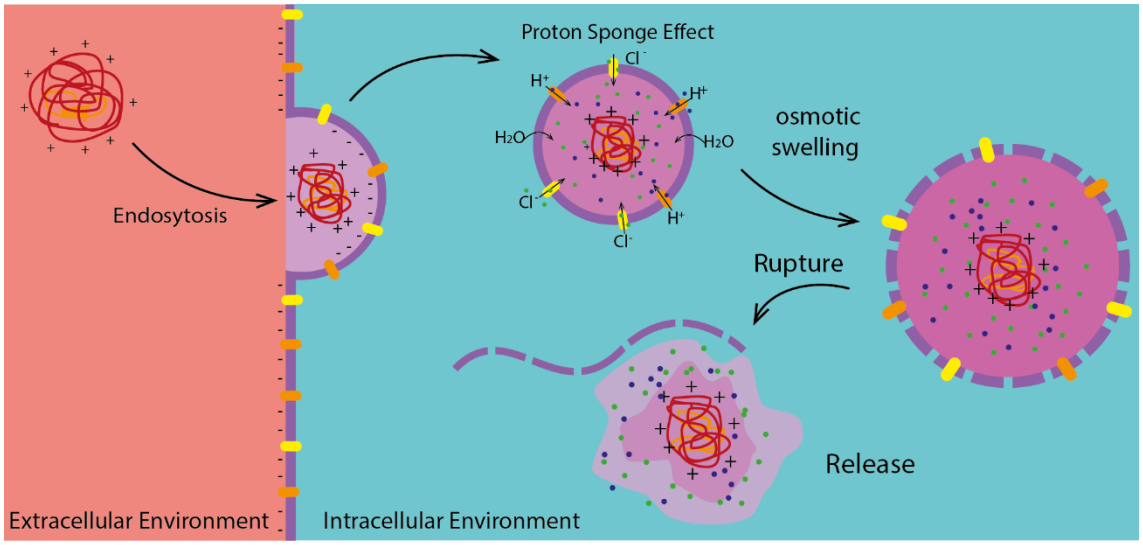

Fig. 3 – Representation of the endosomal escape mechanism based on the proton-sponge properties of polymers. Red string – polymer, and orange string – DNA.

1.2.1 Biodegradable Polymers

Biodegradable polymers go hand in hand with biomedical applications. In particular, hydrolytically degradable aliphatic polyesters, polyamides, polyorthoesters and polycarbonates have become part of biomaterials, devices and drug delivery systems[74]. Polymers that are degradable by cleavage of the disulfide bonds represent a growing class of biodegradable polymers, receiving more attention since the early 2000's, when they began to be explored in nucleic acids delivery[75]. Numerous other disulfide-containing polymers have been extensively used in industrial applications, such as the vulcanized rubber[76]. Disulfide bonds have also been applied to drug-protein conjugations[77].

Due to the unique nature of the disulfide bond, which can be easily formed and cleaved, polymers with this feature can be applied to adaptable and self-repairing materials and in material design[78-79]. From the biodegradable polymers group, the subgroup that is most important for gene delivery is the disulfide-containing polycations. As discussed above, these polymers combined with nucleic acids form polyelectrolyte complexes that serve to protect the nucleic acids and transport them to the desired destination. This protection should be continuous through the extracellular and intracellular environment. Using a simplified view of the nucleic acid delivery process and the known compartmentalization of disulfide reducing activity in the biological environment, it has been hypothesized that bioreducible polycations can provide such extracellular

protection and selective intracellular release of nucleic acids. High disulfide reducing capacity in biological environment coincides with the location in which the nucleic acids are to be released.

Biological Environment

The disulfide-containing bioreducible polycations desire their utility from the complex system of redox processes that are involved in important biological pathways and cell mechanisms. The redox gradient that exist between extracellular, intracellular environments, and subcellular organelles provides a great route for redox stimulus-responsive polycations in gene delivery. The redox environment present in cells is in dynamic equilibrium and may change depending on many factors including stage of cell cycle and biological status of the cell[80]. The most important agent responsible for the redox state of a cell is glutathione (GSH). This agent is the most abundant intracellular thiol and its concentration reaches millimolar levels inside the cell and micromolar levels in the blood plasma[81-82]. Due to its redox properties, GHS is involved is many cellular processes, including DNA and protein synthesis, enzyme activity, and metabolism and cell protection against oxidative stress[83]. The glutathione exists in two main states: the reduced and more abundant form GHS, and the oxidized state GSSG. The GSH/GSSG ratio is an indicator of the redox environment within the cell[80].

The most reducing environment, within the cell, is the microenvironment around the nucleus where the levels of GSH reach up to 20 mM compared with 1-11 mM in the cytosol. This happens because GSH is required for DNA synthesis and repair and to maintain transcription factors in reduced state[84].

Thiol-Disulfide Exchange Reaction

Disulfide bonds and their reactions are very important for biological systems to survive. They help in redox homeostasis, in correct assembly of proteins, and in the metabolic regulation of enzymatic activity. Due to their importance, cells evolved robust mechanisms for the formation, cleavage, and reshuffling of disulfide bonds in proteins[85]. The mechanisms are mainly based in exchange reactions of thiol-disulfide. These reactions involve the exchange of a disulfide with a thiol and the formation of a new disulfide and a thiol, as seen in equation 1 and 2. From a chemical perspective, thiol-

disulfide exchange is remarkable. It involves the cleavage and formation of a strong covalent bond, being reversible at room temperature in water at neutral pH. This reaction has multiple equilibria and leads to the formation of all possible thiols, symmetrical disulfides, as well as mixed disulfides as products.

$$RSH + R'SSR' \rightleftharpoons RSSR' + R'SH \quad (1)$$

$$RSH + RSSR' \rightleftharpoons RSSR + R'SH \quad (2)$$

Thiolate (RS^-) is the active nucleophile in the thiol-exchange and thus the reaction rate depends strongly on the solution pH. The thiol in GSH has a pK_a of 9.65 and therefore only a very small percentage is in the form of thiolate at neutral pH[75]. The thiol-disulfide exchange is effectively switched-off even under slightly acidic conditions[86]. Likewise, the rate of thiol-disulfide exchange depends on the presence of charged substituents in the participating thiols and disulfides. For example, the rate of reaction of GSH with positively charged peptide disulfides has been seen increase by to 2 orders of magnitude compared to the rate of the same reaction with negative counterparts[87].

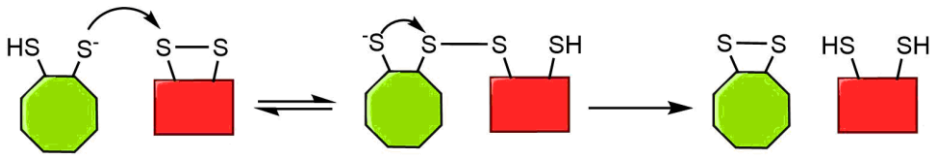

Fig. 4 – Thiol-disulfide exchange reaction between an oxidoreductase (thiolate form) and a disulfide.

There are other pathways for the exchange of thiol-disulfides. In cells, these exchanges can be performed by catalyzation by a class of enzymes named oxidoreductases. The typical enzyme of this group is protein disulfide isomerase. This protein can catalyze thiol-disulfide exchange reaction in a wide range of proteins, peptides, and low molecular thiols and disulfides[88]. The activity of this enzyme depends on a pair of cysteines present on its motif. Depending on the redox environment and the nature of the substrate, the isomerase can catalyze the formation, reduction, or isomerization of disulfide bonds. If the active site is oxidized, the enzyme oxidizes protein thiols, otherwise the thiolate of

the enzyme attacks disulfide bonds. The overall result of this reaction is the oxidation of the enzyme and the reduction of the initial disulfide (figure 4).

1.3 Disulfide bond formation in peptides

Disulfides in proteins play an important role in the maintenance of biological activity and conformational stability. Because of its importance, many studies have focused on the roles of disulfides as constraints to increase biological activity and as transient intermediates in protein folding. For these studies, it is crucial that the disulfide bond chemical synthesis is readily accessible. The chemical synthesis of these peptides, e.g. $Cys(Lys)_5Cys$ – bioreducible poly-L-lysine building block used in this project, containing one or more disulfide bonds, require as final step, the formation of disulfide bonds of cysteine residues. The general procedure to disulfide formation is by using a mild oxidant to form the desired product.

Among the conventional methods for the formation of disulfide bonds, the air oxidation in aqueous medium is one of the most common. Air oxidation usually requires a long-term synthesis, at basic or neutral pH, and a very diluted concentration of peptide or protein to be effective. Nevertheless, it has the advantage of producing a harmless reaction byproduct, H_2O. A variation to the air oxidation method is the thiol-disulfide interchange reaction, with a mixture of oxidized and reduced glutathione. Because the air oxidation and the mixed interchange reaction are slow processes, they produce thermodynamically controlled products, useful for protein synthesis. In contrast, stronger oxidizing agents like I_2 and $K_3Fe(CN)_6$, that produce kinetically controlled products, are often used for simple peptides containing only one or two disulfide bonds. These strong agents are such powerful oxidants that the oxidations are usually performed cautiously to prevent overoxidation. They have the advantage of being applicable in the acidic range, but the byproducts produced by this oxidation require purification. Since the pH should be around the basic region, for air oxidation or mixed disulfides, the basic and hydrophobic peptides tend to aggregate and precipitate from solution at or near the isoelectric points.

It would be highly desirable to devise a new method for the disulfide formation that is similar in mildness to air oxidation, but can be conducted under acidic or neutral conditions with no harmful byproducts at an efficient rate. An oxidation process that appears to satisfy all these requirements is the use of dimethyl sulfoxide (DMSO)[89-91]. This chemical in known to be a mild oxidizing agent for simple organic thiols, producing

H_2O and dimethyl sulfide as harmless byproducts. It is miscible with water at all concentrations[89], and thus a high concentration of DMSO could be envisioned to affect the desirable rate of reactions. Furthermore, oxidation by DMSO could also be designed to be performed at acidic to neutral pH range, to overcome the limitation of the conventional methods of oxidation. This kind of synthesis has been reported to synthesize bioreducible polymers by disulfide bond between cysteine-containing peptides[21, 92].

1.3.1 Mechanism of disulfide formation

The general mechanism of disulfide formation by DMSO has been determined by Wallach and Mahon, and a simplified overall reaction can be represented by the following equation 3.

$$RSH + (CH_3)_2SO \longrightarrow \underset{\text{rate determining step}}{[(CH_3)_2S(OH)SR]} \xrightarrow{+RSH} RSSR + CH_3SCH_3 + H_2O \quad (3)$$

The stoichiometry for the reaction requires 2 mol of a thiol and 1 mol of DMSO, and the reaction shows a second order kinetics[89]. Besides, the reaction is strongly catalyzed by primary and secondary amines and weakly catalyzed by acids. The rate-determining step is the formation of the unstable adduct that is rapidly captured by another free thiol to give the disulfide. For this kind of reaction, a pH dependence may be found for cysteines, with free α-amino group, while protected amino groups do not show that kind of dependence. The pH-dependent kinetics could be rationalized by the rate acceleration of disulfide formation at neutral pH by DMSO, when the cysteine is at the amino terminus with an unprotected α-amino group. It is plausible that the observed acceleration rate for peptides containing a free amino terminal cysteine is due to assistance of the free amino group as a general base, and its ability in the steering of the DMSO to the thiol of the cysteine. Such regiospecificity is due to the weak interaction between the partially negatively charged sulfoxide and the partially positively charged unprotonated α-amine, that facilitates the formation of the unstable adduct (figure 5). This kind of assistance will not be possible when the free amino group is protected, protonated (at acidic pH) or one or more amino acids residues away.

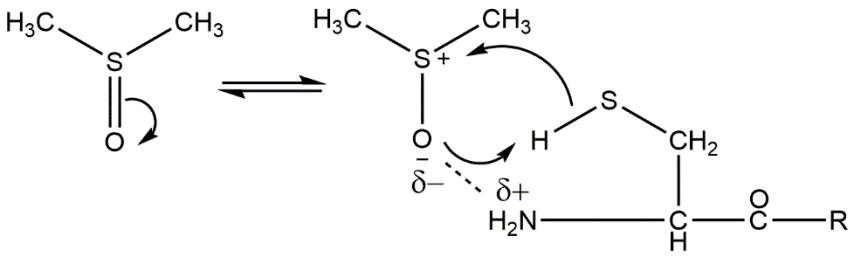

Fig. 5 - Representation of the regiosteering of the DMSO to the thiol of the amino terminal cysteine, this is the rate determining step[89].

1.4 Microfluidics

1.4.1 Outline

The microfluidic technique may be defined as the science and technology of systems that process or manipulate small volumes of fluids (typically 10^{-9} to 10^{-12} L) using channels with dimensions of tens of hundreds of micrometers. The first application of microfluidics has been in chemical analysis, for which they offer several useful abilities such as small quantities of sample, and high resolution and sensitivity of separations and detections. Also, this technology is cost-effective, has short times for analysis, and small footprints for the analytical devices[93]. Microfluidics exploits both its most obvious characteristic – small size – and less obvious characteristic of fluids in microchannels, such as laminar flow.

Some of the initial work on microfluidics used silicon and glass, but these materials have been displaced by plastics. Silicon is expensive and opaque to visible light, hence it cannot be used in optical methods of detection. It is easier to fabricate the components required for these systems in elastomers than in rigid materials. Neither glass nor silicon has all the properties required for work with biological systems.

Thus, microfluidic devices have not developed as clones of silicon microelectronic devices. Instead, much of the exploratory work on microfluidic chips have been carried out in an optically transparent, soft elastomer polymer – poly(dimethylsiloxane), or PDMS – which properties are different from the silicon[94-95]. The ease with which new concepts can be tested in PDMS, and its ability to support certain useful components, such as pneumatic valves, has made it the key material for research. Silicon and other microelectronic materials, like steel or glass, are indispensable to the development of microfluidics with the purpose of building specialized systems that require chemical or thermal stability. For example, PDMS chips cannot be used in organic synthesis involving organic solvents since the microchannels can be partially or totally destroyed.

1.4.2 Microfluidic Environment

A microfluidic chip must have a series of components that allow it to fulfill its purposes, namely as a method to: (i) introduce reagents and samples, probably as fluids; (ii) move, combine and mix those fluids around the chip, and (iii) detect or purify chemical components. Two contributions have been the development of soft lithography in PDMS as a method to fabricate new devices[96], and the development of pneumatically activated valves, mixers and pumps based on soft-lithographic procedures[97]. This lithography procedure is much shorter in time than the silicone-based procedure, with typically 2 days from design to working device for the former compared with one month or more for the latter[98].

The use of microfluidics has enabled the comprehension of certain fundamental differences between the properties of fluids moving through large channels and fluids moving through micrometer channels[99]. On large scales, fluids mix convectively, similarly with the mixing of milk when is swirled into coffee, or with smoke leaving the chimney. In microsystems, the opposite is true as fluids do not mix convectively, because when two fluid streams come together they flow in parallel, without turbulence. The only mixing that occurs is the result of the diffusion of molecules at the interface of the two fluids. When mixing is required, components can be made inside the channels that foment that.

The two most used methods to flow fluids around the microfluidic chip are hydrodynamic and electro-osmotic flows. The hydrodynamic flow works by pumping the fluid into the microchannels. When an ion-containing fluid is placed in a microchannel that has fixed charges on its surface and an electrical potential is applied along the channel, the fluid moves as a plug, rather than a parabolic profile characteristic of hydrodynamic flow. The advantage of using electro-osmotic flow is that it minimizes the broadening of plugs of samples that occur in many pressure-driven systems, and allows very high-resolution separations of ionic species.

1.4.3 Mixing Principles

Commonly, the laws that describe the flow at the macroscale also apply to the microscale. Nevertheless, the miniaturization process confers additional features that can be explored to perform processes otherwise not possible. Microfluidic devices are not the miniature of their macroscale counterpart, because many physical properties do not scale linearly from large to small devices, such as surface area-to-volume ratio,

surface tension and diffusion. The omnipresence of laminar flow is also an important feature because viscous forces dominate in the microchannel. It must be noted that rather than designing a microfluidic mixer as just a scale-down copy of a macroscale mixing device, one should design it in ways that leverage the physical characteristics of the mixing in a confined space.

Reynolds Number and Diffusion

Fluid flow is generally categorized into two flow regimes: laminar and turbulent. Laminar flow is characterized by smooth and constant flow, whereas turbulent flow is characterized by vortices and flow fluctuations. Physically, the two regimes differ in terms of the relative importance of viscous and inertial forces. The relative importance of these two types of forces for a given flow condition is given by the Reynolds number (Re):

$$R_e = \frac{\rho u D_h}{\mu} \tag{4}$$

where ρ and μ are the fluid density and viscosity, respectively; u is the velocity of fluid and D_h is the hydraulic diameter. The hydraulic diameter of the channel is a characteristic number that depends on the cross-sectional geometry of the channel, and is given by:

$$D_h = \frac{4A}{P_{wet}} \tag{5}$$

where A and P_{wet} are the cross-sectional area and the wetted perimeter of the channel, respectively.

At low R_e, the viscous effects dominate inertial effects and a completely laminar flow occurs. In the laminar flow system, the fluid streams flow parallel to each other and the velocity at any location within the fluid stream is invariant with time when boundary conditions are constant. This implies that mass transfer only occurs in the direction of the flow, and mixing can be achieved by molecular diffusion[100]. By contrast, at high Re the opposite is observed. The flow is dominated by inertia and characterized by turbulent flow. In a turbulent flow, the fluid exhibits motion that is random in both space and time, and there is mass transfer in all directions[101], (figure 6.a). The transition Re is generally expected to be in the range of 1.500 and 2.500 for most situations. For microfluidic systems, Re is typically smaller than 100 and the flow is considered essentially laminar (figure 6.b).

In an environment where the flow is strictly laminar, mixing is largely dominated by passive molecular diffusion. Diffusion may be defined as the process of spreading molecules from a zone of higher concentration to one of lower concentration by Brownian motion, which results in the gradual mixing of material.

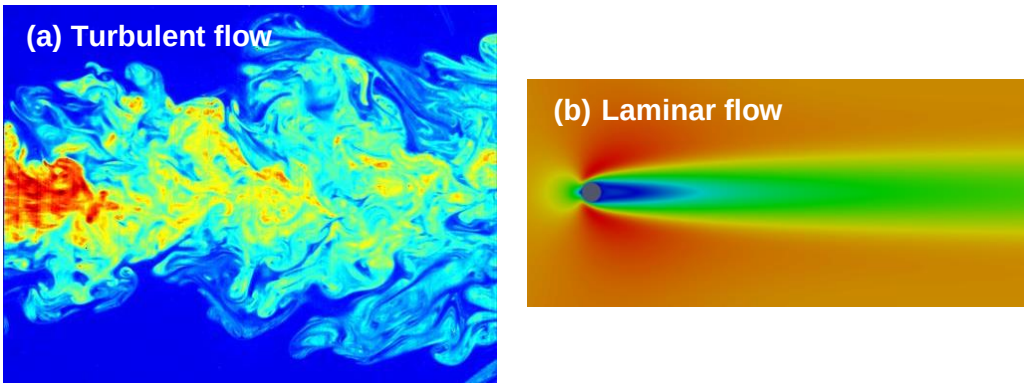

Fig. 6 - Images of different flow patterns. (a) Laminar flow with low Re; (b) Turbulent flow with high Re.

Mixing in the Microfluidic Devices

At a macroscale level, mixing is achieved by turbulent flow, which makes possible the segregation of the fluid in small domains, thereby decreasing the mixing path. As discussed, R_e is small for microfluidic systems, implying that hydrodynamic instability does not develop; so the flow cannot be turbulent. Owing to this limitation, mixing in microfluidic devices is generally achieved by taking advantage of the relevant small length, which dramatically increases the effect of diffusion.

Micromixers are generally design with channel geometries that decrease the mixing path and increase contact surface area. Micromixers are generally classified as being active or passive. Active micromixers use external energy input to introduce perturbations that stir and perturb the fluid for accelerating the mixing process. The type of external input employed can be further categorized as pressure field-driven[102], ultrasound-driven[103], temperature-driven[104] or magneto-hydrodynamic[105]. Generally, active micromixers have higher mixer efficiency[106]. However, the implementation of these kind of peripheral devices for the external power source into the microdevice, and the complex and expensive fabrication process, limit the usage of such devices in practical applications. In addition, conditions such as high ultrasound waves or high temperature gradients may damage the biological samples. Therefore, active mixers are not a popular choice to study biological systems[107].

Passive mixing devices rely entirely on fluid pumping energy and use special channel design and structure in a way that minimizes flow length and maximizes contact surface area. These are more convenient to fabricate, less expensive and can be easily integrated into more complex devices. This is achieved by splitting the fluid stream using serial or parallel lamination[108], by hydrodynamically focusing mixing streams[109], or by introducing ribs or grooves designed on the channel walls, called chaotic advection method[110].

Passive Micromixers

These devices are designed with a specific geometry that increases surface area and decreases the diffusion path. The modified flow pattern is characterized by a shorter diffusion path that improves the mixing velocity. As seen before, there are many categories of passive mixers, but, in this work, the main emphasis will be on the focusing-enhanced micromixers.

Flow Focusing

The basic design for hydrodynamic focusing is a long microchannel with three inlets - the point of entry of reagents - and one outlet - the point of exit of any possible products (figure 7). In hydrodynamic focusing, a central sample solution (supplied from the middle inlet) flows within the sheath of outer fluids (supplied from the side inlets), which constrain laterally the inner sample flow to achieve a smaller stream and thinner lamination width. The extent of the width decrease depends of the volumetric flow rate ratio between the sample flow and sheath flows. The greater the flow rate difference, the greater the degree of width reduction. The advantage of hydrodynamically focusing the central stream is that by doing so, the mixing – by diffusion – will be faster. Notably, the position of the focused stream is a function of the relative flow rate ratio of the three inlets, so it is possible to direct the stream to a specific outlet, in those cases where there is more than one, by changing the relative flow rate of the two side streams[111].

The relative flow rates of the three inlets are generally controlled by pressure sources or pumps, already mentioned. The analysis and predictions of the focused stream width is based on a simple model on mass conservation principles. The 2D focused stream width is computed under these simplified assumptions:

i. Flow in the microchannel is steady and laminar;
ii. Fluids are Newtonian;
iii. Fluids have the same density in the four channels;
iv. Fluids flow in a rectangular microchannel;
v. The four channels have the same height.

According to the mass conservation principle, the volume of liquid sample that passes through the inlet channel (Q_2) must match the volume of the focused stream:

$$Q_2 = v_2 w_2 h = v_f w_f h = Q_f \quad (6)$$

Leading to:

$$w_f = \frac{Q_2}{v_f h} \quad (7)$$

where w_2 and w_f represent the width of the central stream and focused stream, respectively. Q_2 and Q_f are the volumetric flow rates of the central inlet channel and the focused stream. h is the height of the channel, and v_2 and v_f are the average velocity of the flow in the central inlet channel and of the focused stream. It can also be concluded that the amount of fluid passing the outlet channel must be equal to the total amount of fluid supplied from the three inlets:

$$Q_c = w_c v_c h = Q_1 + Q_2 + Q_3 \quad (8)$$

$$w_c = \frac{Q_1 + Q_2 + Q_3}{v_c h} \quad (9)$$

where Q_1 and Q_3 are the volumetric flow rates for the two lateral channels, and v_o and w_o are the average velocities of the flow and width of the mixing channel, respectively. When combining (4) and (7), assuming v_c and v_f have the same values, it is possible to obtain the relationship between the width of the focused stream and volumetric flow rate of the inlets:

$$\frac{w_f}{w_c} = \frac{Q_2}{Q_1 + Q_2 + Q_3} \tag{10}$$

This equation provides a simple guideline for predicting the focused stream width. However, it does not reflect the effect of other factors such as device structure, channel surface, and fluidic property, which could affect the focusing process.

$$Q_{ratio} = \frac{Q_1 + Q_3}{Q_2} \tag{11}$$

$$Q_{Total} = Q_1 + Q_2 + Q_3 \tag{12}$$

The ratio of volumetric flow rates, equation 11, and the total flow rate, equation 12, can also be used to describe the flow system, and be used to characterize and predict the width of the focused stream.

Typically, focusing-enhanced micromixers focus the sample flow only in the horizontal dimension. Different authors have proposed microfabricated devices capable of focusing the sample vertically and horizontally[112-113]. Such devices are referred as 3D hydrodynamic focusing devices because they add a new dimension to the traditional 2D. The problem with these devices is that they have to be prepared by multistep photolithography, leading to an increase in fabrication cost.

It is also important to refer that the velocity profile inside a microfluidic channel in laminar flow is typically of the Poiseuille type, i.e. a parabolic shape where the velocity is maximum in the center of the channels, and zero at the walls, due to the no-slip boundary condition (figure 8.a). This slower velocity near the walls leads to a higher dispersion or enlargement of the focused stream near the surface, resulting in a concave shape[114] (figure 8.b). Hence there is a wider distribution of mixing times, which can limit slightly time resolution.

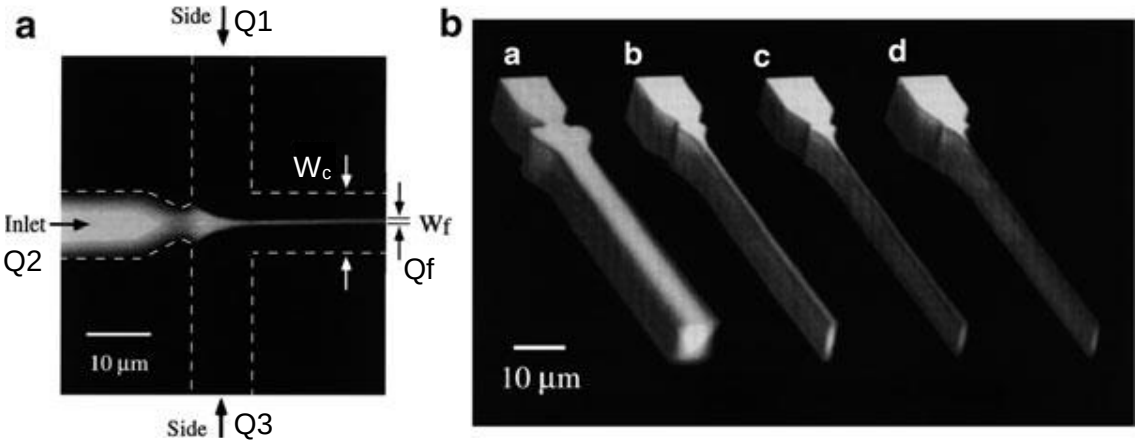

Fig. 7 - (a) Focusing enhanced mixer. (b) Effect of the ratio of the side pressure to the central pressure on the width of the focused stream: (a) 0.5, (b) 1.0, (c) 1.1, and (d) 1.2. Adapted from [115].

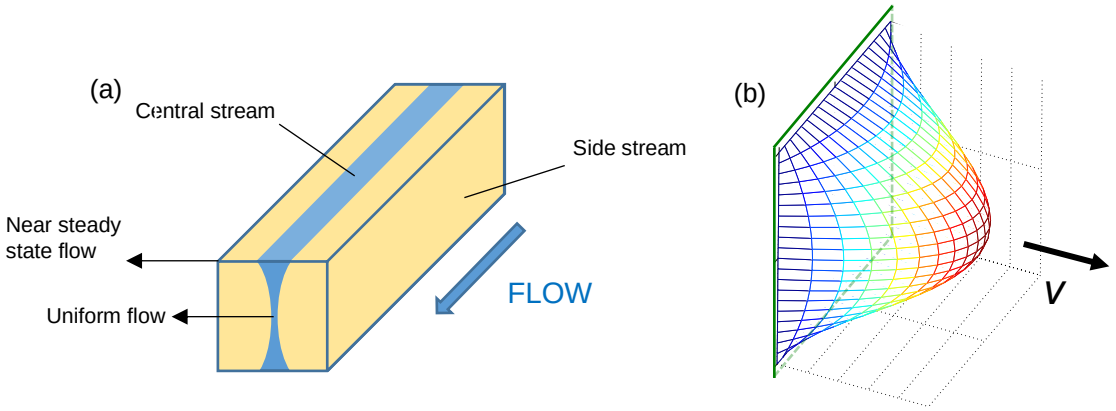

Fig. 8 – (a) The velocity profile inside the channel is of the Poiseuille flow type, where the velocity is maximum in the center of the channel and zero at the walls (no slip condition). This slower velocity near the walls typically leads to dispersion and/or enlargement of the focused stream, resulting in a concave profile (b).

1.5 Scope and aim of this work

Gene delivery efficiency depends significantly on the delivery system chosen. This system has to be able to withstand or surpass many biological barriers, and safely deliver the genetic cargo inside the cells. Many delivery systems can be adopted for this purpose. The system described in this work is based on polymeric colloidal carriers for DNA.

In this project, our aim is to produce and characterize bioreducible polyplexes. The bioreducibility property makes the polyplex sensitive to the redox environment of cytosol, resulting in degradation of the polymer. This property tackles one of the major barriers of nonviral gene delivery, which is the unloading of the gene content. Also, traditional bulk self-assembly methods do not allow a fine control of size and polydispersity in the production of these nanoparticle. Thus, we propose the application of the microfluidic technique that allows a better control over the process of mixing the different components and hence on the properties of the polyplexes.

To achieve our general goals, the following steps will be undertaken: (1) synthesis of the bioreducible polymer and plasmid DNA; (2) bulk preparation and characterization of bioreducible polyplexes; (2) study of the effect of physiological buffer and ionic strength on their colloidal stability; (3) comparison of the physicochemical properties of bioreducible polyplexes with non bioreducible polyplexes; (4) study of the effect of microfluidics on the structure of polyplexes.

2. Materials and Methods

2.1 Materials and reagents

Polyplex preparation

Poly-L-lysine 0.1% (w/v) H_2O wt. 125 000-300 000, and calf thymus DNA (Type I, fibers) were purchased at Sigma. HEPES powder (99%) was acquired at Acros Organics. NaCl (98%) was acquired at Sigma. Plasmid DNA was obtained by bacteria propagation (Appendix I). Glutathione (pharmaceutical second standard) was purchased at Sigma. The DNA solution concentration was measured by NanoDrop™ 2000c spectrophotometer. The microscope used for the microfluidic experiments was a Nikon Eclipse Ti, with a Plain Fluor 20x/0.45 objective, and a Lambda LS 145W Xenon bulb as fluorescence excitation source. The camera was a Andor™ Neo.

Bioreducible poly-L-lysine

Bioreducible poly-L-lysine monomer (88.9%) was purchased at POP-UP, a service unit of peptide synthesis provided by the Faculty of Sciences of the University of Porto. DMSO (99.5%) and PBS tablets were purchased at Sigma. The Amicon 10 000 MW centrifuging filters were acquired at Merck.

2.2 Charge ratio calculation

Throughout the work, the polymer/DNA charge ratio, *CR*, is defined according to

$$CR = \frac{C^+}{C^-} \tag{13}$$

where C^+ is the molar concentration of positive charge present in the protonated amine groups of lysine and C^- is molar concentration of negative charge due to the phosphate groups of DNA.

The negative charge of the phosphate groups of DNA present in solution were determined by

$$C_{-} = \frac{C_{DNA}}{MW_{bp}} * 2 \quad (14)$$

where MW_{bp} = 618 g·mol^{-1} and C_{DNA} is the concentration of DNA in the solution in g·L^{-1}. The MW_{bp} does not take into consideration the sodium counter ions because their mass contribution is not measured when using nanodrop to determine DNA concentration of the solution. The factor of 2 is due to the two negative charges per base pair (bp) of DNA.

The positive charge of the amino groups of PLL present in solution were determined by

$$C_{+} = \frac{C_{PLL}}{MW_{PLL}} \quad (15)$$

where MW_{PLL} = 129.18 g·mol^{-1} and C_{PLL} is the concentration of PLL in the solution in g·L^{-1}. The MW_{PLL} does not take into consideration the bromide counter-ions because the PLL solution, bought from Sigma, only considers PLL mass contribution. There is only one charge for which lysine, so the molar concentration of positive charges is equal to the molar concentration of poly-L-lysine.

The positive charge of the amino groups of bPLL present in solution were determined by

$$C_{+} = \frac{C_{bPLL}}{MW_{bPLL}} * 5 \quad (16)$$

where MW_{bPLL} = 906.47 g·mol^{-1} and C_{bPLL} is the mass concentration of the solution. The MW_{bPLL} was obtained by mass spectroscopy. The factor of 5 is due to the five positive charges of each building block.

All stock solutions of DNA, PLL and bPLL, used to prepare all samples, had a concentration of 1.00 g·L^{-1}.

2.3 Bulk preparation

All polyplex systems were prepared similarly, following the procedures stated below. These systems are poly-L-lysine with calf thymus DNA (PLL-cfDNA), poly-L-lysine with plasmid DNA (PLL-pDNA), bioreducible poly-L-lysine with plasmid DNA (bPLL-pDNA), and monomeric bioreducible poly-L-lysine CK_5C-pDNA.

2.3.1 Poly-L-lysine and DNA system preparation in water

The PLL-DNA complexes were prepared as follows: a fixed volume of PLL (0.500 mL) of variable concentration was added to a solution containing DNA (0.500 mL) on a magnetic mixer. The final concentration of DNA was 11.5 $\mu g \cdot mL^{-1}$ (0.0115 mg per sample). The samples were subsequently vortexed for 10 seconds at 1200 rpm and left for 30 min on a mixing board before measurements.

2.3.2 Poly-L-lysine and DNA system preparation in buffer

Buffer preparation

The following buffer solutions were prepared: 80 mM HEPES with 80, 120, 280, 400 and 600 mM of monovalent salt. In a falcon tube, a mass of 0.1906 mg of HEPES (99%) was dissolved in 10 mL of DI water. The pH was then adjusted to 7.4, normally 100 µL of 1 M NaOH. To complete the monovalent salt concentration, NaCl was added. To determine the quantity of NaCl to add, one needs to consider de sodium ions present from the pH adjustment, and the ionization of HEPES.

The concentration of Na^+, in this case, was 10 mM. At pH 7.4, the concentration of ionized HEPES was 35.4 mM. To prepare a buffer with 80 mM of monovalent salt, the quantity of NaCl to add was only 34.6 mM equivalent to 0.0215 g.

Addition of buffer after formation (Path I)

A stock solution of 80 mM HEPES and 80 mM monovalent salt at pH 7.4 was used to prepare the samples. A fixed volume of PLL solution (0.188 mL) was added to the DNA solution (0.188 mL) on a magnetic mixer. The final concentration of pDNA was 11.5 µg

mL^{-1}. The samples were subsequently vortexed for 10 seconds at 8000 rpm and left for 30 min on the mixing board. Finally, 0.125 mL of buffer was added to the polyplex solution. The solution was vortexed at 8000 rpm for 5 seconds and left to rest for 30 minutes before measurements.

The same procedure was applied to the other buffered samples.

Formation in buffer (Path II)

A stock solution of 80 Mm HEPES and 80 Mm monovalent salt at pH 7.4 was used to prepare the PLL and DNA solutions. To a fixed volume of PLL (0.188 mL) of variable concentration, 0.062 mL of buffer was added. The same was done for the DNA solution. Then, the PLL solution (0.250 mL) was added to the DNA solution (0.250 mL) on a magnetic mixer. The final concentration of DNA was 11.5 µg mL^{-1}. The samples were subsequently vortexed for 10 seconds at 8000 rpm and left to rest for 30 min before measurements.

Same procedure was applied to the other buffered samples.

2.3.3 Glutathione test

All polyplex systems were prepared similarly, following the procedures stated below. These systems are poly-L-lysine with plasmid DNA (PLL-pDNA), bioreducible poly-L-lysine with plasmid DNA (bPLL-pDNA), and monomeric bioreducible poly-L-lysine CK_5C-pDNA.

A stock solution of 208.6 mM GSH at pH 7.3 was used to prepare the samples. A fixed volume of polymer solution of variable concentration, was added to the pDNA solution on a magnetic mixer. The final concentration of pDNA was 11.5 µg mL^{-1} (0.00575 mg per sample). The samples were subsequently vortexed for 10 s at 1200 rpm and left for 30 min on the mixing board. Finally, it was added a determined volume of GSH to the polyplex solution, to a variable final concentration ranging from 10-40 mM. In table 1 are shown the volumes of reagents to prepare samples stated in this section. The DLS measurements were performed immediately afterwards, unless otherwise stated.

Table 1 – Volumes of polymer, DNA and GSH added to prepare samples for the study of the effect of glutathione on polyplexes.

Final concentration of GSH /mM	$V_{polymer}$ /mL	V_{DNA} /mL	V_{GSH} /mL
10	0.238	0.238	0.0240
20	0.226	0.226	0.0479
40	0.202	0.202	0.0959

2.4 Microfluidic preparation

2.4.1 Microfluidic device fabrication

PDMS microfluidic devices were fabricated by using a microfabrication protocol establish by the microfluidics group at INL and a Sylgard® 184 PDMS kit. The silicon master is prepared at the cleanroom with photolithography techniques. The silicon wafer with the requested design (figure 9.a) is then put into a Petri dish and covered with PDMS:crosslinker (10:1). The master is placed under vacuum for 40-60 min. This removes trapped air in the PDMS. The next step is the curing process which involves the hardening of the PDMS. For this, the master is maintained in an oven for 3 h at 65 ºC. After curing, the PDMS is cut around the channels, and then peeled from the master. A puncher is used to create the inlets and outlet. The PDMS stripes and a coverslip are washed with water and ethanol. The PDMS surface with the channels and the coverslip are then exposed to an oxygen plasma treatment. Finally, the exposed surfaces are gently pressed together. A solution of 1%(w/w) of F127 is slowly flown through the microchannels. This compound adheres to the channels walls making them hydrophilic.

2.4.2 Poly-L-lysine and plasmid DNA in water

For the flow visualization, the MF device was mounted on an inverted microscope stage (Nikon Eclipse Ti) with a s Point Fluor 20x/0.45 objective. Two programable syringe pumps were used to control the fluid flow rates independently. The setup is shown in figure 9.b. The device consists of three inlets and one outlet. The side inlets were connected to PLL and the mid inlet was connected to pDNA with fluorescein (11.7 μM). After the DNA stream has entered and the hydrodynamic focusing established, the products in the outlet stream are collected after 3-5 minutes to allow steady state, tracked by fluorescence microscopy. The magnitude of shear stresses applied to DNA was

controlled by altering the ratio of the flow rate (Q_R) in the side streams to the middle stream, see table 2.

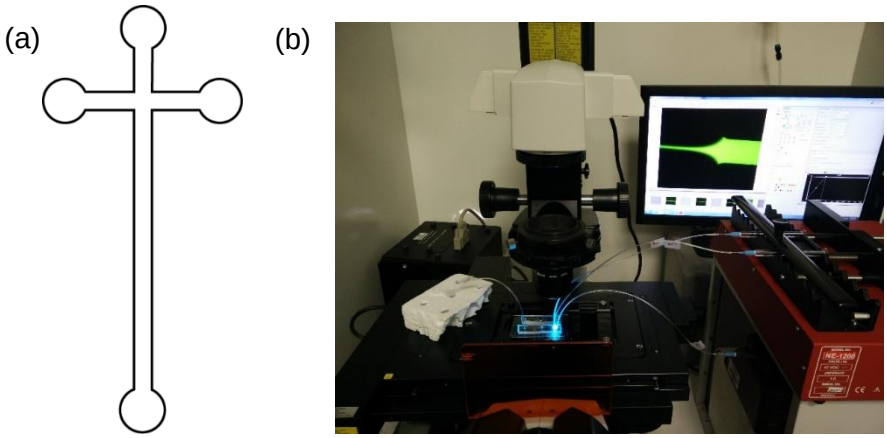

Fig. 9 – (a) Representation of the design of the channels on the microchip; (b) microfluidic setup used to prepare PLL/pDNA polyplexes.

Applying equation 17, one can determine the initial concentrations of PLL and pDNA to use for each flow rate ratio for charge ratio 7. The concentrations can be found in table 3.

$$[PLL]_{seringe} = \frac{Q_i}{2Q_s} CR[pDNA]_{seringe} \quad (17)$$

Table 2 – Selected flow ratios to prepare the polyplexes. Flow rates Qi and Qs were determined by applying equations 11 and 12 (Q2=Qi, DNA inlet, and Q1=Q3=Qs, PLL inlet).

Q_{total}	Q_{ratio}	Q_i /µL.min^{-1}	Q_s /µL.min^{-1}
11	**2**	3.667	3.667
	10	1.000	5.000
	30	0.355	5.323
	50	0.216	5.392
55	**2**	18.333	18.333
	10	5.000	25.000
	30	1.774	26.613
	50	1.078	26.961

Table 3 – Determined concentrations of pDNA, fluorescein and PLL, for charge ratio 7, for microfluidic-assisted preparation of polyplexes.

Q_{ratio}	$[pDNA]_{syringe}$ /µg.mL^{-1}	[Fluorescein] /µM	$[PLL]_{syringe}$ /µg.mL^{-1}
2	23.0	11.7	33.4
10	115		33.4
30	345		33.4
50	575		33.4

2.5 Synthesis of bioreducible polymer

Procedure

The bioreducible poly-L-lysine was synthesized by oxidative polycondensation as described by many authors[21, 89, 92, 116]. Briefly, 61.7 mg of CKKKKKC was dissolved in 1.420 mL phosphate buffered saline (PBS) and 0.426 mL DMSO. The reaction was carried out at room temperature for 5 days. The bPLL was then purified by centrifuging using a centrifugal filter with a 10 000 MW cut-off. The purified bPLL was resuspended and lyophilized. A total of 9.1 mg of bPLL were synthesized. A scheme of the synthesis is shown in figure 10.

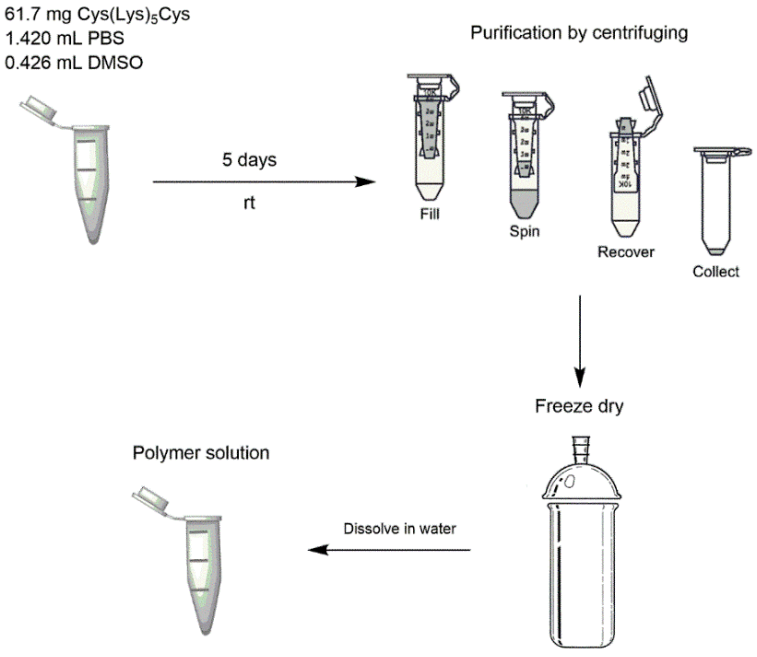

Fig. 10 - Scheme of the polycondensation of CK_5C and purification process.

2.6 Characterization techniques

2.6.1 Dynamic light scattering

The two main characteristics of colloids that are used by DLS are the Tyndall effect (scattering) and Brownian motion. Among other factors, the intensity of scattered light depends on the scattering angle (θ) and the observation time (t). This leads to the development of DLS in which the time dependence of the intensity is measured[117].

This time dependence of scattering intensity arises from the fact that colloidal particles are not static in suspension, rather they move in a random fashion by the Brownian motion effect. When a monochromatic radiation goes through a collection of particles, it scatters due to physical interaction. Since particles are moving in space, the distance travelled by the scattered light from the particle to the detector differs with time[117-118].

In DLS, the characteristic time of fluctuations in the scattered intensity is measured, and it depends on the diffusion coefficient of the particles undergoing Brownian motion. Larger particles have inherently slower Brownian motions, diffusing slower than smaller particles[119]. In terms of scattered light, large agglomerates with slow Brownian motion will have slower intensity fluctuations than the smaller particles with high Brownian motion, thus allowing the system to correlate slow intensity fluctuations with large size particle (figure 11). Quantitative information regarding the time scale of these fluctuations is obtained by a signal processing technique known as autocorrelation[120]. The essence of this technique lies in analyzing the correlation function to determine the particle size information. For a particle suspension undergoing Brownian motion, the autocorrelation function decays exponentially with the delay of time τ, and is given as,

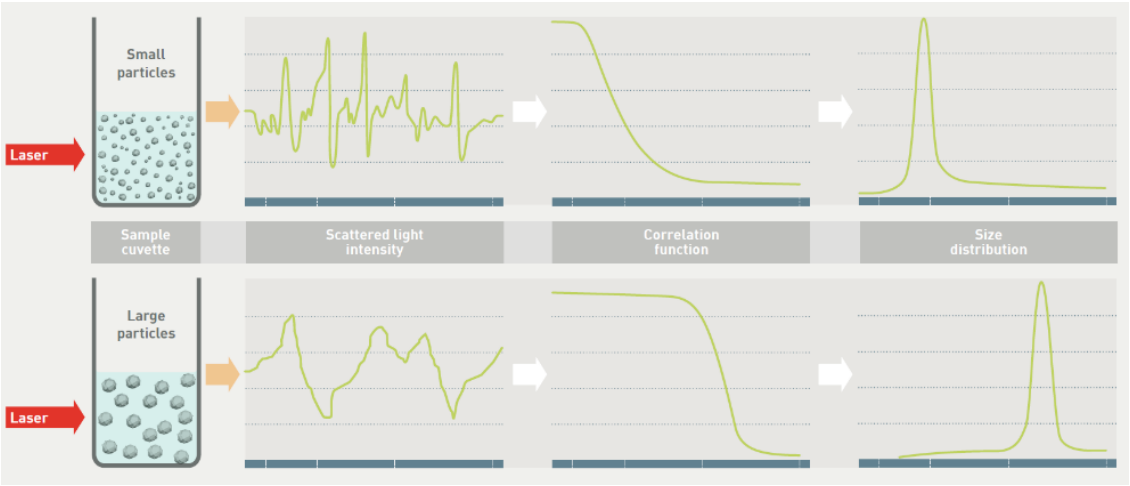

Fig. 11 – Schematic illustration of a Dynamic Light Scattering measurement, highlighting the differences between small and large particle signals. Adapted from [119].

where A is the amplitude of the correlation function, B is the baseline, *D* is the translational diffusion coefficient of the particles, and *q* is the magnitude of the scattering vector. The hydrodynamic diameter, d_H, is obtained from the translational diffusion coefficient, D, using the Stokes-Einstein relationship:

$$d_H = \frac{k_B T}{3\pi\mu D} \tag{19}$$

where d_H is the hydrodynamic diameter, k_B is Boltzmann's constant, *T* is the absolute temperature, *μ* is the viscosity and *D*, already mentioned above[118]. The diffusion coefficient is acquired by fitting the correlation function with a suitable algorithm, resulting in mean size, z-average, and polydispersity index values.

In many practical systems, there exists a distribution of particle sizes and scattering from such polydisperse population of particles leads to deviation from the expected single exponential decay of the correlation function. For a polydisperse distribution of diffusion coefficient, equation 18 can be written as a sum of exponentials, weighted by their amplitudes. For a continuous distribution, each *D* contributes its own exponential, and the observed correlation function can be represented as an integral weighted by the distribution function, which can be expressed as

$$g^1(\tau) = \int_0^\infty G(\Gamma) \exp(-\Gamma\tau)\, d\Gamma \tag{20}$$

where $\Gamma = Dq^2$ is the decay constant for a given size. The distribution G(Γ) represents the relative intensity of light being scattered with decay constant Γ and will depend on the volume fraction and size of scatterers. The occurrence of measurement noise, baseline drifts, dust interference and the exponential function under the integral all put together make this equation ill-conditioned.

There are different ways to extract the diffusion coefficient (particle size) information from the measured data in polydisperse samples. One approach is to calculate the mean and variance of the distribution. Under this approach, the method of cumulants [121] has been widely used to analyze narrow polydispersity in DLS experiments and is the only method that is currently recommended[122].

In this method used in DLS analysis, the term exp*(-Γτ)* in equation 20 can be expanded about a mean value $\bar{\Gamma}$ such that,

$$\begin{aligned} exp(-\Gamma\tau) &= exp(-\bar{\Gamma}\tau)\times \exp(-[\Gamma-\bar{\Gamma}]\tau) \\ &= \exp(-\bar{\Gamma}\tau)\times[1-(\Gamma-\bar{\Gamma})\tau+(\Gamma-\bar{\Gamma})^2\frac{\tau^2}{2!}+\cdots] \end{aligned} \quad (21)$$

The relative magnitude of contributions of the term in the bracket falls of rapidly with increasing order. When G(Γ) is relatively narrow, terms with order 3 and above can be neglected [117, 120], substituting equation 21 in equation 20,

$$\begin{aligned} g^1(\tau) = e^{(-\bar{\Gamma}\tau)}[&\int_0^\infty G(\Gamma)d\Gamma \\ &-\tau\int_0^\infty G(\Gamma)\Gamma d\Gamma+\bar{\Gamma}\tau\int_0^\infty G(\Gamma)d\Gamma+\frac{\tau^2}{2}\int_0^\infty(\Gamma-\bar{\Gamma})^2G(\Gamma)d\Gamma] \end{aligned} \quad (22)$$

By definition, the mean ($\bar{\Gamma}$) and variance (μ_2) of the distribution G(Γ) are

$$\bar{\Gamma} = \int_0^\infty G(\Gamma)\Gamma d\Gamma \quad (23)$$

$$\mu_2 = \int_0^\infty G(\Gamma)(\Gamma-\bar{\Gamma})^2 d\Gamma \quad (24)$$

Thus, equation 22 becomes,

$$g^1(\tau) = e^{-\bar{\Gamma}\tau}[1+\frac{\mu_2\tau^2}{2}] \quad (25)$$

When $\mu_2\tau^2 \ll 1$, equation 25 can be simplified,

$$g^1(\tau) = e^{-\bar{\Gamma}\tau+\frac{\mu_2\tau^2}{2}} \quad (26)$$

Taking the natural logarithm, adding the background B in equation 26 gives

$$\ln[g^1(\tau)] = lnB - \bar{\Gamma}\tau + \frac{\mu_2\tau^2}{2} \quad (27)$$

This equation is the one that is traditionally used in cumulants analysis. By fitting $\ln[g^1(\tau)]$ to quadratic in τ, one can obtain the mean, $\bar{\Gamma}$ and the variance, μ_2. The ratio of variance to the square of the mean is a measure of the polydispersity of the diffusion coefficient and this is very often represented as a polydispersity index, equation 28.

$$PI = \frac{\mu_2}{\bar{\Gamma}^2} \quad (28)$$

Finally, the mean $\bar{\Gamma}$ is then used to determine the diffusion coefficient,

$$\bar{\Gamma} = Dq^2 \quad (29)$$

where q is a constant associated with the angle of the detector.

2.6.2 Electrophoretic mobility

Zeta potential is a physical parameter which is related to the surface charge of any particle in suspension. It helps predict the long-term colloidal stability. When a charged particle is dispersed, and adsorbed double layer develops on its surface. The inner layer consists of ions/molecules of the opposite charge to that of the particle – Stern layer. The outer layer, the electrostatic effects due to the surface charge on the particle decreases, making it dynamic – diffuse layer.

Due to the electrostatic field of the charged nanoparticles, a diffuse layer consisting of both same and opposite charged ions/molecules grow beyond the Stern layer. The Stern layer along with the diffuse layer forms the electrical double layer – EDL[123] (figure 12). The composition of the diffuse layer may vary depending on pH, ionic strength, concentration etc. When an electric field is applied to such dispersion, the charged particles move towards the opposite electrode. Within the diffuse layer there is a hypothetical plane which acts as the interface between the moving particle and the dispersant around it while the electric field is applied. This plane is the characteristic slipping/shear plane and ZP is the potential at this particle-fluid interface[118].

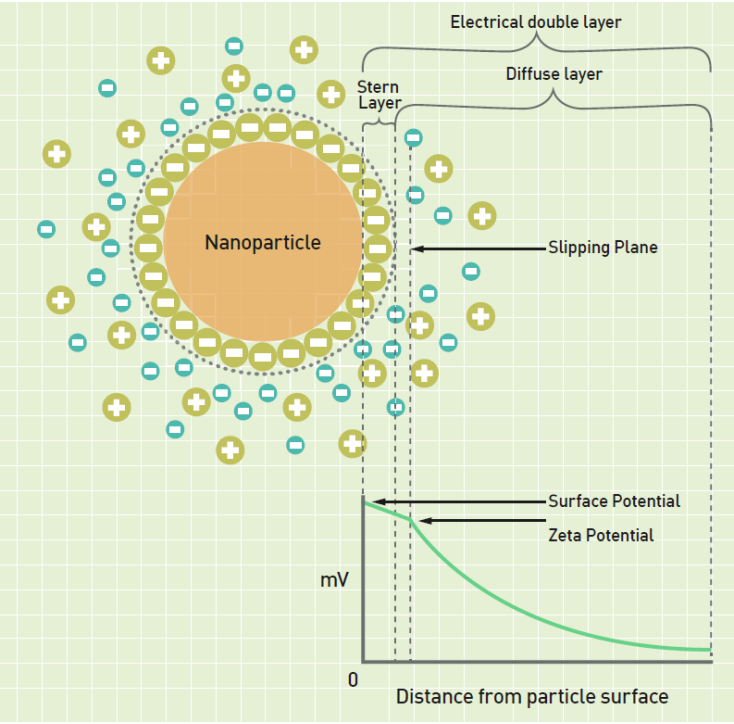

Fig. 12 –Representation showing the electric double layer on a positively charged particle. Immediately on top of the particle surface is a strongly adhered layer (Stern layer) comprising of ions of opposite charge i.e. negative ions. Beyond this layer, a diffuse layer is created consisting of both negative and positive ions. During electrophoresis, the particle with adsorbed EDL moves towards the electrodes i.e. positive electrode in this case, with the slipping plane becoming their interface between the mobile particles and dispersant. The ZP is the electrokinetic potential at this slipping plane. Adapted from [119].

Zeta potential cannot be measured directly and is deduced from electrophoretic mobility of charged particles under an applied electric field. The electrophoretic mobility - μ_e - of the particles is first calculated as in (equation 30)

$$\mu_e = \frac{V}{E} \tag{30}$$

where V is particle velocity and E is electric field, both known quantities. The ZP is then calculated from the obtained μ_e by the Henry's equation (equation 31)

$$\mu_e = \frac{2\varepsilon_r \varepsilon_0 \xi f(K_a)}{3\eta} \tag{31}$$

Where ε_r is the permittivity of vacuum, ε_0 is the dielectric constant, ξ is the ZP, $f(K_a)$ is henry's function and η is the viscosity. When the thickness of EDL is much bigger than the particle itself due to smaller particles dispersed (≤100 nm)[118], the value $f(K_a)$ is taken as 1 and the Henry's equation simplifies to the Hückel equation (equation 32)

$$\mu_e = \frac{2\varepsilon_r \varepsilon_0 \xi}{3\eta} \tag{32}$$

The used method to determine the ZP of the particles described in this work was the electrophoretic light scattering. This is based on the fact that mobile particles scatter light in a different frequency than the original light source, and this frequency is proportional to the speed of particles. In instrument, the laser is split into two and one is used as reference while the other goes through the sample. The scattered light from the sample is combined with the reference beam to determine the shift. The magnitude of particle velocity is deduced from that shift. Then, ZP is measured through the equations listed previously.

ZP data is popular because it can relate to colloid stability. Guidelines classifying NP-dispersion with absolute ZP values of 0-10 mV, 10-20 mV, 20-30 mV, and ≥ 30 mV, as highly unstable, relatively stable, moderately stable and highly stable, respectively, are common[118, 124].

2.6.3 DLS and EM measurements

Bulk measurements procedure

The hydrodynamic radius and the zeta potential of the poly-L-lysine – DNA complexes were determined with a SZ-100 apparatus from Horiba (Japan). Samples were prepared as described in the general procedure. Dynamic light scattering measurements were carried out at 25 °C, at a detection angle of 173° and laser wavelength of 532 nm. Zeta potential measurements were carried out in an electrophoresis cell at 25 °C. The average values of size (z-average) and zeta potential were calculated with data obtained from five runs.

Microfluidic measurements procedure

The hydrodynamic radius and the zeta potential of the poly-L-lysine – DNA complexes were assessed by using a SZ-100 (Horiba, Ltd.). Samples were prepared as described previously. Dynamic light scattering measurements were carried out at 25°C, detection angle of 173° and 90º, and laser wavelength of 532 nm. The average values of size were calculated with a data obtained from five runs.

2.6.4 DLS Characterization

Throughout this work, dynamic light scattering (DLS) was the main characterization method.

The autocorrelation function can be directly fit with different models, such as single or double-exponential decay and cumulants fit, or go through an inverse Laplace transform into an intensity vs. size distribution. Although convenient, the inverse Laplace transform is ill-defined and is not suited for polydisperse samples were the different sizes are not well-separated. Using the inverse Laplace transform in such cases may result in over-

interpretation of the data. Throughout this work we chose the cumulants and double-exponential fits, since they are less model-dependent[125-127].

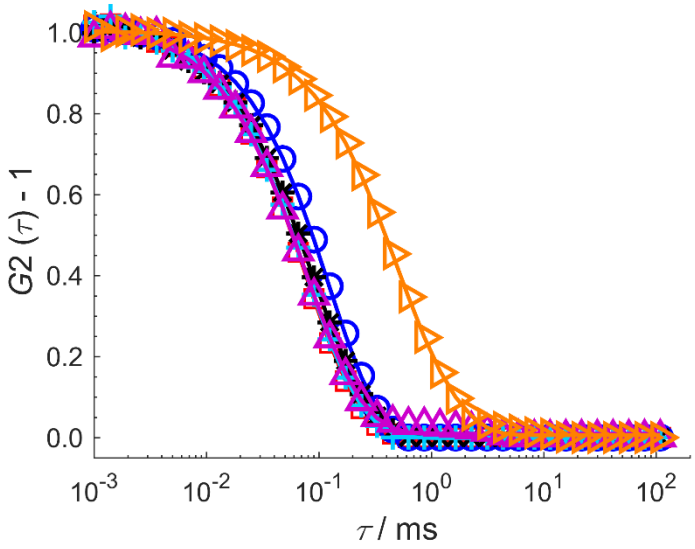

Fig. 13 – Normalized autocorrelation functions obtained from DLS measurements for bioreducible polyplex samples at five different charge ratios and fixed DNA concentration. Autocorrelation curves for (□) polyplexes at CR = 1.5, (○) polyplexes at CR = 2, (▷) polyplexes at CR = 2.1, (*) polyplexes at CR = 2.5, (+) polyplexes at CR = 5, (△) polyplexes at CR = 10.

This technique applies a series of physical concepts, reviewed in section 2.6.1, that results in a mean particle size (z-average) and polydispersity. For the whole bulk preparation of polyplexes, the z-average was determined by the equipment at 25ºC and at a scattering angle of 173º. Some of the autocorrelation curves obtained for bioreducible polyplexes in water at five different charge ratios are illustrated in figure 13.

For the microfluidic preparation, another approach was taken. DLS measurements were made for two scattering angles, 173º and 90º. Then, using a MATLAB routine was implemented that uses a non-linear cumulant analysis[120] to obtain a z-average (diameter) that is weighted by both 173º and 90º measurements. What this routine does is extracts the mean decay constants ($\bar{\Gamma}$) of all the measurements, at 173º and 90º, by fitting the DLS data with this new non-linear fit equation (equation 33).

$$g^{(2)}(\tau) = B + \beta\left\{\exp(-\bar{\Gamma}\tau)\left[1 + \frac{1}{2}\mu_2\tau^2\right]\right\} \quad (33)$$

An example of the application of this equation to fit the DLS data are show in figure 14.a.

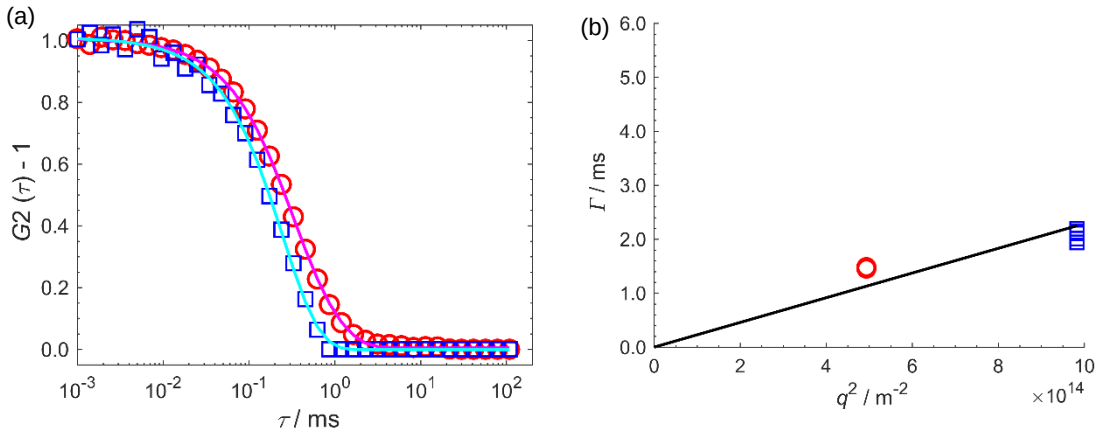

Fig. 14 – Application of the non-linear fit to DLS measurements, at 173º and 90º, of samples PLL-pDNA prepared by microfluidics (Q_R = 2 Q_T = 11 µL.min^{-1}). (a) Illustrative measurement at 173º (□) and 90º (○), (b) Application of equation 34 to extrapolate the diffusion coefficient weighted by both scattering angle data. This extrapolation was done by having five measurements at 173º (□) and five measurements at 90º (○).

After determining the mean decay constants for each measurement, the diffusion coefficient can be extrapolated from equation 34.

$$\bar{\Gamma} = Dq^2 \tag{34}$$

Where $q = (4\pi/\lambda)\sin(\theta/2)$, with θ corresponding to the scattering angle in radians. An example of this extrapolation can be seen in figure 14.b. This extrapolation was done by having five measurements at 173º (high q^2) and five measurements at 90º (low q^2), for each sample. After determining the coefficient, the Stokes-Einstein equation is applied, which results in an averaged hydrodynamic diameter.

3. Results and discussion

3.1 Outline

The basic aims of this project are (i) to provide information about the effect that the bioreducibility property has on the physicochemical properties of the complex and (ii) study the influence of the mixing process on the final structure of the polyplex. The chosen polymer for the production of these particles was poly-L-lysine (PLL), which is a biopolymer composed solely by the amino acid lysine (figure 15.a). This polymer at physiological pH has most of the amine residues protonated (pKa = 10.5[36]). In the case of the bioreducible poly-L-lysine (bPLL) used in this work, most of the features remain, with the difference that between every sequence of five lysines, there is a disulfide bond resulting from the oxidation of monomeric CK_5C. Cysteine-terminal groups allow the formation of disulfide bonds, which are cleavable in the reducing environment of the intracellular medium[81, 128] (figure 15.b). This property also has the advantage of being less toxic than regular polymers, due to the fast-intracellular degradation by cleavage of the disulfide bonds[129].

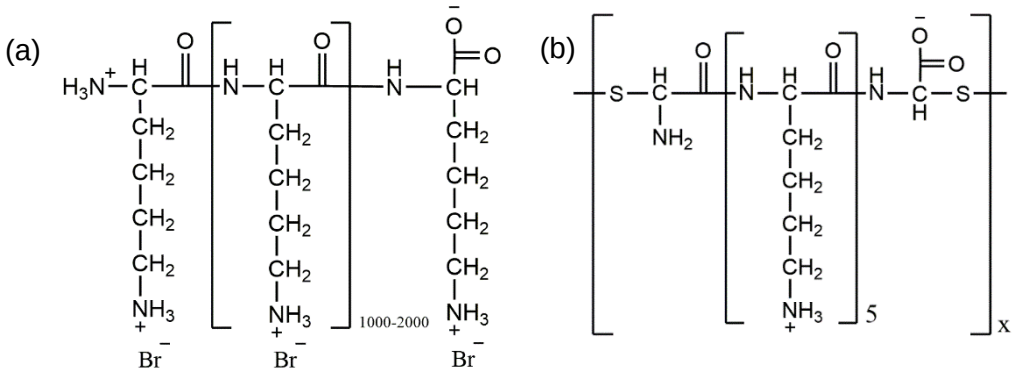

Fig. 15 – Polymer backbones used to prepare the polyplexes described in this work. (a) poly-L-lysine – PLL; (b) bioreducible poly-L-lysine – bPLL.

The structure and size of polyplexes can be influenced by various parameters, such as: (i) the properties of the constituting polymers (e.g. molecular weight and charge density), (ii) overall composition (e.g. mixing ratio between DNA and PLL), (iii) preparation method, and (iv) the properties of the medium in which polyplexes are present (e.g. pH and ionic strength). In order to achieve a greater control over the size and structure of these particles, the influence of some of these parameters was investigated. The systems that we investigated were: ctDNA-PLL, pDNA-PLL and pDNA-bPLL.

3.1.1 Mixing order of PLL and DNA

It has been reported that the mixing order of polyelectrolytes not only affects the size of the resulting particles, causing up to a 2-fold change in size, but also the stability of these complexes to NaCl[130]. For example, at CR=3, if the DNA is added to the polymer, there is always an excess of positive charge in the complexes and repulsive forces between them help maintain colloidal stability. However, if the same polyplex mixture is prepared by addition of polymer to DNA, the negative charge of the initial coacervates will reach a neutral value half way through the addition of polymer. As a result, neutral particles can flocculate if polyelectrolytes are mixed in the wrong order[34, 131]. Hence, in this work we wanted to determine whether this was the case in the pDNA-PLL system, i.e. if adding pDNA to PLL or PLL to pDNA could result in observable differences. Two sets of polyplexes were prepared. In the first set the pDNA was added to the PLL for CR = 1 and 3 (DNA on PLL). In the second set the opposite was done (PLL on DNA). Table 4 shows the results.

Table 4 – Study of the effect of the mixing order for the PLL-pDNA system, at fixed concentrations, CR = 1 and 3.

	DNA on PLL			PLL on DNA		
CR	**Size /nm**	**Std /nm**	**PDI**	**Size /nm**	**Std /nm**	**PDI**
1	93.4	2.9	0.162	85.9	1.5	0.182
3	65.5	3.0	0.224	69.1	3.0	0.204

DLS is especially useful to provide information on the hydrodynamic diameter and polydispersity. Figure 16.a and 16.b show the autocorrelation functions measured with DLS for both CR = 1 and CR = 3, respectively. Each sample is measured in triplicate and the reproducibility across these replicates is very good. For CR=3, the two samples have almost perfectly overlapping autocorrelation curves, indicating very small differences. Indeed, the fitting algorithm of the instrument software (based in the cumulants method) yielded sizes that are essentially identical (table 4). For CR=1, there is some mismatch between the autocorrelation curves for the two different orders of addition. The instrument software fit also provided results that were more different than for the CR=3 case, but taken together, these differences do not seem very significant.

This leads to the assumption that for these conditions, whether pDNA is added to PLL or vice-versa seems to be of small significance. This is in agreement with other studies in the literature, where the mixing order did not have an effect on the final structure of

the polyplex[131-133]. Nonetheless, for consistency, unless otherwise noticed, the polypeptide was always added to pDNA.

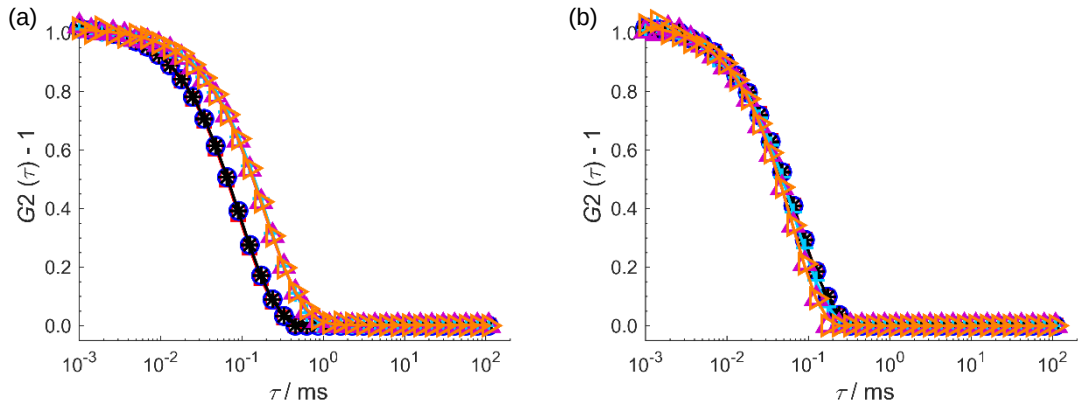

Fig. 16 – DLS autocorrelation functions for PLL-pDNA polyplexes with different charge ratios, at fixed DNA concentration (11.5 μg.mL^{-1}). The data were collected at 25ºC with scattering angle θ = 173º. (a) Study of mixing order at CR 1, (□) first measurement for PLL, (○) second measurement for PLL, (*) third measurement for PLL, (+) first measurement for pDNA, (△) second measurement for pDNA, (▷) third measurement for pDNA; (b) study of mixing order at CR 3 (□) first measurement for PLL, (○) second measurement for PLL, (*) third measurement for PLL, (+) first measurement for pDNA, (△) second measurement for pDNA, (▷) third measurement for pDNA.

Other study[134] addresses the influence of solution inhomogeneity on structure and morphology of polyplexes. The inhomogeneity is induced by mixing two solutions containing, respectively, protamine and DNA, with different relative concentrations, but aiming to produce the same final concentration. This study showed that the relative population of compacted and unfolded structures are very highly dependent on the method of preparation of the mixtures containing polymer/DNA. In this study, the solution inhomogeneity increases with increasing charge ratio. Different populations of compacted and unfolded may be obtained.

3.1.2 Effect of physiological buffer, ionic strength and order of mixing

As mentioned previously, pH influences the protonation of the peptide, and therefore its charge density. Hence, together with the ionic strength, these two parameters are expected to influence the electrostatic attraction between the two oppositely charged polymers, and the colloidal stability of the resulting polyplexes. This becomes significant if one recalls that these particles have applications in biological systems, and hence, complexation and stability in a buffer that resembles physiological media should be studied.

With this in mind, an experimental design was created to understand what kind of influence the buffer pH and ionic strength have on the aggregation and structure of the polyplexes. Thus, several 20 mM HEPES buffers at pH 7.4 with an ionic strength ranging from 20 to 150 mM were prepared and tested on the polyplexes. Two different experiments were performed. In the first, the buffer was added to the reagents (PLL and pDNA), and then the polyplexes were prepared (figure 17.a). In other words, PLL and pDNA are mixed at physiological pH and ionic strength. In a second experiment, the polyplexes were prepared first in water and the buffer was added after (figure 17.b). In other words, PLL and pDNA are mixed at very low ionic strength.

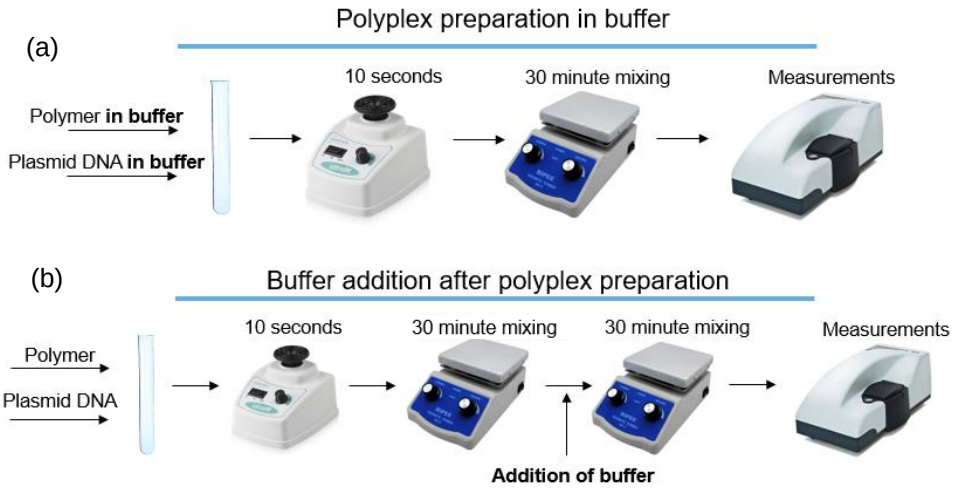

Fig. 17 – Experimental design for the two buffer addition methods. (a) polyplex preparation in buffer, with the polymer and pDNA already in the presence of buffer; (b) Buffer is added after mixing of polymer and pDNA in water.

3.2 Bulk preparation

3.2.1 Poly-L-lysine and DNA

Preparation in water: size differences between ctDNA and pDNA polyplexes

For studies with poly-L-lysine (125k – 300k), two types of DNA were studied, calf thymus DNA and plasmid DNA (pGL3, control vector, 5256 base pairs). While the plasmid DNA is a small circular DNA double helix, and very monodisperse, calf thymus is long and polydisperse.

In an initial study, our aim was to investigate the dependence of polyplex size with concentration. The charge ratio between positive (from PLL) and negative charges (from DNA) was fixed at 3. The results can be seen in figure 18. Aside from the relationship between size and DNA concentration, this study helped to determine the optimum quantity of DNA to use in the following experiments, which was 11.5 $\mu g.mL^{-1}$. In this way, it was possible to minimize plasmid expenditure and maintain a good DLS signal.

As it is easy to see, there is an overall decrease in size of the polyplexes prepared with the circular monodispersed DNA. This difference is most likely to be a result of the structural differences between both types of DNA. While pDNA is circular and highly monodisperse, ctDNA is very polydisperse ($M_w/M_n=5.2$[135]) with an average molecular weight of 13 kbp, indicating that not only the polymer is longer, but there is also a significant fraction with much longer lengths. We hypothesize that while complexation between DNA and PLL is occurring, longer DNA chains are most likely to interact with a larger amount of PLL, nucleating into longer particles.

Along with the size differences between ctDNA and pDNA, it is also clearly noticeable that in both cases, the size increases with increasing DNA concentration. The maximum concentration tested in these experiments is 200 $\mu g.ml^{-1}$ DNA and 249 $\mu g.ml^{-1}$ PLL (CR=3), together resulting in a mass fraction of roughly 0.05%. This means that these samples are all highly dilute, which help exclude the possibility of having obstruction effects from the particles to each other that would slow down the apparent diffusion coefficient and provide overestimated sizes. Hence, the increase in size observed by DLS is a real effect. A possible justification for this behavior is that a larger concentration of the individual polymers in the beginning of the complexation process facilitate nucleation into larger particles.

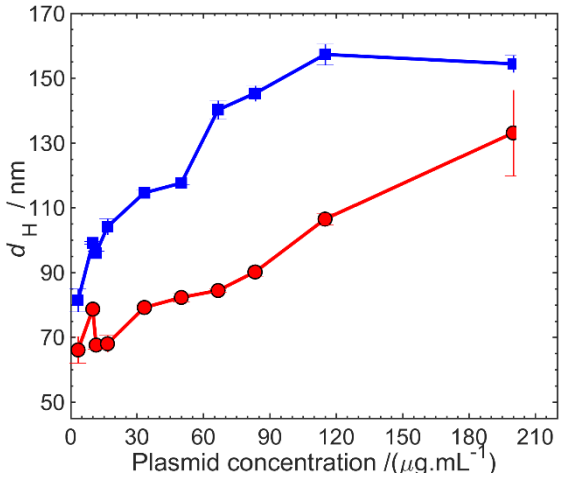

Fig. 18 – Size dependence of polyplexes of poly-L-lysine with calf thymus (■) and plasmid (●) in water, as a function of DNA concentration, and CR=3.

After fixing the DNA concentration at 11.5 μg.mL^{-1}, PLL / DNA system was study varying the charge ratio from 0.5 to 10. The size profile, obtained by DLS, can be observed in figure 19.a, and the zeta potential profile can be seen in figure 19.b.

In terms of size, both preparations have a diameter peak at CR = 1.6, that coincides with a low zeta potential. This means that the polyplex is near charge neutrality. When zeta potential is around 0 mV, an increase in size may be detected due to the formation of particle aggregates. Visually, the CR = 1.6 samples precipitate not long after the measurements, further supporting the near charge neutrality idea. At higher charge ratios, it is observed a stabilization of the size at around 130 nm for calf thymus and 60 nm for pDNA. Zeta potential measurements allow to see an inversion of surface electric potential from negative at low CR (i.e. excess of DNA) to positive at high CR, which was expected. The negative surface potential may indicate that the DNA is partially condensed. Other studies have also found similar size and zeta potential shifts using PEI[136] and polystyrene-based[137] polymers, observing a point of particle charge neutralization at CR = 3 and 0.6, respectively.

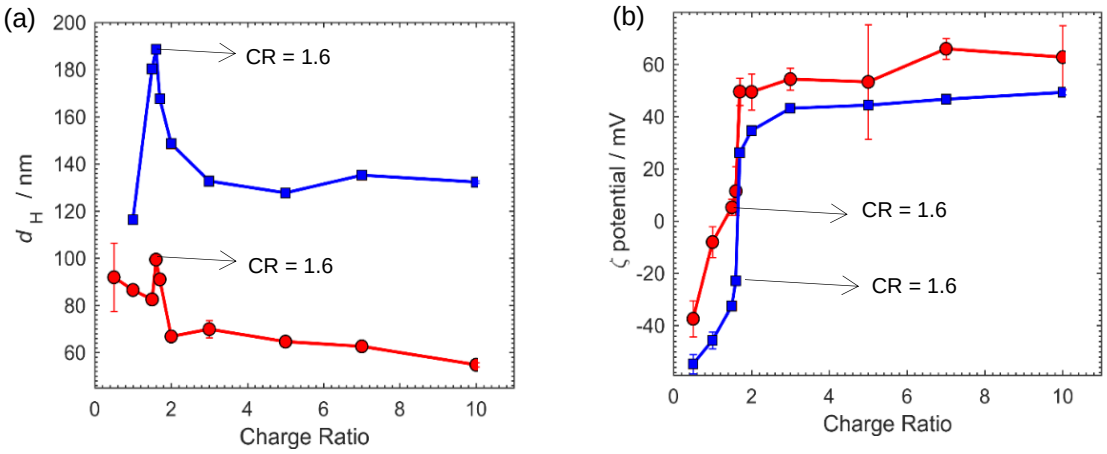

Fig. 19 - Study of complexation of poly-L-lysine with DNA, calf thymus (■) and plasmid (●), in water as a function of charge ratio, at fixed DNA concentration (11.5 μg.mL^{-1}). **(a)** size of polyplexes against charge ratio; **(b)** zeta potential of polyplexes against charge ratio.

Table 5 – Size and polydispersity values obtained by DLS for bioreducible poly-L-lysine/pDNA systems, at fixed concentration (11.5 μg.mL^{-1}).

	PLL / Calf thymus system			PLL-pDNA system		
CR	**Size /nm**	**Std /nm**	**PDI**	**Size /nm**	**Std /nm**	**PDI**
0.5	118.1	2.9	0.338	91.9	14.5	0.505
1	116.4	0.4	0.25	86.5	2.2	0.092
1.5	180.4	1.5	0.209	82.5	1.2	0.145
1.6	188.6	1.8	0.201	99.4	2.3	0.198
1.7	167.6	1.6	0.156	91.0	1.3	0.218
2	148.5	1.8	0.176	66.8	1.0	0.249
3	132.7	0.8	0.197	69.9	3.6	0.415
5	127.7	0.8	0.204	64.6	1.2	0.306
7	135.2	0.5	0.208	62.6	1.1	0.322
10	132.3	0.5	0.208	54.8	0.9	0.249

The polydispersity index (PDI) should also be mentioned. The PDI results from the cumulants fit to the autocorrelation function determined in the DLS instrument, and provides an indication about the size distribution of the particles in the sample. In general, systems with PDI smaller than 0.05 are very monodisperse, and above 0.7 are very polydisperse. PDI values between 0.05 and 0.7 display a moderate polydispersity. The PDI of both systems can be found in table 5. Although the PLL / ctDNA has an overall bigger size, its polydispersity is equivalent to the PLL-pDNA. The sample with higher PDI is that of CR = 0.5. This sample contains the least amount of polymer making the particles a little less uniform. The rest of the samples yielded a PDI between 0.1-0.2, which may be considered a monodispersed system.

A study of the stability over time regarding PLL and pDNA was made. Figure 20 shows that polyplexes with high charge ratio have a tendency to maintain their size for at least 3 weeks. This is likely due to the excess of PLL that is expected to reside at the surface of the polyplexes, conferring them colloidal stability by electrostatic repulsions. At low CR (CR < 2) polyplexes show significant differences but are able to remain below 200 nm.

These findings seem to be in agreement with other works. On a study regarding the gene delivery vectors for extended systemic circulation[138], the system PLL (205k) / pDNA was studied at CR = 2 and at DNA concentration of 20 μg.mL^{-1}. Particles with 84±2 nm in diameter with a PDI of 0.160 were obtained, which compares reasonably well with 67±1 nm with PDI of 0.249 obtained here. In terms of zeta potential, they obtained a 39.3±0.4mV, while 49.5±6.9mV was measured here. Also, in that work, cryo-TEM images of PLL-pDNA at CR = 2 were obtained, displaying particles with a distorted spherical and rod-like shapes. Given the similarities in size and shape with this study, the polyplexes PLL-pDNA described here are likely to have a similar structure.

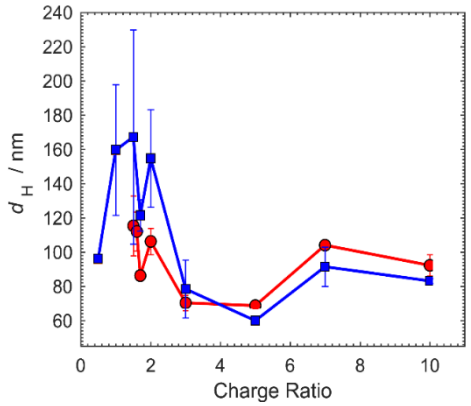

Fig. 20 - Study of stability of poly-L-lysine and pDNA polyplexes in water, upon preparation (●) and three weeks later (■), as a function of charge ratio, and fixed DNA concentration (11.5 μg.mL-1).

Physiological ionic strength and pH effects on polyplex formation: the path matters

When developing particles for biological applications, one has to consider the environment in which they will be used. In order to achieve conditions more closely related to physiological ones, we used a 20 mM Hepes buffer with pH 7.4 (similar to blood pH) and added NaCl to complete a total monovalent salt concentration of 150 mM (also similar to physiological ionic strength)[139]. As mentioned in section 3.1.2, two different experiments were performed. In the first experiment (path I), polyplexes are formed in water and the buffer is added only afterwards. In the second experiment (path II), polyplexes are formed in the presence of the buffer.

Path I: In this first experiment, polyplexes were prepared by mixing PLL and pDNA in water, at fixed pDNA concentration of 11.5 µg.mL^{-1}, in the same range of CR described previously. Then, buffer was added to the solution to achieve 150 mM ionic strength and pH 7.4. Figure 21 shows a comparison of the sizes and zeta potential of polyplexes in water and buffer.

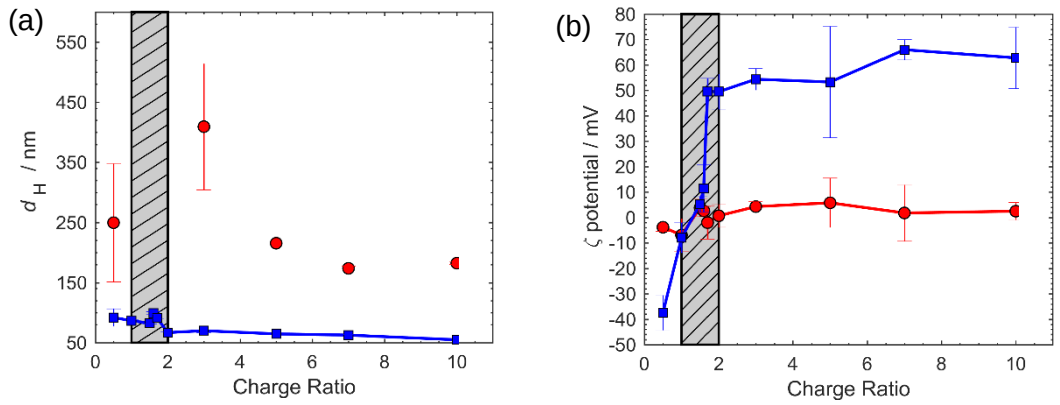

Fig. 21 - Study of the effect of buffer at pH7.4 and 150 mM NaCl on the stability of polyplexes (path I), at fixed DNA concentration of 11.5 µg.mL^{-1}. (a) Size profile of polyplexes in buffer (●) and in water (■); (b) zeta potential profile of polyplexes in buffer (●) and in water (■). The macroscopic aggregation region is shown in grey.

Upon addition of the buffer, an overall increase in the size is observed, but the profile remains similar to the studies made in water. A decrease in size is observed for bigger charge ratios (figure 21.a). From CR 1-2, an aggregation gap is obtained, grey area marked in the figure 21 plots, this gap coincides with the zeta potential inversion zone observed in water (figure 19.b). These changes in size are likely to result from the screening of the particles' surface charge by the salt present in the buffer (this screening effect will be more evident in the study of the effect of intermediate ionic strength on polyplexes). This screening leads to a weakening in electrostatic repulsions which were important in providing colloidal stability to the particles, and this effect is likely to result in

aggregation. These observations are supported by the decrease in the magnitude of the zeta potential as shown in figure 21.b. In addition, some signs of macroscopic aggregation become visible in all the samples in less than one week, indicating that besides an increase in size, indeed these particles are colloidally less stable in this buffer than in water.

Path II: In the second experiment on the effect of the buffer, PLL-pDNA were already prepared in the presence of the buffer. Polyplexes were prepared by mixing PLL and pDNA in 20 mM HEPES and 150 mM ionic strength, at fixed pDNA concentration of 11.5 $\mu g.mL^{-1}$. Figure 22 shows the results of DLS measurements and visual observations for the polyplexes prepared in buffer.

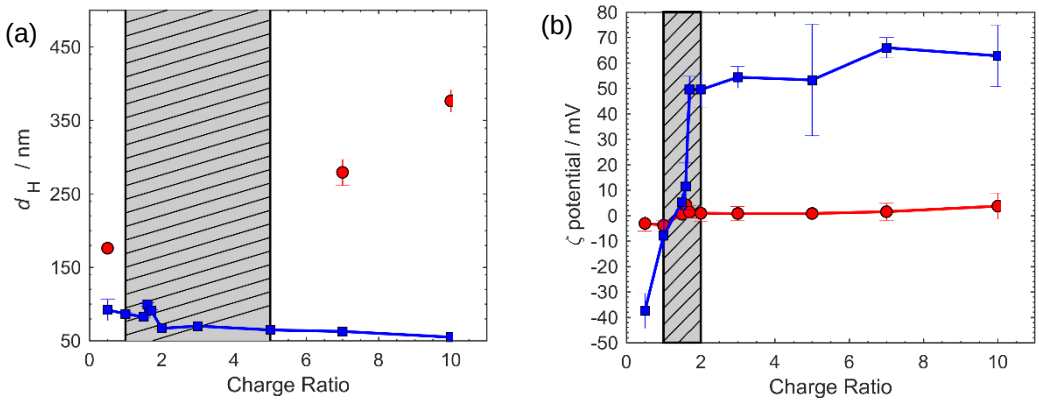

Fig. 22 - Study of the effect of buffer at pH7.4 and 150 mM NaCl on the formation of bioreducible polyplexes (path II), at fixed DNA concentration of 11.5 $\mu g.mL^{-1}$. (a) Size profile of polyplexes in buffer (●) and in water (■); (b) zeta potential profile of polyplexes in buffer (●) and in water (■).The macroscopic aggregation region is shown in grey.

As can be seen, there is a much larger aggregation gap (from CR 1-5), where macroscopic aggregation is visually observed. Simultaneously, the samples that did not show macroscopic aggregation showed a significant increase in size as compared to the sizes observed in path I (polyplexes prepared in water and buffer added later). Overall it seems evident that although the final composition is the same for samples in both path I and path II, the sizes of the polyplexes are very different. Since the major driving force for complexation between pDNA and PLL is the electrostatic interaction, which ultimately results in a large entropy gain due to the release of the sodium and bromide counter ions (from DNA and PLL, respectively), one can hypothesize that the higher ionic strength at the moment of complexation in path II makes complexation slightly less favorable. This may result in a slowing down of complexation, which like most nucleation processes, by being slower, can grow into larger particles.

Effect of intermediate ionic strength in PLL-pDNA polyplexes

To gain further insight on the role of the ionic strength in the formation of polyplexes, we studied the effect of intermediate ionic strength in complexation. For these experiments, the procedure was the same as for the study of the effect of buffer, but varying the ionic strength. The tested ionic strengths were 20 mM, 30mM, 70mM, 100 mM and 150mM at pH 7.4. These buffers were tested for charge ratios, CR = 3, 5 and 7. CR = 10 was excluded because it uses a lot of reagent and the size results can be comparable to CR = 7.

Figure 23 summarizes the results from the addition of buffer with variable ionic strength on polyplexes previously prepared in water (path I). Until 70 mM, the differences are very subtle, but become more significant at 100 mM and especially at 150 mM ionic strength. It is also evident that these effects are more striking at lower CR (CR = 3), which suggests that at CR 5 and 7 the polyplexes are more highly charged, making them colloidally more stable. Table 6 show the sizes obtained by DLS, and also the Debye screening length for each ionic strength. With increasing ionic strength, the screening length decreases, which means that the net electrostatic effect of polyelectrolytes in solution is weakened. To compare, in water, the Debye screening length is around 20 nm.

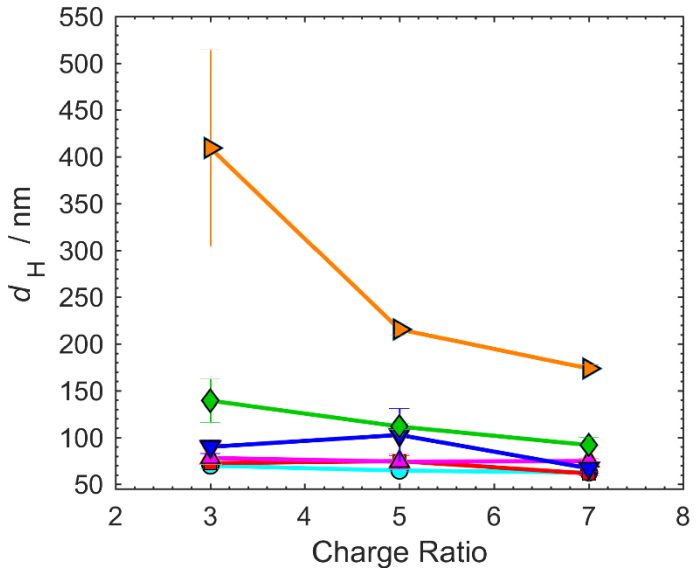

Fig. 23 – Influence of the ionic strength on the size of polyplexes prepared in water (path I), at fixed DNA concentration of 11.5 µg.mL^{-1} and pH 7.4. Polyplexes in water (●), in 20 mM (■), in 30 mM (▲), in 70 mM (▼), in 100 mM (♦), and in 150 mM (►).

Table 6 - Size of polyplexes regarding the study of the effect of buffer at pH7.4 and ionic strength on the stability of polyplexes (path I), at fixed DNA concentration of 11.5 μg.mL^{-1}. Debye screening length was calculated considering the ionic strength of the medium.

Ionic Strength	CR = 3		CR = 5		CR = 7		Screening Length
I /mM	Size /nm	Std /nm	Size /nm	Std /nm	Size /nm	Std /nm	κ^{-1} /nm
20	72.5	1.8	74.8	5.8	61.5	2.3	2.1
30	78.1	5.5	74.2	7.9	74.8	2.6	1.8
70	90.0	7.3	102.7	28.3	67.0	5.1	1.1
100	139.4	23.1	111.7	3.1	91.9	8.2	1.0
150	409.4	105.1	215.5	6.5	173.7	3.9	0.8

Figure 24 summarizes the results on the effect of ionic strength on polyplexes prepared in buffer (path II). In this path, the differences between increasing ionic strengths are more visible. For the buffer with 30 mM ionic strength, the size of polyplexes with CR = 3 and 5 is already significantly larger, and this trend keeps increasing with increasing ionic strength. At 150 mM, only semi stable particles at CR = 7 are observed. Table 7 shows the sizes obtained by DLS, and also the Debye screening length for each ionic strength.

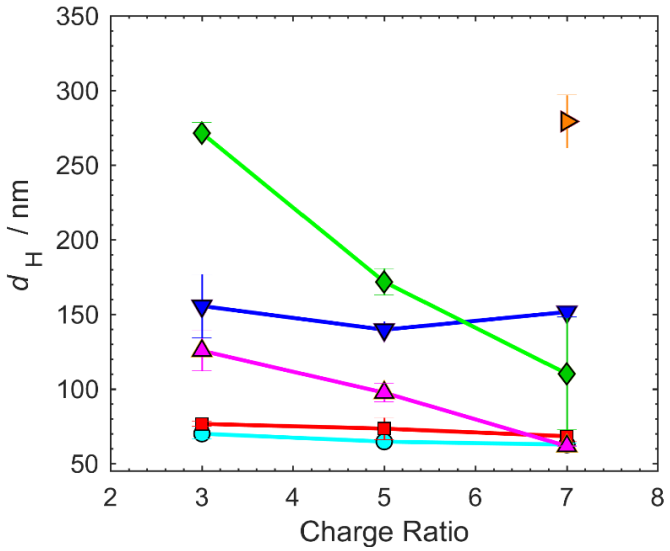

Fig. 24 - Influence of the ionic strength on the size of polyplexes prepared in buffer (path II), at fixed DNA concentration of 11.5 μg.mL^{-1} and pH 7.4. Polyplexes in water (●), in 20 mM (■), in 30 mM (▲), in 70 mM (▼), in 100 mM (♦), and in 150 mM (►).

Table 7 - Size of polyplexes regarding the study of the effect of buffer at pH7.4 and ionic strength on the formation of polyplexes (path II), at fixed DNA concentration of 11.5 μg.mL^{-1}. Debye screening length was calculated considering the ionic strength of the medium.

Ionic Strength	CR = 3		CR = 5		CR = 7		Screening Length
I /mM	Size /nm	Std /nm	Size /nm	Std /nm	Size /nm	Std /nm	κ^{-1} /nm
20	76.5	1.7	73.3	7.4	68.2	3.7	2.1
30	125.5	13.5	97.4	6.1	61.6	0.4	1.8
70	155.5	21.3	139.6	5.6	151.5	3.3	1.1
100	271.4	7.1	171.7	8.9	110.1	37.4	1.0
150	aggr.		aggr.		279.2	17.8	0.8

3.2.2 Bioreducible poly-L-lysine and plasmid DNA

The bioreducible poly-L-lysine was obtained by oxidation of the respective monomers (CKKKKKC) by DMSO. This reaction allows little control over the extent of polymerization and hence, little control over the chain length. Thus, the polymer is expected to be significantly polydisperse.

Preparation in water of bPLL-pDNA polyplexes

For the bPLL and pDNA system in water, the size and zeta profiles can be observed in figure 25. The quantity of pDNA used in these studies is the same as for the PLL studies, so that the results from both studies are more readily comparable.

The size profile can be observed in figure 25.a, and the zeta potential profile can be seen in figure 25.b. The peak observed in the PLL system has now shifted to CR = 2.1 with bPLL. This may be due to structural differences caused by the cysteines or to the presence of non-polymerized CK_5C or impurities that do not contribute to complexation, but cause a systematic error in the weighing of the polymer. Despite this shift, the similarities between the PLL-pDNA and bPLL-pDNA systems are striking. Both

preparations have quite similar sizes, with the size observed for high CR being close to 70 nm in the bPLL complexes. The same inversion of surface electric potential is also observed in both cases. Polyplexes with low CR (CR 0.5-1.7) have highly negative zeta potentials, around -50 mV, while high CR polyplexes (CR 2.5-10) have highly positive zeta potentials.

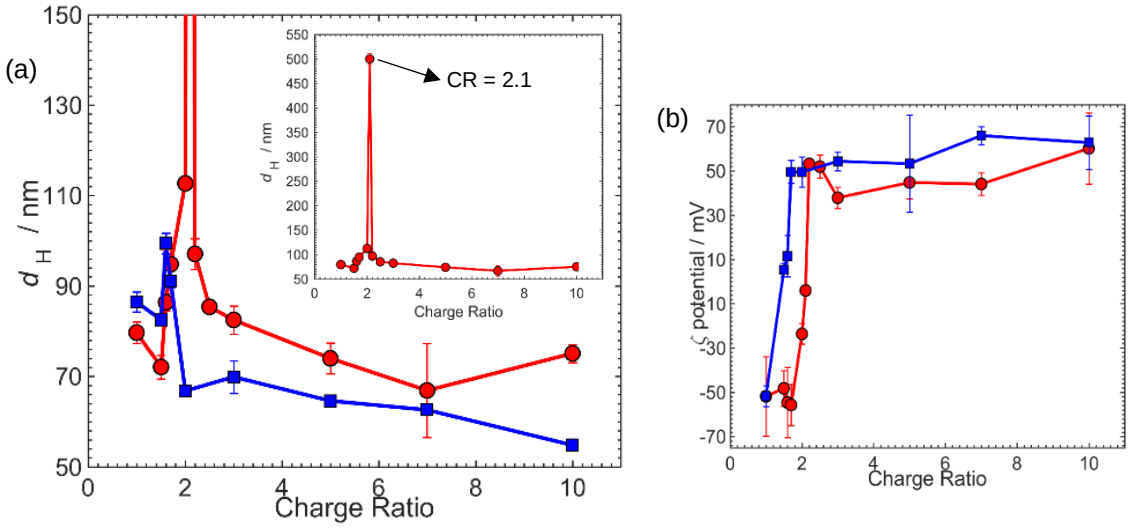

Fig. 25 – Comparison between polymers, bPLL (●) and PLL (■), with plasmid DNA, in water with variation of charge ratio, at fixed DNA concentration (11.5 µg.mL-1). (a) Size of polyplexes against charge ratio; (b) zeta potential of polyplexes against charge ratio.

The polydispersity index (PDI) results from the cumulants fit to the DLS data and gives an indication about the size polydispersity of the system. The PDI of bPLL-pDNA can be found in table 8. These indexes indicate a higher level of polydispersity when compared to the PLL-pDNA. This difference is likely to be associated with the bioreducible poly-L-lysine and it is possible high level of polydispersity.

We also investigated the colloidal stability of bPLL and pDNA polyplexes in water. Figure 26 shows that polyplexes are able to maintain their size in water for at least 3 weeks, mainly due to high cationic repulsions. Polyplexes with CR = 2.1 and 2.5 were the only that aggregated.

Table 8 – Size and polydispersity values obtained by DLS for bioreducible poly-L-lysine/pDNA systems, at fixed concentration (11.5 μg.mL^{-1}).

bPLL-pDNA system			
CR	**Size /nm**	**Std /nm**	**PDI**
1	79.7	2.4	0.368
1.5	72.1	2.6	0.228
1.6	86.4	1.9	0.227
1.7	94.8	3.9	0.257
2	112.7	1.4	0.321
2.1	500.1	11.2	0.351
2.2	97.1	3.4	0.294
2.5	85.4	1.0	0.331
3	82.5	3.1	0.279
5	74.0	3.4	0.331
7	66.9	10.4	0.187
10	75.1	2.0	0.250

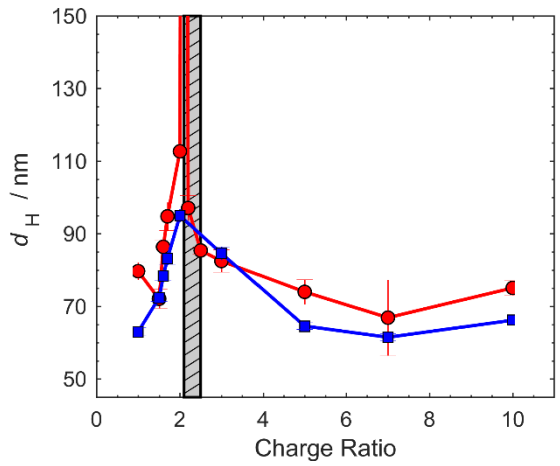

Fig. 26 - Study of the stability of bioreducible poly-L-lysine with pDNA polyplexes in water, upon preparation (●) and three weeks later (■) as a function of charge ratio, at fixed pDNA concentration (11.5 μg.mL-1). Aggregation zone showed in grey.

Physiological ionic strength and pH effects on bPLL-pDNA polyplexes

We further investigated the effect of physiological ionic strength and pH on the complexation between bPLL with pDNA. The tests with 20 mM HEPES, 150 mM ionic strength at pH 7.4 made for the PLL-pDNA system were repeated for the bioreducible polymer, including the order of addition of the buffer.

For the case of bioreducible polyplexes prepared in water, with buffer added after complexation (path I), it was observed little stability on physiological buffer. Results can be seen in Table 9. Aggregation was observed from basically every sample, except for CR = 1.

For the case of preparation of polyplexes in buffer (path II), the results are similar to path I. Table 10 shows the size and zeta potential of those polyplexes. Aggregation occurs for all charge ratios, except CR = 1. Also, zeta potential indicates low surface electrical potential in a similar way to what was found for the PLL/pDNA system.

Table 9 - Values of size and zeta potential acquired for the study of the effect of buffer at pH7.4 and 150 mM NaCl on the stability of bioreducible polyplexes (path I), at fixed DNA concentration of 11.5 $\mu g.mL^{-1}$.

bPLL-pDNA in physiological buffer					
CR	**D_H /nm**	**PDI**	**Std /nm**	**ζ-potential /mV**	**Std /mV**
1	160.6	0.779	13.0	-0.4	0.8
1.7				-1.9	1.2
2				-1.9	3.7
2.1				-0.2	1.8
2.2		Aggregated		-0.5	2.4
3				7.0	8.7
5				6.9	0.2
7				4.6	1.8
10				5.5	1.7

Table 10 - Values of size and zeta potential acquired for the study of the effect of buffer at pH 7.4 and 150 mM NaCl on the formation of bioreducible polyplexes (path II), at fixed DNA concentration of 11.5 μg.mL^{-1}.

bPLL-pDNA in physiological buffer					
CR	**D_H /nm**	**PDI**	**Std /nm**	**ζ-potential /mV**	**Std /mV**
1	242.8	0.451	27.0	-3.1	1.7
1.7				-1.3	1.5
2				-1.8	0.3
2.1				-1.4	1.9
2.2		Aggregated		2.0	4.1
3				0.9	0.6
5				-0.6	0.6
7				2.6	2.0
10				2.3	1.0

Effect of intermediate ionic strength in bPLL-pDNA polyplexes

To investigate the influence of the ionic strength on the bioreducible polyplexes, and to determine the maximum ionic strength in which polyplexes remain somewhat stable, we performed measurements at increasing ionic strengths (20 mM, 30 mM, 50 mM and 70 mM) at pH 7.4. Here, owing to the smaller amount of bPLL available, the number of ionic strength concentrations investigated was reduced. These buffers were tested for charge ratios, CR = 3, 5 and 7. Figure 27 shows the results obtained for the case of bioreducible polyplexes prepared in water, with buffer added after complexation (path I), These bioreducible polyplexes show very little stability at higher ionic strengths. Whereas regular polyplexes are able remain colloidally stable in 150 mM, bioreducible polyplexes show macroscopic aggregation already at 50 mM. Table 11 shows the sizes obtained by DLS, and also the Debye screening length for each ionic strength. With increasing ionic strength, the screening length decreases, which means that the net electrostatic effect

of polyelectrolytes in solution is less predominant. To compare, in water, the Debye screening length is around 20 nm.

Figure 28 shows the results obtained for the case of bioreducible polyplexes prepared in buffer (path II). Like in path I, the stability is very reduced, and above 30 mM ionic strength macroscopic aggregation is observed for all charge ratios. Table 12 shows the sizes obtained by DLS, and also the Debye screening length for each ionic strength.

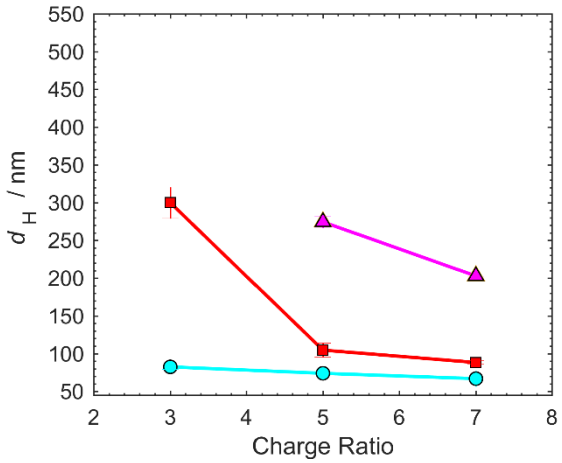

Fig. 27 - Size of bioreducible polyplexes regarding the study of the effect of buffer at pH7.4 and ionic strength on the stability of polyplexes (path I), at fixed DNA concentration of 11.5 μg.mL^{-1}. Ionic strength ranging from 20-150 mM. Polyplexes in water (●), in 20 mM (■), in 30 mM (▲).

Table 11 - Size of bioreducible polyplexes regarding the study of the effect of buffer at pH 7.4 and ionic strength on the stability of polyplexes (path I), at fixed DNA concentration of 11.5 μg.mL^{-1}. Debye screening length was calculated considering the ionic strength of the medium.

Ionic Strength	**CR = 3**		**CR = 5**		**CR = 7**		**Screening Length**
I /mM	**Size /nm**	**Std /nm**	**Size /nm**	**Std /nm**	**Size /nm**	**Std /nm**	**κ^{-1} /nm**
20	300.0	20.8	104.7	9.3	88.3	2.3	2.1
30	aggr.		274.5	7.9	202.9	0.6	1.8
50	aggr.		aggr.		aggr.		1.1

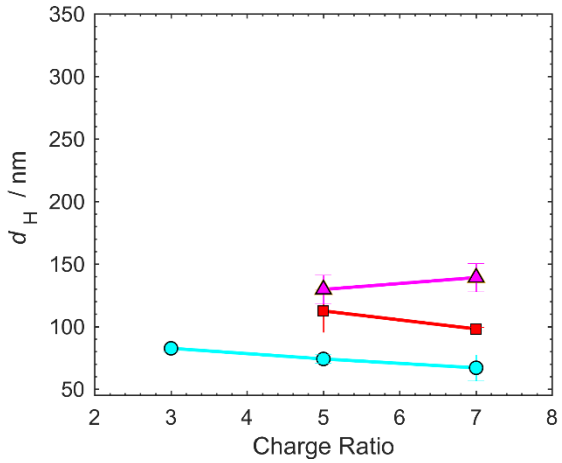

Fig. 28 - Size of bioreducible polyplexes regarding the study of the effect of buffer at pH 7.4 and ionic strength on the formation of bioreducible polyplexes (path II), at fixed DNA concentration of 11.5 μg.mL^{-1}. Polyplexes in water (●), in 20 mM (■), in 30 mM (▲).

Table 12 - Size of bioreducible polyplexes regarding the study of the effect of buffer at pH7.4 and ionic strength on the formation of polyplexes (path II), at fixed DNA concentration of 11.5 μg.mL^{-1}. Debye screening length was calculated considering the ionic strength of the medium.

Ionic Strength	**CR = 3**		**CR = 5**		**CR = 7**		**Screening Length**
I /mM	**Size /nm**	**Std /nm**	**Size /nm**	**Std /nm**	**Size /nm**	**Std /nm**	**κ^{-1} /nm**
20	aggr.		112.5	17.1	98	1.2	2.1
30	aggr.		129.6	11.5	139.1	11.3	1.8
50	aggr.		aggr.		aggr.		1.1

3.2.3 Glutathione test

The main purpose of the bioreducible polymers is the ability to degrade when exposed to cellular cytosol, more specifically to glutathione (GSH) present in the cell matrix[80-81, 140]. Here, to test the ability of the bioreducible polyplexes to degrade, we performed a series of experiments where glutathione is added.

Two GSH concentrations, 20 mM and 40 mM, were studied. These concentrations are believed to be the normal cell cytosol and the cancerous cell concentration, respectively. After GSH addition a waiting time of 1 hour.

Polyplexes were prepared for charge ratios 3, 5, 7 and 10, and before GSH addition, DLS measurements were taken. Those results are shown in figure 29.a. The size profile is as seen before, small complexes which diameter decreases with increasing CR. Upon addition and incubation of GSH, the size profile was taken again. Results are shown in figure 29.b. Although one was expecting a decrease in size due to the bPLL degradation, the size of all samples increased drastically to the point where they fall out the size range of the equipment. They are between 10 000 – 30 000 nm, i.e. 10 – 30 µm. This difference displays that some surface destabilization occurred that led to the formation of big particles. This destabilization could be either by electrostatic screening or degradation of particle surface polymer[50].

In figure 30.a and 30.b, it is possible to see the difference in delay time from samples before and after glutathione, 20 mM and 40 mM, respectively. It is important to notice that after the addition of the GSH, the fitting becomes more complex, existing possibly more than one population.

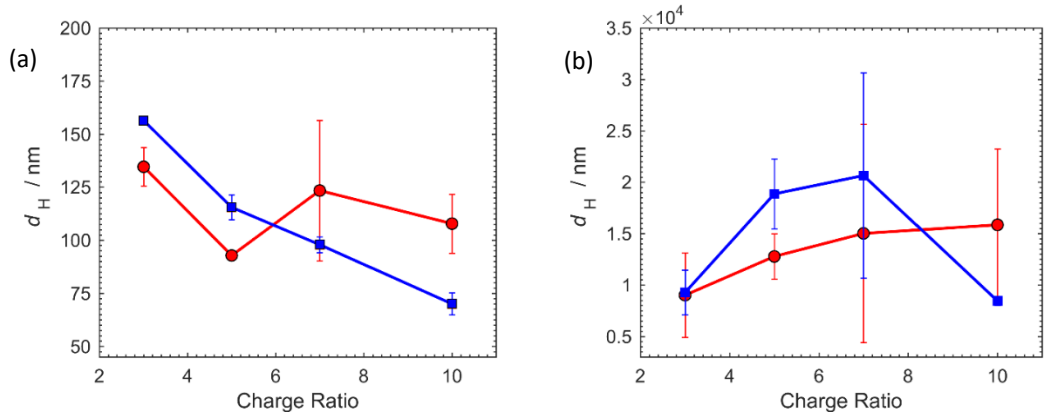

Fig. 29 - Study of the effect of glutathione in bioreducible polyplexes with variation of charge ratio, at fixed concentration (11.5 µg.mL^{-1}). (a) Size results before GSH addition, 20 mM (●) and 40 mM (■); (b) size results after GSH addition incubating for 1h, 20 mM (●) and 40 mM (■).

Additional tests using GSH were performed. Optimum GSH concentration, to observe gradual increase in size of polyplexes over time, was found to be 10 mM of glutathione for polyplexes with CR = 3. This experiment was also done on PLL-pDNA as a control. Figure 31.a show the study of the effect of glutathione over time. The point x = 0 refers to the measurement before addition of GSH. The DLS measurements were taken with

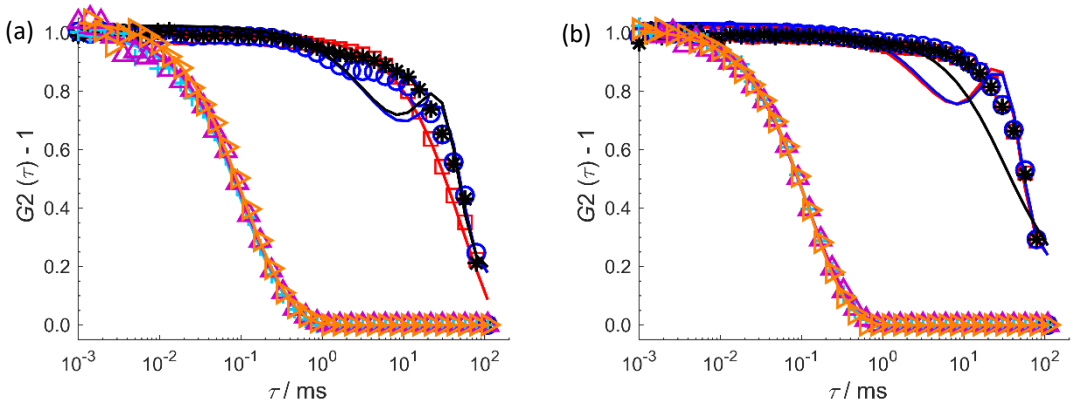

Fig. 30 - Normalized autocorrelation functions obtained from DLS measurements for the study of addition of GSH to bioreducible polyplexes at CR=5, and at fixed DNA concentration (11.5 μg.mL^{-1}). (a) Study of the effect of 20 mM GSH. Measurements made before GSH addition (+), (△), (▷), and after incubation for 1h at room temperature (□), (○), (*); (b) Study of the effect of 20 mM GSH. Measurements made before GSH addition (+), (△), (▷), and after incubation for 1h at room temperature (□), (○), (*).

2 minutes of each other. Within 10 minutes of addition, the size has already increased around 4 times. It keeps increasing for that point on. The last measurement was made 4 weeks after the addition, with no signs of any possible particle disassembly. On the other end, poly-L-lysine polyplexes are able to maintain their size throughout all time, see figure 31.b. The last measurement was also made 4 weeks after addition, at this time polyplexes were not stable anymore and had aggregated.

A study regarding vectors based on reducible polycations[141] studied the bioreducibility of the system $CK_{10}C$ polymer (187k) / pDNA in 25 mM DTT – dithiothreitol. DTT is a reducing agent, similar to GSH. Bioreducible polyplexes at CR = 2 and DNA concentration of 20 μg.mL^{-1} suffered an increase in size, while non-reducible polyplexes - PLL-pDNA - remained stable. This finding agrees with the study described here. Cryo-TEM images were taken of the before and after the addition of 25 mM DTT. Before the

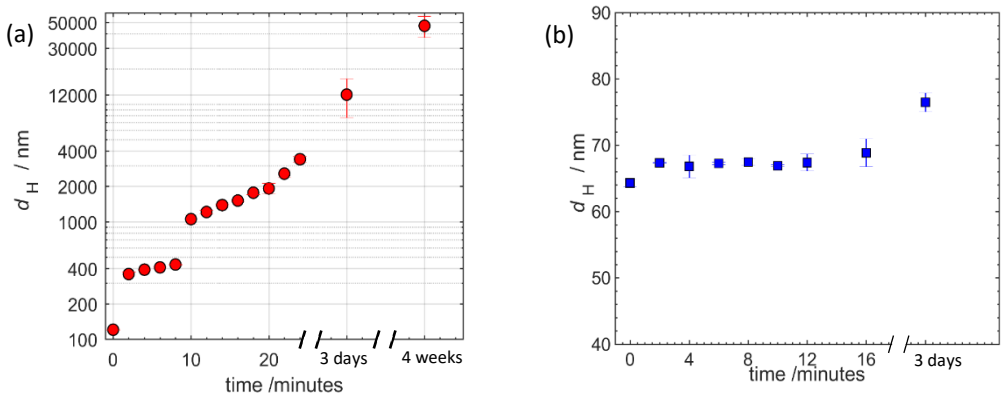

Fig. 31 - Study of the effect of 10 mM glutathione at pH 7.4 in bioreducible polyplexes with variation of charge ratio, at fixed concentration (11.5 μg.mL^{-1}). x = 0 is the measurement before addition of GSH. (a) Bioreducible polyplexes, and (b) regular polyplexes.

addition, polyplexes were very discrete particles with diameters ranging from 50-200 nm with quasi-spherical shape, however treatment with DTT caused extensive aggregation of the sample.

Polyplex preparation with CK_5C

Apart from using regular poly-L-lysine as a glutathione control, samples containing monomeric bioreducible poly-L-lysine were prepared to be tested in 10 mM of glutathione. For this purpose, we mixed pDNA with CK_5C (i.e. monomeric bPLL) at a fixed charge ratio of 3, and fixed DNA concentration (11.5 $\mu g.mL^{-1}$) to check whether polyplexes would form with the short peptide of 5 positive charges. Table 13 shows the size results obtained for this experiment.

Table 13 − Study of the addition of GSH to polyplexes prepared with monomeric bPLL / pDNA, at CR = 3, and at fixed DNA

CR = 3	**Size /nm**	**Std /nm**
Without GSH	8326.5	75.2
After GSH		
Time	**Size /nm**	**Std /nm**
3 minutes	14128.6	4671.1
3 days	36264.7	14486.1
4 weeks	55756.0	14747.1

.

Upon addition of the CK_5C to the pDNA solution, a visible white precipitate formed in the solution, suggesting that large polyplexes form, although without colloidal stability. Even though there is a large excess of positive charges (like in the case of PLL and bPLL at CR=3), perhaps due to the much smaller size of the monomers it becomes more difficult to overcharge the polyplexes (i.e. the smaller peptides make it very easy to find the exact match for charge neutrality) which leads to very favourable aggregation of CK_5C with pDNA but without a stop mechanism caused by excess charge repulsion. However, other studies show successful preparation of polyplexes using polymer monomers[21, 142]. This also provides a clue to the aggregation of polyplexes followed by addition of GSH: most likely, the excess of bPLL overcharge on the surface of polyplexes is cleaved away,

leading to the loss of positive charge on the surface, and consequent loss of colloidal stability.

GSH was also added to these CK_5C-pDNA complexes, to a final concentration of 10 mM. A continuously increase in size after the addition was observed, but it is likely that the size would increase with aging independently of GSH addition.

Overall this experiment demonstrates that even though the bPLL degrades (at least partially) in reducing media, this degradation by itself is not enough to disassemble polyplexes in our *in vitro* conditions (physiological pH and ionic strength). This by itself does not mean that bioreducible polyplexes will be inefficient *in vivo*. As interactions *in vivo* are more difficult to assess, transfection efficiency experiments are required. It is important to point out that in a similar study using bioreducible multivalent lipids instead of bPLL, the transfection efficiency did not improve when compared to non-bioreducible analogue lipids, but the cytotoxicity of the vector was significantly reduced, which is also an important aspect[143]. Furthermore, in a continuation of that study[16], small-angle x-ray scattering (SAXS) was able to elucidate that after the bioreducible multivalent cationic lipid is cleaved, the initial structures containing the DNA were destabilized, but a new structure with the DNA condensed by the cleaved multivalent headgroups as formed, indicating that the DNA release is more complex than initially assumed.

In a recent study using a bioreducible poly-L-lysine block copolymer with plasmid DNA, a better transfection efficiency was achieved when compared to polyplexes from nonbioreducible block copolymers analogues. Also, these bioreducible polyplexes showed lower cytotoxicity[144]. In another study, bioreducible PEI polyplexes were shown to have lower cytotoxicity as well as higher transfection efficiency when compared with low molecular and high molecular nonbioreducible analogues[145]. The same result regarding improved transfection efficiency when using bioreducible polyplexes may be found elsewhere[50, 146].

3.3.3 Microfluidics

3.3.1 Microfluidic assembly of Poly-L-lysine and plasmid DNA polyplexes

Microfluidics constitutes a promising platform for the controlled self-assembly of more complex materials, including liposomes[147-149], multiple emulsions[150-151] and polyplexes[152-155]. One of the goals of this project was to use microfluidic-based methods to control the assembly of bioreducible polyplexes and achieve a better control over their size and polydispersity.

To perform these experiments, we started by using a simple 2D cross-shaped microfluidic hydrodynamic focusing (MF) device (figure 9.a), made of polydimethylsiloxane (PDMS) with microchannels 200 μm width and 50 μm depth. The device consists of three inlets and one outlet. The side inlets are connected to two syringes containing PLL, while the central inlet is connected to the pDNA solution. The syringes are mounted on two syringe pumps that control the flow rate of each syringe independently: Q_2, which is the flow rate of the central stream (pDNA) is controlled by one syringe pump, whereas Q_1 and Q_3, which are the flow rates of the side streams (PLL), are controlled by the other syringe pump. This allows to fine tune the flow rate ratio (Q_R) of the PLL to pDNA streams. The pDNA solution is hydrodynamically focused by the PLL streams from the side channels into a narrowly focused stream. For the flow visualization, the MF device was mounted on an inverted microscope stage NIKON Eclipse Ti with a Plain Fluor 20x/0.45 objective. The focused stream containing DNA and the side streams containing PLL have no optical contrast and therefore are not distinguishable under normal light. As such, fluorescein dye (11.7 μM) was added to the DNA solution to color the focused stream, and allow a suitable monitoring of the flow within the device. A range of flow rates were studied to assess their influence in the formation of polyplexes (table 2), and in an attempt to find suitable conditions for optimal polyplex formation, i.e. conditions that allow a control over the size and polydispersity. The microfluidic-produced polyplexes were characterized by DLS.

For MF, the charge ratio was fixed at CR=7. The pGL3 and PLL solutions were injected at individual flow rates to satisfy the conditions Q_R=2, 10, 30 and 50, and Q_T = 11 and 55 μL.min^{-1} (table 3). Fluorescence images of the hydrodynamic focusing can be found in figure 32. By analyzing fluorescence images an approximate measurement of the central stream width (w_f) can be obtained. As mentioned in section 1.4.3, w_f is not constant through the depth of the channel, but rather has a concave shape because of the slower

fluid velocity near the walls. Hence, these measurements are likely to be slightly overestimated, especially at high Q_R (i.e. narrow widths), because the projection imaged in the microscope is likely to capture the larger width of the stream. From equation 10, it is also possible to roughly estimate the width of the focused streams. Eq. 10 is suitable for 2D geometries like the one used here, but is limited by the assumption that w_f is constant throughout the channel depth, which is not true like mentioned above. With these limitations in mind, both in the measured and estimated widths, the discrepancies are expected, and these values should be taken as qualitative indicators of hydrodynamic flow focusing (table 14). As expected, for higher Q_R, the width of the central stream decreases, allowing faster mixing by diffusion[99].

Table 14 - Comparison between the measured and estimated widths of the central stream (w_f) at fixed Q_T = 11 µL.min^{-1}.

	Q_T=11 µL.min^{-1}			Q_T=55 µL.min^{-1}			
Q_R	Q_2	$Q_1 + Q_3$	w_f	Q_2	$Q_1 + Q_3$	w_f	w_f (estimated)
2	3.667	7.334	55	18.33	36.67	53	67
10	1.000	10.00	17	5.000	50.00	26	18
30	0.355	10.65	14	1.774	53.23	24	6
50	0.216	10.78	10	1.078	53.92	18	4

For the first experiment with MF preparation, all samples were prepared on the same device. Between sample preparations, channels were cleaned with 1 M NaCl, DI water and finally F127 pluronic (commonly used to make the PDMS hydrophilic and avoid particle absorption). To assess the size of the polyplexes prepared by MF, DLS measurements were made at 173º and 90º. Results are shown in table 15. In figure 33.a and 33.b are shown the diameters of the prepared polyplexes measured at 173º for Q_T = 11 µL.min^{-1} and Q_T = 55 µL.min^{-1}, respectively.

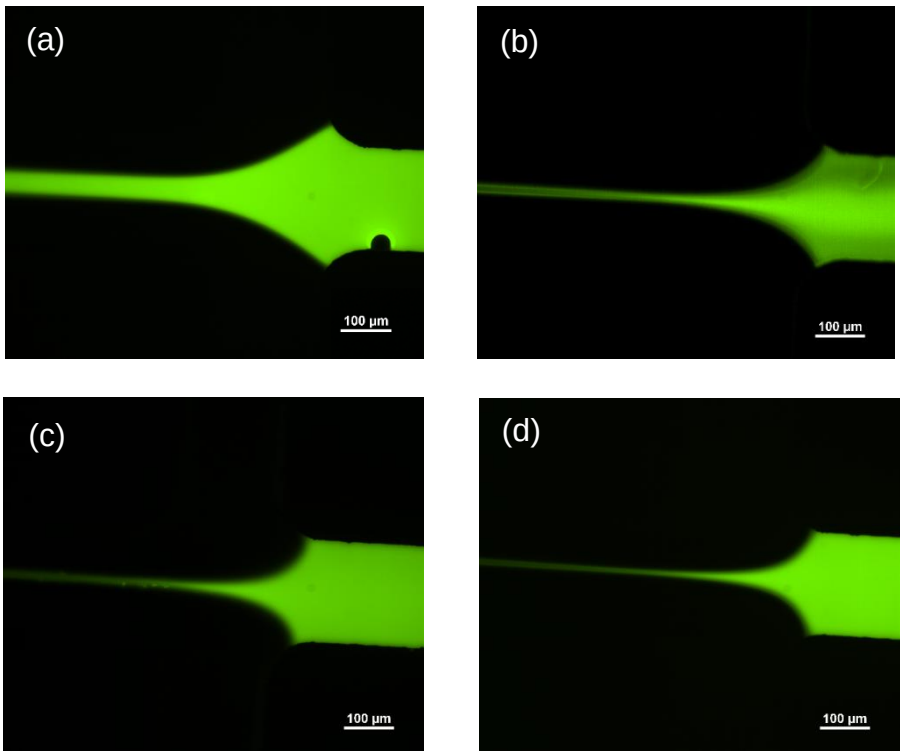

Fig. 32 – Hydrodynamic focusing of a pDNA solution containing fluorescein (11.7 µM) by PLL solution coming from the sides. The polymer concentrations and flow conditions are such that CR is fixed at 7. (a) Q_R = 2 and Q_T = 11 µL.min^{-1} (b) Q_R = 10 and Q_T = 11 µL.min^{-1} (c) Q_R = 30 and Q_T = 11 µL.min^{-1} (d) Q_R = 50 and Q_T = 11 µL.min^{-1}

Table 15 – Assessment of size of polyplexes prepared by MF at varying flow rates, and at fixed CR = 7. Measurements made at 173º and 90º. Also, size results applying a matlab methodology using the output given at 173º and 90º. All preparations were made in the same microchip.

		173º			90º			Matlab
Q_R	Q_T	D_H /nm	Std /nm	PDI	D_H /nm	Std /nm	PDI	D_H /nm
2	**11**	167.9	13.3	0.429	295.7	144.3	0.352	182.3
10	**11**	404.5	35.9	4.507	261.7	100.4	0.409	320.8
30	**11**	272.3	26.8	0.522	617.5	74.9	0.359	132.6
50	**11**	314.5	14.2	1.044	3850.4	3263.6	1.208	415.1
2	**55**	198.2	4.9	0.434	241	193.4	0.339	178.5
10	**55**	150.7	3.2	0.473	251.9	65.5	0.476	264.3
30	**55**	166.5	9.6	0.494	315.9	58.8	0.366	174.2
50	**55**	286.1	19.3	0.361	947.8	114.2	0.493	140.2

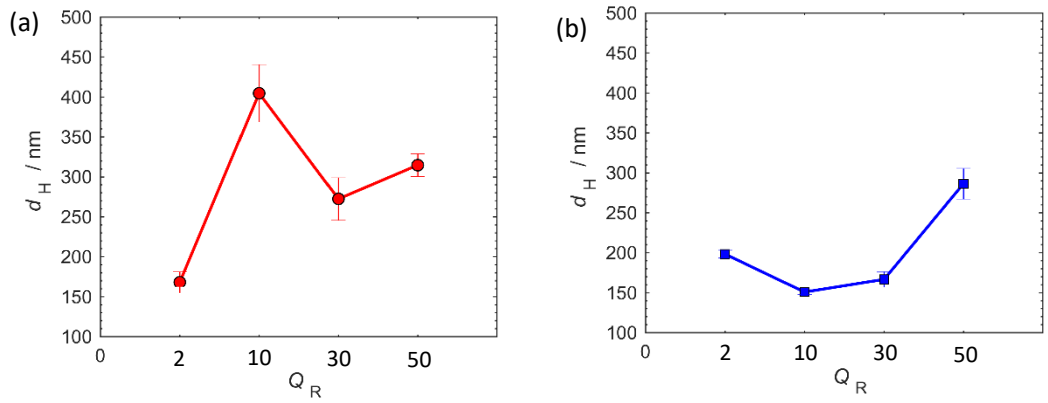

Fig. 33 - Microfluidic-assisted preparation of poly-L-lysine polyplexes at fixed CR = 7. DLS measurements obtained at 173º. All preparations were made in the same microchip. (a) Diameter with varying flow rate ratio at fixed total flow rate (QT = 11 µL.min^{-1}); (b) Diameter with varying flow rate ratio at fixed total flow rate (QT = 55 µL.min^{-1}).

Although the expectation was that with the enhanced fluid manipulation and mixing control given my MF, one could produce monodisperse polyplexes and control their size, the results showed the opposite. For CR=7, polyplexes became more polydisperse, and furthermore, the size dependence with Q_R was erratic (table 15 and figure 33). Unexpectedly, repeatability was also very low. This hinted at problems with the device. Indeed, during flow, we noticed that some macroscopic aggregates would form at the interface of pDNA and PLL, in the top and bottom microchannel walls. These aggregates would get stuck to the walls, and rarely would come off, not even with a 1 M NaCl solution pumped through the channels. The aggregates can be seen in figure 34.a and 34.b. We hypothesize that this uncontrolled aggregation at the walls can act as a source of larger particles that spoil a hypothetical narrower size distribution that we were expecting to obtain.

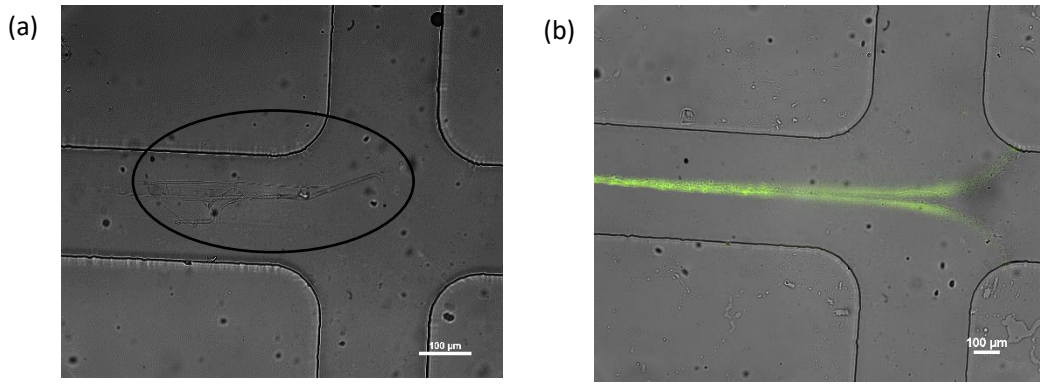

Fig. 34 – Imagens of aggregation occurred during MF preparation of polyplexes. (a) Aggregates form during flow at Q_R = 2 and Q_T = 11 µL.min^{-1} (b) Aggregates adhered to the wall after flow at Q_R = 10 and Q_T = 11 µL.min^{-1}

Because in the first experiment only one device was used for all the different flow conditions, we hypothesized that the surface aggregation could have formed at Q_R=2, which was the first tested flow rate ratio, and then contaminated all the subsequent conditions. As such, a second experiment was attempted by preparing each Q_R on a different device. This way one can avoid the influence of the previous aggregation on the new preparation. PDMS replicas were made from the same silicon master. All solutions and flow rates were kept the same. Results are shown in table 16.

Table 16 - Assessment of size of polyplexes prepared by MF at varying flow rates, and at fixed CR = 7. Measurements made at 173º and 90º. Also, size results applying a matlab methodology using the output given at 173º and 90º. All preparations were made in the same microchip.

		173º			90º			Matlab
QR	**QT**	**D_H /nm**	**Std /nm**	**PDI**	**D_H /nm**	**Std /nm**	**PDI**	**D_H /nm**
2	**11**	1076	248.6	0.578	213.1	0.7	0.344	327.9
10	**11**	152.1	22.8	0.590	252.4	13.7	0.408	187.5
30	**11**	364.5	8.1	0.709	1121.8	662.5	0.703	404.1
50	**11**	345.3	7.2	0.892	1644.3	1091.1	0.629	392.2
2	**55**	199.8	19.6	0.880	183.5	18.7	0.355	213.8
10	**55**	944.4	288.2	0.546	935.7	386.5	0.443	1038
30	**55**	470.9	208.3	1.898	894.5	75.1	0.472	344.7
50	**55**	326	10.4	1.000	1172.5	696.1	0.639	371.3

Again, for this second experiment, different sizes were obtained for each Q_R with no visible tendency. The level of polydispersity was also equally high. Furthermore, macroscopic aggregates in the channel walls were again observed for all the flow conditions, indicating that this problem is independent of the flow conditions for this channel geometry, and likely to be the source of the erratic results. Such behavior was likely caused by the very low fluid velocity expected close to the walls[114] (Poiseuille flow), which might facilitate the polymers (either condensed or non-condensed) sticking in an almost irreversible way to the channel walls. This occurred even though the PDMS

channels were coated with F127 As an improvement to the future, we will develop a 3D flow focusing microfluidic device to avoid contact of PLL and pDNA with the walls[156].

These results were unexpected, especially bearing in mind that there are some successful cases already described in the literature, even for a simple 2D geometry like the one used here. Successful preparation of polyplexes by microfluidics using PEI – polyethylenimine – and pDNA – pGL3 – using a 2D hydrodynamic focusing has been described[157]. The preparation was made on a device made of PMMA, with microchannel width of 254 μm and depth of 70 μm, at Q_R = 10 and Q_T = 110 μL.min^{-1}. The fact that the authors were able to produce polyplex smaller polyplexes with a more homogeneous size distribution can be related with a different material used to fabricate the device, or with the use of PEI instead of PLL.

Recently, droplet microfluidics were used successfully to prepare polyplexes of pDNA (pGL3) and a poly(amidoamine), reporting a significant improvement compared to bulk preparation[154]. The confinement of the oppositely charged polyelectrolytes within droplets allowed a more controlled aggregation process, with each droplet acting as a microreactor. This allowed an improvement of size and polydispersity, although a tailoring of size was not mentioned (BM: d = 165.8±21 nm PDI = 0.342; MF: d = 100.8±13.3 nm, PDI = 0.152).

Recently, an ingenious experimental setup was described using relatively cheap commercial parts like a 23G needle, tee union tube fittings, and 3 mm inner diameter tubing, to create a 3D turbulent flow-focusing device[155]. The dimensions of the tubing (which act as the channels) are 3 mm so this is not a real microfluidic device, and indeed the flow conditions favor more turbulent regimes. Yet, the turbulent flow proved very useful for rapid and controlled mixing, which allowed the preparation of polyplexes of poly(2-hydroxyprpyleneimine) with pDNA. These polyplexes showed smaller size, slower aggregation rate, and higher transfection efficiency, while exhibiting reduced cytotoxicity compared to those prepared by bulk mixing. Also, this method proved reproducible for synthesizing these complexes. Importantly, the size of the particles was controlled (in this case decreased) by increasing the total flow rate (Q_T). Another especially attractive feature of this setup was the 3D focusing which helped avoid the polymers entering in contact with the tube walls. We expect that the next iteration of our device, including 3D focusing can avoid polymer aggregation to the walls, while adding additional control over particle synthesis owing to the improved flow control at low Reynolds numbers.

3.4 Overview

This project started with the study of complexation of calf thymus with poly-L-lysine, in a range of charge ratios, which resulted in very stable complexes, with charge neutralization around CR = 1.6. Polyplexes with high polymer content (high CR) have smaller sizes and high zeta potentials (>30 mV). When the type of DNA was changed to plasmid DNA, which is significantly smaller and monodisperse, the overall particle size dropped to half. This shows that PLL is able to compact pDNA into smaller structures. Nevertheless, size and zeta profiles were very similar to those of bPLL-pDNA. In conclusion, the interaction of DNA with PLL showed three regimes in the formation of polyplexes: (a) at low CR DNA-PLL polyplexes and partially condensed DNA chains coexist; (b) for CR close to neutrality, a coacervate forms with near-zero charge ($\zeta \sim 0$); and (c) at high CR, positively charged polyplexes are formed with d_H values of 60 to 80 nm (figure 35). Cryo-TEM images of polyplexes prepared with similar pDNA and PLL at CR = 2 showed spherical and rod-like particle shape[138].

We have also observed the impact of DNA concentration on polyplex size. The experiment was made at fixed charge ratio. Larger particles were observed upon increasing DNA concentration. For the bPLL-pDNA system, the size profile showed similar sizes to those obtained for PLL polyplexes, except with a slight shift of particle charge neutralization (CR = 2.1). This may be due to structural differences caused by the disulfide bonds, or impurities resulting from the polymerization of the peptide. Zeta potential profile follows the trend observed for PLL / DNA and also seen in literature[136].

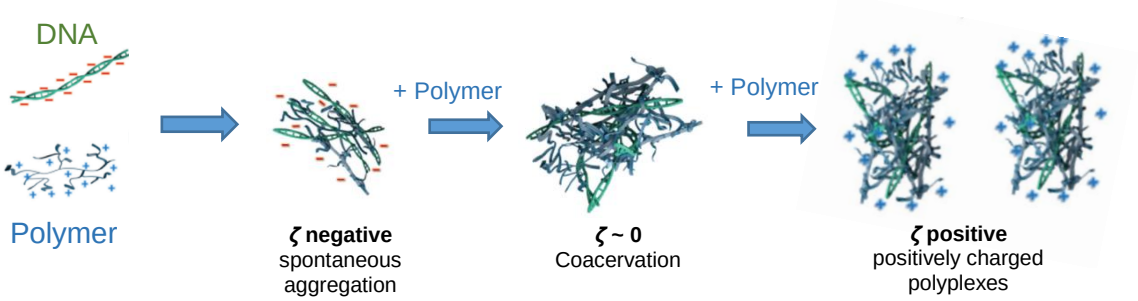

Fig. 35 – Representation of the model for the interaction of DNA / Polymer in aqueous solution, at increasing charge ratio[136].

When studying the effect of quasi-physiological buffer (20 mM HEPES, pH 7.4, 150 mM ionic strength), the order in which the buffer was added was taken into consideration. The PLL-pDNA system showed much higher stability to buffer at high CR. When adding the buffer after the formation of PLL polyplexes in water (path I), a window of aggregation was observed from CR 1-2. Conversely, when the formation of polyplexes was made in

buffer (path II), the aggregation window increased to CR 1-5. In the latter case, the gain of entropy is lessened by the presence of excess ions in solution and this slows the process of nucleation, leading to bigger complexes. Further, the presence of salt also reduced electrostatic repulsions, making polyplexes less stable. Nevertheless, an increase of particle size was observed. For the bPLL system, the effect of buffer was more evident. In both experiments aggregation was observed to all CR, except CR = 1. Perhaps the uncondensed pDNA present was able to stabilize particles.

A study involving buffer (20 mM HEPES, pH 7.4) and varying ionic strength (20, 30, 70, 100 and 150 mM) was performed for both PLL and bPLL systems to assess the effect of these parameters on polyplex stability and complexation. We observed an increase in the size of particles prepared at CR = 3, 5 and 7. For PLL-pDNA, when adding the buffer after polyplex formation in water (path I), polyplexes were not significantly affected until 150 mM ionic strength was reached, whereas for polyplexes formed in buffer (path II), 30 mM was enough to increase their size. Yet, polyplexes formed in up to 100 mM. For the bioreducible polyplexes, less stability was found. Polyplexes were able to remain stable or to form in buffer in an ionic strength up to 30 mM (paths I and II).

Microfluidic preparation of polyplexes containing poly-L-lysine and plasmid DNA was performed. A 3-inlet 2D cross hydrodynamic focusing device was used. The polyplexes were prepared at fixed CR = 7, at different flow rate ratios, and at different total flow rates. Polyplexes were able to form using this device, but an erratic and non-reproducible behavior was observed. This is most likely due to significant aggregation of condensed and non-condensed polymers to the microchannel surface, indicating that the device needs to be optimized to avoid contact of the polyplexes with the walls (e.g. by using a 3D flow focusing geometry).

4. Conclusion and Future Prospects

The structural analysis of polyplexes carried out in this work are relevant for the development of more efficient polymer-based gene delivery systems, which rely on the molecular properties of the complexing agent.

In this thesis, we were able to prepare and synthesize bioreducible poly-L-lysine and plasmid DNA. We successfully characterized the size, polydispersity and zeta potential of PLL-ctDNA, PLL-pDNA and bPLL-pDNA systems, in water and in a variety of buffers with different ionic strengths.

We found that the type of DNA used to prepare polyplexes greatly affected the size of the final complexes. Polyplexes containing ctDNA were much larger than those containing pDNA. This trend may be originating from the different structures of each type of DNA. Both systems containing plasmid DNA had similar structural properties when prepared in water, while in the presence of buffer these properties differed significantly.

We have demonstrated that the microfluidic hydrodynamic focusing method can condense plasmid DNA by PLL, but aggregation is due to happen inside the channel. Therefore, the microfluidic technique applied to this system still needs refining and optimization to achieve better control of particle size and stability (e.g. by using a 3D flow focusing geometry), allowing for further characterization and transfection studies.

As concerning future prospects, further structural studies of small-angle X-ray scattering, fluorescence cross-correlation spectroscopy and cryo-TEM will be required to gain further insight on the interactions between polymer and DNA, and also on the effect of glutathione on bioreducible polyplexes. Optimization of the microfluidics technique applied to this system will be mandatory. Finally, transfection studies will be required to obtain structure-efficiency relationships.

.

References

1. Watson, J. D.; Crick, F. H. C., Molecular Structure of Nucleic Acids - a Structure for Deoxyribose Nucleic Acid. *Nature* **1953,** *171* (4356), 737-738.
2. Crick, F., Central Dogma of Molecular Biology. *Nature* **1970,** *227* (5258), 561-&.
3. Ehsan, A.; Mann, M. J.; Dell'Acqua, G.; Dzau, V. J., Long-term stabilization of vein graft wall architecture and prolonged resistance to experimental atherosclerosis after E2F decoy oligonucleotide gene therapy. *J Thorac Cardiov Sur* **2001,** *121* (4), 714-722.
4. Mann, M. J.; Whittemore, A. D.; Donaldson, M. C.; Belkin, M.; Conte, M. S.; Polak, J. F.; Orav, E. J.; Ehsan, A.; Dell'Acqua, G.; Dzau, V. J., Ex-vivo gene therapy of human vascular bypass grafts with E2F decoy: the PREVENT single-centre, randomised, controlled trial. *Lancet* **1999,** *354* (9189), 1493-1498.
5. Yacyshyn, B. R.; Bowen-Yacyshyn, M. B.; Jewell, L.; Tami, J. A.; Bennett, C. F.; Kisner, D. L.; Shanahan, W. R., A placebo-controlled trial of ICAM-1 antisense oligonucleotide in the treatment of Crohn's disease. (vol 114, pg 1133, 1998). *Gastroenterology* **2001,** *121* (3), 747-747.
6. Compagno, D.; Lampe, J. N.; Bourget, C.; Kutyavin, I. V.; Yurchenko, L.; Lukhtanov, E. A.; Gorn, V. V.; Gamper, H. B., Jr.; Toulme, J. J., Antisense oligonucleotides containing modified bases inhibit in vitro translation of Leishmania amazonensis mRNAs by invading the mini-exon hairpin. *J Biol Chem* **1999,** *274* (12), 8191-8.
7. zu Putlitz, J.; Yu, Q.; Burke, J. M.; Wands, J. R., Combinatorial screening and intracellular antiviral activity of hairpin ribozymes directed against hepatitis B virus. *J Virol* **1999,** *73* (7), 5381-7.
8. Welch, P. J.; Yei, S.; Barber, J. R., Ribozyme gene therapy for hepatitis C virus infection. *Clin Diagn Virol* **1998,** *10* (2-3), 163-71.
9. Macpherson, J. L.; Ely, J. A.; Sun, L. Q.; Symonds, G. P., Ribozymes in gene therapy of HIV-1. *Front Biosci* **1999,** *4*, D497-505.
10. Vile, R. G.; Russell, S. J.; Lemoine, N. R., Cancer gene therapy: hard lessons and new courses. *Gene Ther* **2000,** *7* (1), 2-8.
11. Katz, S. M.; Tian, L.; Stepkowski, S. M.; Phan, T.; Bennett, C. F.; Kahan, B. D., Effect of ICAM-1/LFA-1 blockade on pancreatic islet allograft survival, function, and early cytokine production. *Transplant Proc* **1997,** *29* (1-2), 748-9.
12. Niven, R.; Pearlman, R.; Wedeking, T.; Mackeigan, J.; Noker, P.; Simpson-Herren, L.; Smith, J. G., Biodistribution of Radiolabeled Lipid−DNA Complexes and DNA in Mice. *Journal of Pharmaceutical Sciences* **1998,** *87* (11), 1292-1299.
13. Anderson, W. F., Human gene therapy. *Nature* **1998,** *392*, 25-30.
14. Verma, I. M.; Somia, N., Gene therapy - promises, problems and prospects. *Nature* **1997,** *389* (6648), 239-242.
15. Cardoso, A. M. S.; Faneca, H.; Almeida, J. A. S.; Pais, A. A. C. C.; Marques, E. F.; de Lima, M. C. P.; Jurado, A. S., Gemini surfactant dimethylene-1,2-bis(tetradecyldimethylammonium bromide)-based gene vectors: A biophysical approach to transfection efficiency. *Bba-Biomembranes* **2011,** *1808* (1), 341-351.
16. Shirazi, R. S.; Ewert, K. K.; Silva, B. F. B.; Leal, C.; Li, Y. L.; Safinya, C. R., Structural Evolution of Environmentally Responsive Cationic Liposome-DNA Complexes with a Reducible Lipid Linker. *Langmuir* **2012,** *28* (28), 10495-10503.
17. Silva, S. G.; Oliveira, I. S.; do Vale, M. L. C.; Marques, E. F., Serine-based gemini surfactants with different spacer linkages: from self-assembly to DNA compaction. *Soft Matter* **2014,** *10* (46), 9352-9361.
18. Ferruti, P., Poly(amidoamine)s: Past, present, and perspectives. *Journal of Polymer Science Part A: Polymer Chemistry* **2013,** *51* (11), 2319-2353.

19. Pereira, P.; Jorge, A. F.; Martins, R.; Pais, A. A.; Sousa, F.; Figueiras, A., Characterization of polyplexes involving small RNA. *J Colloid Interface Sci* **2012,** *387* (1), 84-94.
20. Cai, X. J.; Jin, R. R.; Wang, J. L.; Yue, D.; Jiang, Q.; Wu, Y.; Gu, Z. W., Bioreducible Fluorinated Peptide Dendrimers Capable of Circumventing Various Physiological Barriers for Highly Efficient and Safe Gene Delivery. *Acs Appl Mater Inter* **2016,** *8* (9), 5821-5832.
21. Soundara Manickam, D.; Bisht, H. S.; Wan, L.; Mao, G.; Oupicky, D., Influence of TAT-peptide polymerization on properties and transfection activity of TAT/DNA polyplexes. *J Control Release* **2005,** *102* (1), 293-306.
22. Behr, J. P., Synthetic gene-transfer vectors. *Accounts Chem Res* **1993,** *26* (5), 274-278.
23. Pack, D. W.; Hoffman, A. S.; Pun, S.; Stayton, P. S., Design and development of polymers for gene delivery. *Nat Rev Drug Discov* **2005,** *4* (7), 581-93.
24. Tiram, G.; Segal, E.; Krivitsky, A.; Shreberk-Hassidim, R.; Ferber, S.; Ofek, P.; Udagawa, T.; Edry, L.; Shomron, N.; Roniger, M.; Kerem, B.; Shaked, Y.; Aviel-Ronen, S.; Barshack, I.; Calderon, M.; Haag, R.; Satchi-Fainart, R., Identification of Dormancy-Associated MicroRNAs for the Design of Osteosarcoma-Targeted Dendritic Polyglycerol Nanopolyplexes. *Acs Nano* **2016,** *10* (2), 2028-2045.
25. Lachelt, U.; Wagner, E., Nucleic Acid Therapeutics Using Polyplexes: A Journey of 50 Years (and Beyond). *Chem Rev* **2015,** *115* (19), 11043-78.
26. Scholz, C.; Wagner, E., Therapeutic plasmid DNA versus siRNA delivery: Common and different tasks for synthetic carriers. *Journal of Controlled Release* **2012,** *161* (2), 554-565.
27. Schiessel, H., The physics of chromatin. *J Phys-Condens Mat* **2003,** *15* (19), R699-R774.
28. Thoma, F.; Koller, T.; Klug, A., Involvement of Histone-H1 in the Organization of the Nucleosome and of the Salt-Dependent Superstructures of Chromatin. *J Cell Biol* **1979,** *83* (2), 403-427.
29. Bloomfield, V. A., DNA condensation by multivalent cations. *Biopolymers* **1997,** *44* (3), 269-282.
30. Laemmli, U. K., Characterization of DNA condensates induced by poly(ethylene oxide) and polylysine. *Proc Natl Acad Sci U S A* **1975,** *72* (11), 4288-92.
31. Hart, S. L., Lipid carriers for gene therapy. *Curr Drug Deliv* **2005,** *2* (4), 423-8.
32. Zhang, C. N.; Jin, R.; Zhao, P.; Lin, C., A family of cationic polyamides for in vitro and in vivo gene transfection. *Acta Biomater* **2015,** *22*, 120-130.
33. Bloomfield, V. A., Condensation of DNA by Multivalent Cations - Considerations on Mechanism. *Biopolymers* **1991,** *31* (13), 1471-1481.
34. Drogoz, A.; David, L.; Rochas, C.; Domard, A.; Delair, T., Polyelectrolyte complexes from polysaccharides: Formation and stoichiometry monitoring. *Langmuir* **2007,** *23* (22), 10950-10958.
35. Suh, J.; Paik, H. J.; Hwang, B. K., Ionization of Poly(ethylenimine) and Poly(allylamine) at Various pH´s. *Bioorganic Chemistry* **1994,** *22* (3), 318-327.
36. Eckenrode, H. M.; Dai, H. L., Nonlinear optical probe of biopolymer adsorption on colloidal particle surface: poly-L-lysine on polystyrene sulfate microspheres. *Langmuir* **2004,** *20* (21), 9202-9.
37. Moore, N. M.; Sheppard, C. L.; Barbour, T. R.; Sakiyama-Elbert, S. E., The effect of endosomal escape peptides on in vitro gene delivery of polyethylene glycol-based vehicles. *Journal of Gene Medicine* **2008,** *10* (10), 1134-1149.
38. Oba, M.; Kato, T.; Furukawa, K.; Tanaka, M., A Cell-Penetrating Peptide with a Guanidinylethyl Amine Structure Directed to Gene Delivery. *Sci Rep-Uk* **2016,** *6*.
39. Choi, H. S.; Liu, W.; Liu, F.; Nasr, K.; Misra, P.; Bawendi, M. G.; Frangioni, J. V., Design considerations for tumour-targeted nanoparticles. *Nat Nanotechnol* **2010,** *5* (1), 42-7.

40. Maeda, H., The enhanced permeability and retention (EPR) effect in tumor vasculature: the key role of tumor-selective macromolecular drug targeting. *Adv Enzyme Regul* **2001,** *41*, 189-207.
41. Cabral, H.; Matsumoto, Y.; Mizuno, K.; Chen, Q.; Murakami, M.; Kimura, M.; Terada, Y.; Kano, M. R.; Miyazono, K.; Uesaka, M.; Nishiyama, N.; Kataoka, K., Accumulation of sub-100 nm polymeric micelles in poorly permeable tumours depends on size. *Nat Nanotechnol* **2011,** *6* (12), 815-23.
42. Kopatz, I.; Remy Js Fau - Behr, J.-P.; Behr, J. P., A model for non-viral gene delivery: through syndecan adhesion molecules and powered by actin. (1099-498X (Print)).
43. Burke, R. S.; Pun, S. H., Extracellular barriers to in Vivo PEI and PEGylated PEI polyplex-mediated gene delivery to the liver. *Bioconjug Chem* **2008,** *19* (3), 693-704.
44. Merkel, O. M.; Urbanics, R.; Bedocs, P.; Rozsnyay, Z.; Rosivall, L.; Toth, M.; Kissel, T.; Szebeni, J., In vitro and in vivo complement activation and related anaphylactic effects associated with polyethylenimine and polyethylenimine-graft-poly(ethylene glycol) block copolymers. *Biomaterials* **2011,** *32* (21), 4936-4942.
45. Chollet, P.; Favrot, M. C.; Hurbin, A.; Coll, J. L., Side-effects of a systemic injection of linear polyethylenimine-DNA complexes. *Journal of Gene Medicine* **2002,** *4* (1), 84-91.
46. Ruponen, M.; Ronkko, S.; Honkakoski, P.; Pelkonen, J.; Tammi, M.; Urtti, A., Extracellular glycosaminoglycans modify cellular trafficking of lipoplexes and polyplexes. *J Biol Chem* **2001,** *276* (36), 33875-80.
47. Mas, V.; Melero, J. A., Entry of enveloped viruses into host cells: membrane fusion. *Subcell Biochem* **2013,** *68*, 467-87.
48. Duncan, R.; Richardson, S. C. W., Endocytosis and Intracellular Trafficking as Gateways for Nanomedicine Delivery: Opportunities and Challenges. *Mol Pharmaceut* **2012,** *9* (9), 2380-2402.
49. Wan, L.; You, Y.; Zou, Y.; Oupicky, D.; Mao, G., DNA release dynamics from bioreducible poly(amido amine) polyplexes. *J Phys Chem B* **2009,** *113* (42), 13735-41.
50. Chen, S.; Han, K.; Yang, J.; Lei, Q.; Zhuo, R. X.; Zhang, X. Z., Bioreducible polypeptide containing cell-penetrating sequence for efficient gene delivery. *Pharm Res* **2013,** *30* (8), 1968-78.
51. Piao, J. G.; Ding, S. G.; Yang, L.; Hong, C. Y.; You, Y. Z., Bioreducible Cross-Linked Nanoshell Enhances Gene Transfection of Polycation/DNA Polyp lex in Vivo. *Biomacromolecules* **2014,** *15* (8), 2907-2913.
52. Dauty, E.; Verkman, A. S., Actin cytoskeleton as the principal determinant of size-dependent DNA mobility in cytoplasm. *Journal of Biological Chemistry* **2005,** *280* (9), 7823-7828.
53. Lukacs, G. L.; Haggie, P.; Seksek, O.; Lechardeur, D.; Freedman, N.; Verkman, A. S., Size-dependent DNA mobility in cytoplasm and nucleus. *J Biol Chem* **2000,** *275* (3), 1625-9.
54. Pigeon, L.; Goncalves, C.; Gosset, D.; Pichon, C.; Midoux, P., An E3-14.7K Peptide that Promotes Microtubules-Mediated Transport of Plasmid DNA Increases Polyplexes Transfection Efficiency. *Small* **2013,** *9* (22), 3845-3851.
55. Remaut, K.; Symens, N.; Lucas, B.; Demeester, J.; De Smedt, S. C., Cell division responsive peptides for optimized plasmid DNA delivery: the mitotic window of opportunity? *J Control Release* **2014,** *179*, 1-9.
56. Opalinska, J. B.; Gewirtz, A. M., Nucleic-acid therapeutics: basic principles and recent applications. *Nat Rev Drug Discov* **2002,** *1* (7), 503-514.
57. Wagner, E., Polymers for siRNA Delivery: Inspired by Viruses to be Targeted, Dynamic, and Precise. *Accounts Chem Res* **2012,** *45* (7), 1005-1013.
58. McCutchan, J. H.; Pagano, J. S., Enchancement of the infectivity of simian virus 40 deoxyribonucleic acid with diethylaminoethyl-dextran. *J Natl Cancer Inst* **1968,** *41* (2), 351-7.

59. Vaheri, A.; Pagano, J. S., Infectious poliovirus RNA: a sensitive method of assay. *Virology* **1965,** *27* (3), 434-6.
60. Farber, F. E.; Melnick, J. L.; Butel, J. S., Optimal conditions for uptake of exogenous DNA by Chinese hamster lung cells deficient in hypoxanthine-guanine phosphoribosyltransferase. *Biochim Biophys Acta* **1975,** *390* (3), 298-311.
61. Arscott, P. G.; Li, A. Z.; Bloomfield, V. A., Condensation of DNA by trivalent cations. 1. Effects of DNA length and topology on the size and shape of condensed particles. *Biopolymers* **1990,** *30* (5-6), 619-30.
62. Baeza, I.; Gariglio, P.; Rangel, L. M.; Chavez, P.; Cervantes, L.; Arguello, C.; Wong, C.; Montanez, C., Electron microscopy and biochemical properties of polyamine-compacted DNA. *Biochemistry* **1987,** *26* (20), 6387-92.
63. Chattoraj, D. K.; Gosule, L. C.; Schellman, A., DNA condensation with polyamines. II. Electron microscopic studies. *J Mol Biol* **1978,** *121* (3), 327-37.
64. Bareford, L. M.; Swaan, P. W., Endocytic mechanisms for targeted drug delivery. *Adv Drug Deliv Rev* **2007,** *59* (8), 748-58.
65. Luthman, H.; Magnusson, G., High efficiency polyoma DNA transfection of chloroquine treated cells. *Nucleic Acids Res* **1983,** *11* (5), 1295-308.
66. Cheng, J. J.; Zeidan, R.; Mishra, S.; Liu, A.; Pun, S. H.; Kulkarni, R. P.; Jensen, G. S.; Bellocq, N. C.; Davis, M. E., Structure - Function correlation of chloroquine and analogues as transgene expression enhancers in nonviral gene delivery. *Journal of Medicinal Chemistry* **2006,** *49* (22), 6522-6531.
67. Khalil, I. A.; Kogure, K.; Akita, H.; Harashima, H., Uptake pathways and subsequent intracellular trafficking in nonviral gene delivery. *Pharmacol Rev* **2006,** *58* (1), 32-45.
68. Erbacher, P.; Roche, A. C.; Monsigny, M.; Midoux, P., Putative role of chloroquine in gene transfer into a human hepatoma cell line by DNA lactosylated polylysine complexes. *Exp Cell Res* **1996,** *225* (1), 186-194.
69. Maxfield, F. R.; McGraw, T. E., Endocytic recycling. *Nat Rev Mol Cell Bio* **2004,** *5* (2), 121-132.
70. Murphy, R. F.; Powers, S.; Cantor, C. R., Endosome Ph Measured in Single Cells by Dual Fluorescence Flow-Cytometry - Rapid Acidification of Insulin to Ph-6. *J Cell Biol* **1984,** *98* (5), 1757-1762.
71. Behr, J.-P., The Proton Sponge: A Trick to Enter Cells the Viruses Did Not Exploit. *CHIMIA International Journal for Chemistry* **1997,** *51* (1-2), 34-36.
72. Devika Soundara Manickam, D. O., Multiblock Reducible Copolypeptides Containing Histidine-Rich and Nuclear

Localization Sequences for Gene Delivery. *Bioconjugate Chem.* **2006,** (17), 1395-1403.
73. Pichon, C.; Goncalves, C.; Midoux, P., Histidine-rich peptides and polymers for nucleic acids delivery. *Adv Drug Deliv Rev* **2001,** *53* (1), 75-94.
74. Brannigan, R. P.; Dove, A. P., Synthesis, properties and biomedical applications of hydrolytically degradable materials based on aliphatic polyesters and polycarbonates. *Biomater Sci-Uk* **2017,** *5* (1), 9-21.
75. Oupicky, D.; Li, J., Bioreducible polycations in nucleic acid delivery: past, present, and future trends. *Macromol Biosci* **2014,** *14* (7), 908-22.
76. Bang, E.-K.; Lista, M.; Sforazzini, G.; Sakai, N.; Matile, S., Poly (disulfide) s. *Chemical Science* **2012,** *3* (6), 1752-1763.
77. Wu, A. M.; Senter, P. D., Arming antibodies: prospects and challenges for immunoconjugates. *Nat Biotech* **2005,** *23* (9), 1137-1146.
78. Corbett, P. T.; Leclaire, J.; Vial, L.; West, K. R.; Wietor, J. L.; Sanders, J. K. M.; Otto, S., Dynamic combinatorial chemistry. *Chemical Reviews* **2006,** *106* (9), 3652-3711.
79. Yoon, J. A.; Kamada, J.; Koynov, K.; Mohin, J.; Nicolay, R.; Zhang, Y. Z.; Balazs, A. C.; Kowalewski, T.; Matyjaszewski, K., Self-Healing Polymer Films Based on Thiol-Disulfide Exchange Reactions and Self-Healing Kinetics Measured Using Atomic Force Microscopy. *Macromolecules* **2012,** *45* (1), 142-149.

80. Schafer, F. Q.; Buettner, G. R., Redox environment of the cell as viewed through the redox state of the glutathione disulfide/glutathione couple. *Free Radical Bio Med* **2001,** *30* (11), 1191-1212.
81. Filomeni, G.; Rotilio, G.; Ciriolo, M. R., Cell signalling and the glutathione redox system. *Biochem Pharmacol* **2002,** *64* (5-6), 1057-1064.
82. Jones, D. P.; Carlson, J. L.; Samiec, P. S.; Sternberg, P.; Mody, V. C.; Reed, R. L.; Brown, L. A. S., Glutathione measurement in human plasma Evaluation of sample collection, storage and derivatization conditions for analysis of dansyl derivatives by HPLC. *Clin Chim Acta* **1998,** *275* (2), 175-184.
83. Meister, A.; Anderson, M. E., Glutathione. *Annu Rev Biochem* **1983,** *52*, 711-60.
84. Bellomo, G.; Vairetti, M.; Stivala, L.; Mirabelli, F.; Richelmi, P.; Orrenius, S., Demonstration of nuclear compartmentalization of glutathione in hepatocytes. *P Natl Acad Sci USA* **1992,** *89* (10), 4412-4416.
85. Sevier, C. S.; Kaiser, C. A., Formation and transfer of disulphide bonds in living cells. *Nat Rev Mol Cell Biol* **2002,** *3* (11), 836-847.
86. Otto, S.; Furlan, R. L. E.; Sanders, J. K. M., Dynamic combinatorial chemistry. *Drug Discovery Today* **2002,** *7* (2), 117-125.
87. Wu, C.; Belenda, C.; Leroux, J. C.; Gauthier, M. A., Interplay of chemical microenvironment and redox environment on thiol-disulfide exchange kinetics. *Chemistry* **2011,** *17* (36), 10064-70.
88. Gilbert, H. F., Protein disulfide isomerase and assisted protein folding. *Journal of Biological Chemistry* **1997,** *272* (47), 29399-29402.
89. Tam, J. P.; Wu, C. R.; Liu, W.; Zhang, J. W., Disulfide Bond Formation in Peptides by Dimethyl-Sulfoxide - Scope and Applications. *Journal of the American Chemical Society* **1991,** *113* (17), 6657-6662.
90. Son, S.; Singha, K.; Kim, W. J., Bioreducible BPEI-SS-PEG-cNGR polymer as a tumor targeted nonviral gene carrier. *Biomaterials* **2010,** *31* (24), 6344-54.
91. Jeong, H.; Lee, E. S.; Jung, G.; Park, J.; Jeong, B.; Ryu, K. H.; Hwang, N. S.; Lee, H., Bioreducible Cationic Poly(amido amine)s for Enhanced Gene Delivery and Osteogenic Differentiation of Tonsil-Derived Mesenchymal Stem Cells. *J Biomed Nanotechnol* **2016,** *12* (5), 1023-1034.
92. Mok, H.; Park, T. G., Self-crosslinked and reducible fusogenic peptides for intracellular delivery of siRNA. *Biopolymers* **2008,** *89* (10), 881-8.
93. Manz, A.; Harrison, D. J.; Verpoorte, E. M. J.; Fettinger, J. C.; Paulus, A.; Ludi, H.; Widmer, H. M., Planar Chips Technology for Miniaturization and Integration of Separation Techniques into Monitoring Systems - Capillary Electrophoresis on a Chip. *J Chromatogr* **1992,** *593* (1-2), 253-258.
94. Whitesides, G. M.; Stroock, A. D., Flexible methods for microfluidics. *Phys Today* **2001,** *54* (6), 42-48.
95. Ng, J. M. K.; Gitlin, I.; Stroock, A. D.; Whitesides, G. M., Components for integrated poly(dimethylsiloxane) microfluidic systems. *Electrophoresis* **2002,** *23* (20), 3461-3473.
96. McDonald, J. C.; Duffy, D. C.; Anderson, J. R.; Chiu, D. T.; Wu, H. K.; Schueller, O. J. A.; Whitesides, G. M., Fabrication of microfluidic systems in poly(dimethylsiloxane). *Electrophoresis* **2000,** *21* (1), 27-40.
97. Thorsen, T.; Maerkl, S. J.; Quake, S. R., Microfluidic large-scale integration. *Science* **2002,** *298* (5593), 580-584.
98. Whitesides, G. M., The origins and the future of microfluidics. *Nature* **2006,** *442* (7101), 368-73.
99. Squires, T. M.; Quake, S. R., Microfluidics: Fluid physics at the nanoliter scale. *Rev Mod Phys* **2005,** *77* (3), 977-1026.
100. Beebe, D. J.; Mensing, G. A.; Walker, G. M., Physics and Applications of Microfluidics in Biology. *Annual Review of Biomedical Engineering* **2002,** *4* (1), 261-286.
101. Weigl, B. H.; Bardell, R. L.; Cabrera, C. R., Lab-on-a-chip for drug development. *Adv Drug Deliv Rev* **2003,** *55* (3), 349-77.

102. Glasgow, I.; Aubry, N., Enhancement of microfluidic mixing using time pulsing. *Lab Chip* **2003,** *3* (2), 114-120.
103. Yang, Z.; Matsumoto, S.; Goto, H.; Matsumoto, M.; Maeda, R., Ultrasonic micromixer for microfluidic systems. *Sensor Actuat a-Phys* **2001,** *93* (3), 266-272.
104. Tsai, J. H.; Lin, L. W., Active microfluidic mixer and gas bubble filter driven by thermal bubble micropump. *Sensor Actuat a-Phys* **2002,** *97-8*, 665-671.
105. Bau, H. H.; Zhong, J. H.; Yi, M. Q., A minute magneto hydro dynamic (MHD) mixer. *Sensor Actuat B-Chem* **2001,** *79* (2-3), 207-215.
106. Wu, Z. G.; Nguyen, N. T., Convective-diffusive transport in parallel lamination micromixers. *Microfluid Nanofluid* **2005,** *1* (3), 208-217.
107. Nguyen, N. T.; Wu, Z. G., Micromixers - a review. *J Micromech Microeng* **2005,** *15* (2), R1-R16.
108. Kamholz, A. E.; Yager, P., Molecular diffusive scaling laws in pressure-driven microfluidic channels: deviation from one-dimensional Einstein approximations. *Sensor Actuat B-Chem* **2002,** *82* (1), 117-121.
109. Gunther, A.; Jhunjhunwala, M.; Thalmann, M.; Schmidt, M. A.; Jensen, K. F., Micromixing of miscible liquids in segmented gas-liquid flow. *Langmuir* **2005,** *21* (4), 1547-1555.
110. Johnson, T. J.; Ross, D.; Locascio, L. E., Rapid microfluidic mixing. *Anal Chem* **2002,** *74* (1), 45-51.
111. Vestad, T.; Marr, D. W. M.; Oakey, J., Flow control for capillary-pumped microfluidic systems. *J Micromech Microeng* **2004,** *14* (11), 1503-1506.
112. Sundararajan, N.; Pio, M. S.; Lee, L. P.; Berlin, A. A., Three-dimensional hydrodynamic focusing in polydimethylsiloxane (PDMS) microchannels. *J Microelectromech S* **2004,** *13* (4), 559-567.
113. Chang, C. C.; Huang, Z. X.; Yang, R. J., Three-dimensional hydrodynamic focusing in two-layer polydimethylsiloxane (PDMS) microchannels. *J Micromech Microeng* **2007,** *17* (8), 1479-1486.
114. Ismagilov, R. F.; Stroock, A. D.; Kenis, P. J. A.; Whitesides, G.; Stone, H. A., Experimental and theoretical scaling laws for transverse diffusive broadening in two-phase laminar flows in microchannels. *Appl Phys Lett* **2000,** *76* (17), 2376-2378.
115. Knight, J. B.; Vishwanath, A.; Brody, J. P.; Austin, R. H., Hydrodynamic focusing on a silicon chip: Mixing nanoliters in microseconds. *Phys Rev Lett* **1998,** *80* (17), 3863-3866.
116. Oupicky, D.; Parker, A. L.; Seymour, L. W., Laterally stabilized complexes of DNA with linear reducible polycations: Strategy for triggered intracellular activation of DNA delivery vectors. *Journal of the American Chemical Society* **2002,** *124* (1), 8-9.
117. Hassan, P. A.; Rana, S.; Verma, G., Making Sense of Brownian Motion: Colloid Characterization by Dynamic Light Scattering. *Langmuir* **2015,** *31* (1), 3-12.
118. Bhattacharjee, S., DLS and zeta potential - What they are and what they are not? *Journal of Controlled Release* **2016,** *235*, 337-351.
119. Malvern, Zetasizer Nano Series. 2016.
120. Alastair, G. M.; Paul, S. C.; Peter, N. P., Particle sizing by dynamic light scattering: non-linear cumulant analysis. *Journal of Physics: Condensed Matter* **2015,** *27* (14), 145102.
121. Koppel, D. E., Analysis of Macromolecular Polydispersity in Intensity Correlation Spectroscopy: The Method of Cumulants. *The Journal of Chemical Physics* **1972,** *57* (11), 4814.
122. Particle size analysis -- Dynamic light scattering (DLS). In *ISO 22412:2017* 2017; p 34.
123. Ruiz-Cabello, F. J. M.; Trefalt, G.; Maroni, P.; Borkovec, M., Electric double-layer potentials and surface regulation properties measured by colloidal-probe atomic force microscopy. *Phys Rev E* **2014,** *90* (1).

124. Patel, V. R.; Agrawal, Y. K., Nanosuspension: An approach to enhance solubility of drugs. *Journal of Advanced Pharmaceutical Technology & Research* **2011,** *2* (2), 81-87.
125. Frisken, B. J., Revisiting the method of cumulants for the analysis of dynamic light-scattering data. *Appl Opt* **2001,** *40* (24), 4087-91.
126. Patty, P. J.; Frisken, B. J., Direct determination of the number-weighted mean radius and polydispersity from dynamic light-scattering data. *Appl Opt* **2006,** *45* (10), 2209-16.
127. Hassan, P. A.; Kulshreshtha, S. K., Modification to the cumulant analysis of polydispersity in quasielastic light scattering data. *J Colloid Interface Sci* **2006,** *300* (2), 744-8.
128. Draghici, B.; Ilies, M. A., Synthetic Nucleic Acid Delivery Systems: Present and Perspectives. *Journal of Medicinal Chemistry* **2015,** *58* (10), 4091-4130.
129. Ou, M.; Wang, X. L.; Xu, R.; Chang, C. W.; Bull, D. A.; Kim, S. W., Novel biodegradable poly(disulfide amine)s for gene delivery with high efficiency and low cytotoxicity. *Bioconjug Chem* **2008,** *19* (3), 626-33.
130. Dautzenberg, H.; Jaeger, W., Effect of charge density on the formation and salt stability of polyelectrolyte complexes. *Macromol Chem Phys* **2002,** *203* (14), 2095-2102.
131. Insua, I.; Wilkinson, A.; Fernandez-Trillo, F., Polyion complex (PIC) particles: Preparation and biomedical applications. *Eur Polym J* **2016,** *81*, 198-215.
132. Dautzenberg, H., Polyelectrolyte Complex Formation in Highly Aggregating Systems. 1. Effect of Salt: Polyelectrolyte Complex Formation in the Presence of NaCl. *Macromolecules* **1997,** *30* (25), 7810-7815.
133. M¨¹ller, M.; Ke£¿ler, B.; Fr£¿hlich, J.; Poeschla, S.; Torger, B., Polyelectrolyte Complex Nanoparticles of Poly(ethyleneimine) and Poly(acrylic acid): Preparation and Applications. *Polymers-Basel* **2011**.
134. Pinto, M. F.; Moran, M. C.; Miguel, M. G.; Lindman, B.; Jurado, A. S.; Pais, A. A., Controlling the morphology in DNA condensation and precipitation. *Biomacromolecules* **2009,** *10* (6), 1319-23.
135. Porsch, B.; Laga, R.; Horsky, J.; Konak, C.; Ulbrich, K., Molecular weight and polydispersity of calf-thymus DNA: static light-scattering and size-exclusion chromatography with dual detection. *Biomacromolecules* **2009,** *10* (11), 3148-50.
136. Bellettini, I. C.; Fayad, S. J.; Machado, V. G.; Minatti, E., Properties of polyplexes formed through interaction between hydrophobically-modified poly(ethylene imine)s and calf thymus DNA in aqueous solution. *Soft Matter* **2017,** *13* (14), 2609-2619.
137. Delisavva, F.; Mountrichas, G.; Pispas, S., Quaternized Poly[3,5-bis(dimethylaminomethylene)hydroxystyrene]/DNA Complexes: Structure Formation as a Function of Solution Ionic Strength. *Journal of Physical Chemistry B* **2013,** *117* (25), 7790-7796.
138. Oupicky, D.; Ogris, M.; Howard, K. A.; Dash, P. R.; Ulbrich, K.; Seymour, L. W., Importance of Lateral and Steric Stabilization of Polyelectrolyte Gene Delivery Vectors for Extended Systemic Circulation. *Mol Ther* **2002,** *5* (4), 463-472.
139. Leclercq, L.; Boustta, M.; Vert, M., Roles of hydrophobicity and charge density on the dynamics of polyelectrolyte complex formation and stability under modeled physicochemical blood conditions. *J Bioact Compat Pol* **2012,** *27* (2), 161-173.
140. Kim, T. I.; Lee, M.; Kim, S. W., A guanidinylated bioreducible polymer with high nuclear localization ability for gene delivery systems. *Biomaterials* **2010,** *31* (7), 1798-1804.
141. Read, M. L.; Bremner, K. H.; Oupicky, D.; Green, N. K.; Searle, P. F.; Seymour, L. W., Vectors based on reducible polycations facilitate intracellular release of nucleic acids. *Journal of Gene Medicine* **2003,** *5* (3), 232-245.
142. Nayvelt, I.; Thomas, T.; Thomas, T. J., Mechanistic differences in DNA nanoparticle formation in the presence of oligolysines and poly-L-lysine. *Biomacromolecules* **2007,** *8* (2), 477-484.

143. Shirazi, R. S.; Ewert, K. K.; Leal, C.; Majzoub, R. N.; Bouxsein, N. F.; Safinya, C. R., Synthesis and characterization of degradable multivalent cationic lipids with disulfide-bond spacers for gene delivery. *Bba-Biomembranes* **2011,** *1808* (9), 2156-2166.
144. Tappertzhofen, K.; Beck, S.; Montermann, E.; Huesmann, D.; Barz, M.; Koynov, K.; Bros, M.; Zentel, R., Bioreducible Poly-L-Lysine-Poly[HPMA] Block Copolymers Obtained by RAFT-Polymerization as Efficient Polyplex-Transfection Reagents. *Macromol Biosci* **2016,** *16* (1), 106-120.
145. Xia, W.; Wang, P.; Lin, C.; Li, Z.; Gao, X.; Wang, G.; Zhao, X., Bioreducible polyethylenimine-delivered siRNA targeting human telomerase reverse transcriptase inhibits HepG2 cell growth in vitro and in vivo. *J Control Release* **2012,** *157* (3), 427-36.
146. Kim, T. I.; Lee, M.; Kim, S. W., A guanidinylated bioreducible polymer with high nuclear localization ability for gene delivery systems. *Biomaterials* **2010,** *31* (7), 1798-804.
147. Jahn, A.; Vreeland, W. N.; Gaitan, M.; Locascio, L. E., Controlled vesicle self-assembly in microfluidic channels with hydrodynamic focusing. *Journal of the American Chemical Society* **2004,** *126* (9), 2674-2675.
148. Jahn, A.; Stavis, S. M.; Hong, J. S.; Vreeland, W. N.; Devoe, D. L.; Gaitan, M., Microfluidic Mixing and the Formation of Nanoscale Lipid Vesicles. *Acs Nano* **2010,** *4* (4), 2077-2087.
149. Arriaga, L. R.; Datta, S. S.; Kim, S. H.; Amstad, E.; Kodger, T. E.; Monroy, F.; Weitz, D. A., Ultrathin Shell Double Emulsion Templated Giant Unilamellar Lipid Vesicles with Controlled Microdomain Formation. *Small* **2014,** *10* (5), 950-956.
150. Utada, A. S.; Lorenceau, E.; Link, D. R.; Kaplan, P. D.; Stone, H. A.; Weitz, D. A., Monodisperse double emulsions generated from a microcapillary device. *Science* **2005,** *308* (5721), 537-541.
151. Shah, R. K.; Shum, H. C.; Rowat, A. C.; Lee, D.; Agresti, J. J.; Utada, A. S.; Chu, L. Y.; Kim, J. W.; Fernandez-Nieves, A.; Martinez, C. J.; Weitz, D. A., Designer emulsions using microfluidics. *Mater Today* **2008,** *11* (4), 18-27.
152. Koh, C. G.; Kang, X. H.; Xie, Y. B.; Fei, Z. Z.; Guan, J. J.; Yu, B.; Zhang, X. L.; Lee, L. J., Delivery of Polyethylenimine/DNA Complexes Assembled in a Microfluidics Device. *Mol Pharmaceut* **2009,** *6* (5), 1333-1342.
153. Debus, H.; Beck-Broichsitter, M.; Kissel, T., Optimized preparation of pDNA/poly(ethylene imine) polyplexes using a microfluidic system. *Lab Chip* **2012,** *12* (14), 2498-2506.
154. Grigsby, C. L.; Ho, Y. P.; Lin, C.; Engbersen, J. F. J.; Leong, K. W., Microfluidic Preparation of Polymer-Nucleic Acid Nanocomplexes Improves Nonviral Gene Transfer. *Sci Rep-Uk* **2013,** *3*.
155. Lim, J. M.; Swami, A.; Gilson, L. M.; Chopra, S.; Choi, S.; Wu, J.; Langer, R.; Karnik, R.; Farokhzad, O. C., Ultra-High Throughput Synthesis of Nanoparticles with Homogeneous Size Distribution Using a Coaxial Turbulent Jet Mixer. *Acs Nano* **2014,** *8* (6), 6056-6065.
156. Brennich, M. E.; Nolting, J. F.; Dammann, C.; Noding, B.; Bauch, S.; Herrmann, H.; Pfohl, T.; Koster, S., Dynamics of intermediate filament assembly followed in micro-flow by small angle X-ray scattering. *Lab Chip* **2011,** *11* (4), 708-716.
157. Koh, C. G.; Kang, X.; Xie, Y.; Fei, Z.; Guan, J.; Yu, B.; Zhang, X.; Lee, L. J., Delivery of Polyethylenimine/DNA Complexes Assembled in a Microfluidics Device. *Mol Pharmaceut* **2009,** *6* (5), 1333-1342.

Appendix I

Plasmid preparation

Materials and reagents

Granulated tryptone, granulated yeast extract and powder agar were acquired at Fisher Scientific. JM109 competent cells (*E. coli*), high efficiency, were purchased at Promega (cat. L2001). Plasmid DNA (pGL3 control vector) was purchased at Promega (cat. E1741). NaOH powder (99.99%), Tris-Cl powder (99.8%), isopropanol (99.8%), ethanol (99.8%) were purchased at Sigma. Giga Prep plasmid purification kit was purchased at Qiagen. The final pDNA solution concentration was acquired by NanoDrop 2000c spectrophotometer.

Preparing Lysogeny Broth Media

Materials:

1. Tryptone
2. Yeast Extract
3. NaCl
4. 2L flask
5. 5M NaOH

Procedure:

To a Flask of volume 2L, add 5 g of tryptone, 2.5 g of yeast extract and 5 g of NaCl. Add 500 mL of pure water and dissolve by magnetic stirring. Adjust the pH to 7.5 with 5M NaOH (typically 300 µL). Remove the magnetic bar. Cover the Flask with aluminum foil and autoclave. When finished, remove and allow to cool, but always keep covered with AL foil. This solution can be stored at 4°C.

Making LB Ampicillin Selection Plates

Materials:

1. Tryptone
2. Yeast Extract
3. NaCl
4. Granulated Agar
5. 2L Flask
6. 5M NaOH
7. Ampicillin

Procedure:

To a Flask of volume 2L, add 5 g of tryptone, 2.5 g of yeast extract and 5 g of NaCl. Add 500 mL of pure water and dissolve by magnetic stirring. Adjust the pH to 7.5 with 5M NaOH (typically 300 µL). Add 7.5 g of granulated agar to the mixture and stir until partial dissolution. Remove the magnetic bar. Cover the Flask with aluminum foil and autoclave. When finished, remove and allow to cool. Sterilize hood surface with a UV cycle. Open a bag of sterile 3'' empty plates and place them on stacks of 10. The 500 mL mixture will allow the preparation of 10-15 plates. When the mixture is cooled down enough, add 1 mL of Ampicillin 50 $mg.mL^{-1}$. Pour the LB agar into a sterile 500 mL beaker for easier transfer onto the plates. Fill the plates until half-full then allow them to set for 1 hour. Place lid on the plates and flip upside down to prevent condensation. Put the plates, upside down, inside the bag and store them at 4°C.

Transforming Competent Bacteria Cells

Materials:

1. JM109 Cells
2. LB Media
3. LB Selection Plates
4. Cryo-Safe
5. ThermoMixer®
6. 1.5 mL Eppendorf tubes

7. Sterile Cell Spreader
8. Incubating Orbital Shaker

Procedure:

Remove cells form -79ºC and let them thaw on the Cryo-Safe. After mixing gently, aliquot 25 µL of cells into a chilled, 1.5 mL Eppendorf tube. Add 0.500 µL of plasmid DNA 0.25 $mg.mL^{-1}$. Gently swirl tube on ice for a few seconds to mix by finger flicking tube. Then incubate tube on cryo-tablet for 30 minutes. Heat shock tube by placing in the ThermoMixer® at 42ºC for 45 seconds without shaking. Replace tube on ice for 2-5 minutes. Add 500 µL of chilled LB media. Gently shake and incubate tube by placing in the ThermoMixer at 300 rpm for 90 minutes at 37ºC. After incubation, centrifuge Eppendorf tubes at 12000 rpm for 30 seconds to pellet the bacteria. Pour off most of the supernatant but leave behind around 120 µL. Resuspend bacteria by pipetting up and down. Spread 10 µL of bacteria solution on LB selection plates with a sterile cell spreader. Place the plate upside down in the 37ºC Orbital Shaker. Incubate overnight and remove to fridge (4ºC). The growth of cell colonies should be noticeable.

Growing up Bacteria Cultures

Material:

1. LB media with ampicillin
2. Cultures grown on selection plates
3. 5x 2L flasks
4. 50 mL Centrifuge Tubes
5. Centrifuge
6. 15 mL Falcon Tube
7. Incubating Orbital Shaker
8. Qiagen Giga Kit

Procedure:

Pick a colony from the selective plate by using a sterile 200 µL pipette tip and just scoop up a colony. Then place the whole tip right into a 10mL Falcon tube containing 5 mL of LB. Grow at 37ºC for 8 hours at 275 rpm. Dilute the grown culture 1/500 into a larger

volume of selective LB medium. Use a flask of at least 4 times the volume of culture to ensure sufficient aeration. For the Qiagen Giga kit, 2.5 L of culture are needed. So, five 2L Flask filled with 500 mL of selective LB. Aliquot 1 mL from the grown culture into each Flask. Grow the culture at 37ºC with vigorous shaking for 12/16h. NOTE: The growth of 12/16h corresponds to the transition from logarithmic into stationary growth phase, when the cell density is high and the RNA content is low. Collect the bacteria by centrifugation at 6000 rpm for 15 minutes at 4ºC. Make sure all centrifuge tubes have the same weight. Remove all supernatant.

Plasmid Prep – Qiagen Giga Kit

Materials:

1. Centrifuge
2. 50 mL Centrifuge Tubes
3. 1L flask
4. Isopropanol
5. 70% Ethanol
6. 10 mL of 10 mM Tris-Cl, pH=8.5 buffer solution

All the buffers and separation column are provided by the Qiagen Giga Kit.

Procedure:

Harvest bacterial overnight culture by centrifuging at 6,000 rpm for 15 minutes at 4ºC. Try to re-use the 50mL tubes to reduce the number of pellets obtained. To a clean 1L flask, pour the bacteria pellets and resuspend them in 125 mL of Buffer P1. Add 125 mL of Buffer P2, mix thoroughly by inverting 4-6 times, and incubate at room temperature for 5-10 minutes. Add 31.25 ml of prechilled Buffer P3, mix thoroughly by vigorously inverting 4-6 times, and incubate on ice for 30 minutes. Centrifuge at 20,000 rpm for 30 minutes at 4ºC. While centrifuging, calibrate the separation column with 75 mL of Buffer QBT. Then, apply the supernatant obtained to the column and wash it with 600 mL of Buffer QC. Elute DNA with 100 mL of Buffer QF into a clean vessel. Precipitate DNA by adding 70 mL room-temperature isopropanol and mix. Centrifuge at 15,000 rpm for 30 minutes at 4ºC. Carefully decant the supernatant. Wash the DNA pellet with 10 mL room-

temperature 70% ethanol, centrifuge at 15,000 rpm for 10 minutes. Carefully decant supernatant without disturbing the pellet. Finally, air-dry pellet for 10-20 minutes and redissolve DNA in a suitable volume of 10mM Tris-Cl, pH=8.5.

It was possible to obtain 19.92 mg of pDNA pGL3. Value obtained by using NanoDrop™.